DOSIMETRY
OF
PULSED AND MIXED RADIATION FIELD
WITH
IONIZATION CHAMBER

1983

KEIJI ODA

DOSIMETRY
OF
PULSED AND MIXED RADIATION FIELD
WITH
IONIZATION CHAMBER

（電離箱によるパルス混成放射線場のドシメトリ）

1983

KEIJI ODA

CONTENTS

CHAPTER 1 GENERAL INTRODUCTION

According as high-energy particle accelerators and apparatus for nuclear fusion research are enlarged in scale, the fluence rate of radiations produced there becomes extremely high.[1] Such radiations, in principle, consist of various species distributed in the wide energy region. Furthermore, they in general are pulsed and often appears as a single burst. We now face new problems of dosimetry of high fluence rate, single burst and mixed radiation fields.

The term *dosimetry* originates from the measurement of *dose* by means of *dosimeters*. In this thesis, the author defines *radiation dosimetry* as (1) measuring a radiation field at a point of interest, (2) evaluating the absorbed energy in the matter placed in the radiation field, and (3) evaluating the radiation effects on the matter in biology, chemistry, physics, etc.[2]

The basic concept of radiation dosimetry is summerized in Table 1.1, where the main purposes of dosimetry are classified into four categories. The first is the measurement of radiation field, i.e. the number of particles and their energy at a given point, Fundamental quantities in dosimetry are *particle fluence* or *energy fluence* as a function of particle energy and its temporal variation. Dosimetric quantities of *exposure* and *air-kerma*, which represent the strength of the field, are also important. The second purpose is the evaluation of the energy absorbed in the matter placed in the radiation field. The *aborbed dose* is defined as the amount of energy imparted to matter by ionizing particles per unit mass of materials.[3,4] The third is the evaluation of the radiation effects on the matter. It is considered that the effects in general are

PURPOSE	QUANTITY	DETECTORS
Specification of Radiation Field	Energy Spectrum Fluence Rate	Semiconductor Detector Proportional Counter
Evaluation of Absorbed Energy in Material	Absorbed Dose	Ionization Chamber Calorimeter Fricke Dosimeter
Evaluation of Radiation Effect	RBE Dose dpa	
Radiation Protection	Dose Equivalent	

Table 1.1. Main puposes of radiation dosimetry.

proportional to the absorbed dose, and that the dose-to-effect conversion factor should depend on the radiation quality, i.e. species, energy and stopping power. It is also important in dosimetry to evaluate the conversion factor for every radiation quality and every effect of interest. In the present, there are many quantities representing the effects, e.g. RBE dose, displacement per atom, color center formation, radical formation, and so on. It is desirable to express these effects universally, for instance, by entropy change in near future. Finally, the fourth purpose is the evaluation of radiation safety. From a viewpoint of radiation protection is defined the *dose equivalent* corresponding to RBE dose.[5,6] The dose-to-dose equivalent conversion factor is called the *quality factor*, which is given by ICRP as a function of the collision stopping power of directly ionizing particles.[5,6]

It is most important for radiation dosimetry that before one practice the measurement, one should establish the principle, that is, (1) which dosimetric quantity among exposure, kerma, absorbed dose and dose equivalent, (2) which particle among photons, electrons, protons, neutrons, etc., (3) with which dosimeter among ionization chamber, TLD, scintillation detector, calorimeter, etc., and (4) how one measures.

In this thesis, the dosimetry of such a radiation field as is generated by high-energy particle accelerators or high-temperature plasmas is discussed. The field has characteristics of extremely high fluence rate, pulsed field (often single pulse) and a mixture of neutrons and X-rays in a wide energy region. It is the purpose of the thesis to establish a method for evaluating the exposure or air-kerma, the absorbed dose in tissue, and the dose-equivalent in the radiation fields. An ionization chamber has been selected as dosimeter, because the first two quantities

are proportional to the number of ion pairs liberated in materials according to their definition by ICRU.[3,4] It is a problem how to measure these dosimetric quantities in such radiation fields with an ionization chamber.

Almost all types of detectors will suffer the so-called high-dose-rate effect[7,8] in a radiation field of high fluence rate. The effect on an ionization chamber appears as the underestimate of the number of ion pairs liberated in the chamber by ionizing particles. In such a situation, a large amount of both positive and negative ions will disappear during their collection by an electric field owing to recombination between them. The ratio of the number of collected ions to that of generated ones is called *collection efficiency, f-value.*[9] Theoretical treatment of the f-value for pulsed X-rays have been carried out by several authors.[10-13] Their formulations, however, have not been experimentally confirmed for pulsed radiations of extremely high dose rate of 10^{10} rad s^{-1}. Furthermore, a method for determining the f-value in a single-burst radiation field has never been established. In addition, few methods have been proposed for evaluating the dose equivalent in a pulsed and mixed radiation field. In view of such problems, the author proposes a new method with an ionization chamber.

In Chap. 2, the f-value of a parallel-plate ionization chamber exposed to pulsed X-rays is obtained by numerical calculations of the partial differential equations which describe the temporal and spatial varistions of both positive and negative ions in the chamber, and furthermore the calculated results are compared with the well-known Boag's formula.[9] The effects of the space charge and the difference in mobility between positive and negative ions on the f-value are also

clarified quantitatively. A method based on the calculated results is proposed in Chap. 3 for determining the f-value for single-burst X-rays. An abreast-type ionization chamber for the method is designed and constructed. The method is applied to a pulsed X-ray field generated by an electron linear accelerator, and its applicability is experimentally confirmed. In Chap. 4 is described the f-value in a pulsed X-ray field of which duration is comparable with the ion transit time of the ionization chamber. The effects of the pulse duration or the pulse shape on the f-value are theoretically clarified. Experiments with an X-ray tube for medical diagnosis show that the proposed method is applicable to X-rays of long pulse duration. In Chap. 5, the evaluation of the dose equivalent in a mixed field is carried out. Two different approaches are made in a mixed radiation field consisting of bremsstrahlung X-rays and photo-neutrons generated by an electron linear accelerator. The results by the methods agree well within 10 % deviation with others by neutron spectrum measurement by TOF and activation methods, LET spectrum measurement with a Rossi counter and the separate measurement with two types of ionization chambers. The conclusions of this thesis are summerized in Chap. 6.

REFERENCES

1) M. Kawanishi: *Proc. 6th Int. Cong. Rad. Res., Tokyo, 1979,* p.192.

2) W.C.Roesch and F.H.Attix: *Radiation Dosimetry vol.I,* eds. F.H. Attix and W.C.Roesch (Academic, New York, 1968) Chap.1.

3) ICRU Report 6 (1954).

4) ICRU Report 19 (1971).

5) ICRP Publication 4 (1964).

6) ICRP Publication 15 (1970).

7) *High-Dose-Rate Effect Caused by Ionizing Radiations*, ed. S.Okabe (Atomic Energy Society of Japan, Tokyo, 1980) [in Japanese].

8) D.K.Nichols: IEEE Trans. Nucl. Sci. NS-23 (1980) 1016.

9) J.W.Boag: *Radiation Dosimetry vol.II,* eds. F.H.Attix and W.C. Roesch (Academic, New York, 1966) Chap.9.

10) J.W.Boag: Brit. J. Radiol. 23 (1950) 601.

11) P.M.Livingstone: J. Appl. Phys. 35 (1964) 2341.

12) R.E.Ellis and L.R.Read: Phys. Med. Biol. 14 (1969) 293.

13) R.E.Ellis and L.R.Read: Phys. Med. Biol. 14 (1969) 411.

CHAPTER 2 COLLECTION EFFICIENCY OF IONIZATION CHAMBER IN PULSED X-RAY FIELD*

2.1. Introduction

The exposure in an X-ray field or the absorbed dose in matter is generally proportional to the number of ion pairs liberated in materials.[1,2] A most convenient method of absolute measurement of the exposure or the absorbed dose is to collect ionic charge by applying an electric field. Some of ions, however, will disappear owing to recombination between positive and negative ions. The ratio of the charge (number) of collected ions to that of ions initially produced is so-called collection efficiency, f-value. The f-value is one of the most important correction factors for absolute measurement of the exposure or the absorbed dose with an ionization chamber, especially in a pulsed X-ray field of high exposure rate.[3]

High energy particle accelerators and apparatus for fusion research will easily generate an extremely high-exposure-rate X-rays of 10^{10} R s^{-1}. The f-value of ionization chambers in common use exposed to such a field becomes much less than unity. It induces an underestimate of the exposure and the absorbed dose. In this situation one must determine an accurate f-value from measurable values only, i.e. ionic charge collected under the unsaturated region ($f < 1.0$). It is very difficult to determine the f-value, because the value itself is a function of the generated charge which is intended to be evaluated.

The main part of this work is presented in Nucl. Instrum. & Methods 172 (1980) 447.

According to the prevailing techniques, the ionic charge has been measured by applying a high voltage enough for the recombination loss to be negligible. The saturation voltage becomes higher with increasing the exposure rate of the X-rays. With further increase in the exposure rate, the voltage will enter into the proportional region beyond the saturation one. It is necessary to develop a new technique for the f-value determination until such a high exposure rate is realized.

It is essential and most important to understand a saturation characteristics of ionization chambers and to know the dependence of the f-value on various parameters, e.g. the exposure rate, pulse duration and chamber constants of recombination coefficient, ion mobility, applied voltage, gap distance, diffusion constant, and cavity size. In 1950's and 1960's a lot of expressions about the f-value for continuous X-rays have been published by many authors.[4-20] Few formulations for pulsed X-rays,[21-24] however, have been proposed. Among them, Boag's formula[21] is most excellent and is still in common use. Surely the formula has been applicable to pulsed X-rays for those days, but it deviates gradually as the exposure rate of pulsed X-rays becomes higher.

In this chapter, more accurate description of a relation between f-value and various parameters is numerically obtained. The output current of ionization chambers is also discussed, and then a correlation with the f-value is clarified.

2.2. Boag's approximation

In a parallel-plate ionization chamber exposed to pulsed X-rays, ion pairs are uniformly generated until an X-ray pulse ceases. The

positive and negative ions drift in the opposit direction by an external electric field as illustrated in Fig. 2.1. In this situation, Boag made the following assumptions:

(1) All ions generated during pulse distribute uniformly in the chamber when the pulse ceases.

(2) The densities of positive and negative ions are equal in the region of overlap of both ion distributions.

(3) Both the space charge effect and diffusion loss are neglected.

The ion density in the overlap region, n [cm^{-3}], decreases with time at the following rate:

$$\frac{dn}{dt} = -\alpha n^2 , \qquad (2.1)$$

where α [$m^3 s^{-1}$] is the recombination coefficient. The equation can be solved explicitly and gives the following solution:

$$n = (q_0 \tau_0)/(1 + \alpha q_0 \tau_0 t) , \qquad (2.2)$$

where q_0 [$m^{-3} s^{-1}$] is the ion production rate which is proportional to the exposure rate, and τ_0 [s] is the pulse duration. Let $k_\pm$ [$m^2 s^{-1} V^{-1}$] be the ion mobilities, d [m] the gap distance between the electrodes, and V [V] the applied voltage, the width of the overlap region is expressed by $\{d - (k_+ + k_-)Vt/d\}$. This region exists only for a time of $d^2/(k_+ + k_-)V$. Thus, the amount of recombination loss per unit area, R [m^{-2}], is expressed as follows:

$$R = \int_0^{d^2/(k_+ + k_-)V} \alpha n^2 \left[d - (k_+ + k_-)\frac{Vt}{d} \right] dt. \qquad (2.3)$$

Substituting eq. (2.2) into eq. (2.3), the following formula is obtained:

$$R = q_0 \tau_0 d \left[1 - \frac{1}{u} \ln(1 + u) \right] , \qquad (2.4)$$

where $u = \alpha q_0 \tau_0 d^2/(k_+ + k_-)V$. Accordingly, Boag's expression of

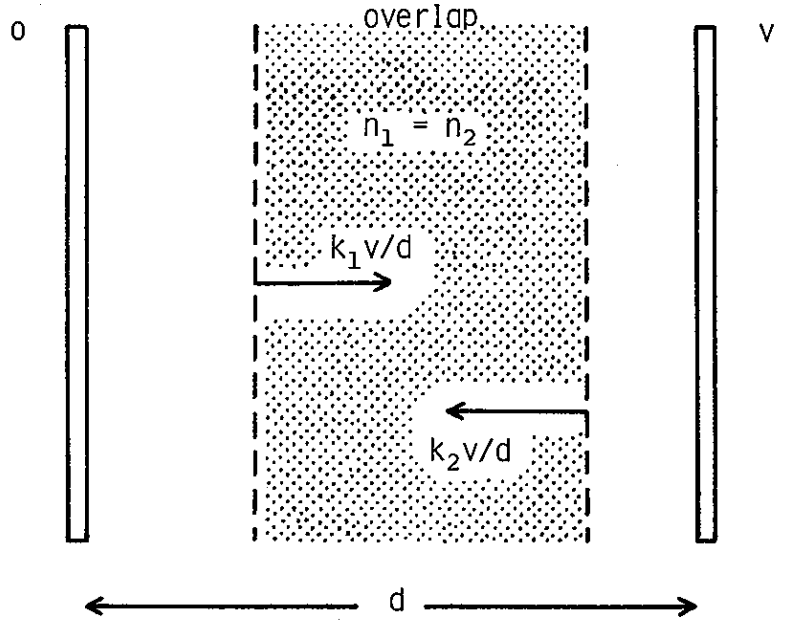

Fig. 2.1. Overlap of positive and negative ion distributions in a parallel-plate ionization chamber after an X-ray pulse.

the f-value is obtained as follows:

$$f_B = 1 - R/q_0 \tau_0 d = 1 - \frac{1}{u}\ln(1+u). \qquad (2.5)$$

2.3. Normalized rate equations

The Boag's formula is applicable to most cases of pulsed X-ray fields. But the assumptions are not acceptable in special cases of an X-ray field of extremely high exposure rate and of an X-ray field of relatively long pulse duration. In the former field the recombination during pulse cannot be neglected. In the latter, the drift of both ions is considerable and the densities of positive and negative ions in the overlap region are not equal. Thus, the Boag's assumptions become invalid in both cases. In order to ascertain the fact, the rate equation with respect to both positive and negative ions should be solved as strictly as possible.

The rate of increase in the ion density at a point, x, at a time, t, is in general expressed by the following equations:[5,6,26]

$$\frac{\partial n_+}{\partial t} = q - \alpha n_+ n_- - k_+ \frac{\partial (n_+ E)}{\partial x} + D_+ \frac{\partial^2 n_+}{\partial x^2}, \qquad (2.6)$$

$$\frac{\partial n_-}{\partial t} = q - \alpha n_+ n_- + k_- \frac{\partial (n_- E)}{\partial x} + D_- \frac{\partial^2 n_-}{\partial x^2}, \qquad (2.7)$$

where q [$m^{-3}s^{-1}$] is the ion production rate as a function of the time, $D_\pm$ [$m^2 s^{-1}$] are the diffusion constants, and E [Vm^{-1}] is the electric field strength, which is related with the ion densities through Poisson's equation as follows:

$$\frac{\partial E}{\partial x} = \frac{e}{\varepsilon_0}(n_+ - n_-), \qquad (2.8)$$

where e [C] is the electronic charge and ε_0 the permittivity. Four

terms on the right hand side of eqs. (2.6) and (2.7) represent production, recombination, divergence and diffusion, respectively.

It is known that minor change in the density is caused by diffusion,[27] but the term is here neglected for simplicity. Then, eqs. (2.6), (2.7) and (2.8) become

$$\frac{\partial \nu_+}{\partial s} = \Lambda - M \nu_+ \nu_- - \frac{\partial (\nu_+ \varepsilon)}{\partial \xi} , \tag{2.9}$$

$$\frac{\partial \nu_-}{\partial s} = \Lambda - M \nu_+ \nu_- + \eta \frac{\partial (\nu_- \varepsilon)}{\partial \xi}, \tag{2.10}$$

$$\frac{\partial \varepsilon}{\partial \xi} = M \lambda (\nu_+ - \nu_-) . \tag{2.11}$$

All the variables in eqs. (2.6), (2.7) and (2.8) are normalized by appropriate constants to be dimensionless.[28,29] Namely, $\nu_\pm = n_\pm / q_0 \tau$, $s = t/\tau$, $\xi = x/d$, $\Lambda(s) = q(t)/q_0$, $M = \alpha q_0 \tau^2$, $\varepsilon = Ed/V$, $\eta = k_-/k_+$ and $\lambda = ek_+/\varepsilon_0 \alpha$. For simplicity the following assumptions are made:

(1) The mobilities of positive and negative ions are equal: $\eta = 1$.

(2) The space charge effect is negligible: $\varepsilon = 1$ for all ξ.

(3) The pulse shape is rectangular: $\Lambda = 1$ when $0 \leq s \leq s_0 = \tau_0/\tau$ and 0 when $s_0 < s \leq 1 + s_0$.

The validity of the assumptions is discussed in the succeeding section and Chap. 4. Allowing for the assumptions, the normalized partial differential equation is obtained as follows:

$$\frac{\partial \nu_\pm}{\partial s} = \Lambda - M \nu_+ \nu_- \mp \frac{\partial \nu_\pm}{\partial \xi} \tag{2.12}$$

The temporal and spatial variations of the normalized ion densities are calculated numerially by the method described in Appendix 2.A. Figures 2.2 (a), (b) and (c) are typical results of numerical calculations.

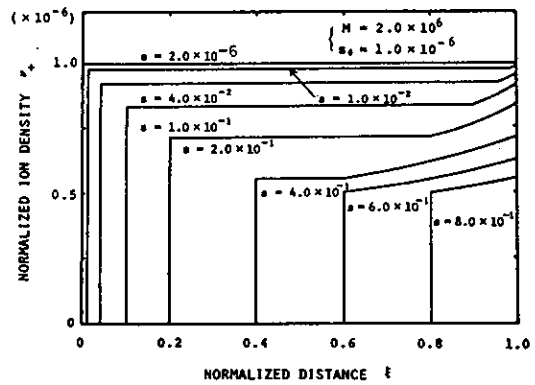

(a)

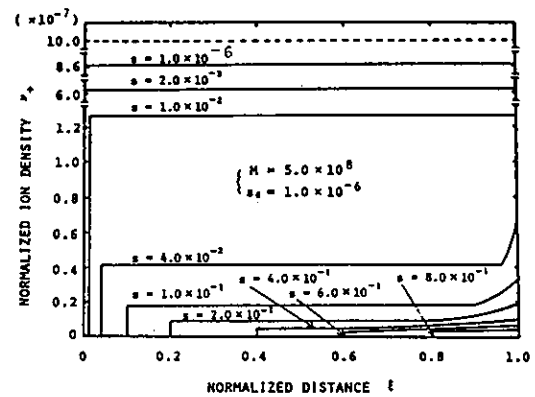

(b)

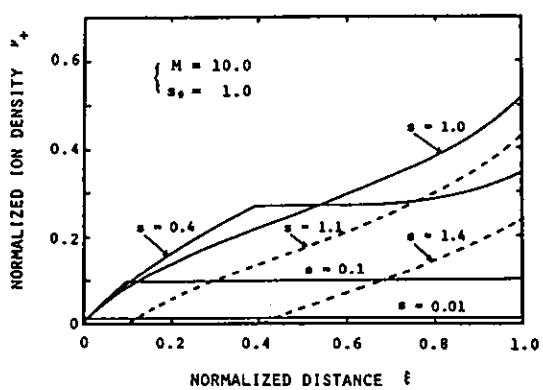

(c)

Fig. 2.2. Temporal variation of the spatial distribution of normalized ion density for pulsed X-rays. (a) $M = 2.0 \times 10^6$ and $s_0 = 1.0 \times 10^{-6}$, (b) $M = 5.0 \times 10^8$ and $s_0 = 1.0 \times 10^{-6}$, (c) $M = 10.0$ and $s_0 = 1.0$.

The abscissa in the figures denotes the normalized distance in the chamber, and the ordinate the normalized density of ions drifting toward the right electrode. The spatial distribution of the density of oppositely charged ions is symmetric with respect to a vertical line $\xi = 0.5$. The parameter, s, corresponds to the time.

Figure 2.2 (a) corresponds to the case where a parallel-plate ionization chamber is placed in an X-ray field with a very short pulse duration, which is generated, for example, by particle accelerators and experimental apparatus for laser induced fusion. Without recombination the density, n_+, would become $q_0\tau_0$ when $t = \tau_0$. In other words, when $s = s_0 = 1.0 \times 10^{-6}$, ν_+ becomes s_0 at any place. It is just right in this case as shown in Fig. 2.2 (a). Namely, the result shows that the Boag's approximation is valid.

The temporal variations of the density distribution for an X-ray field of extremely high exposure rate are ahown in Fig. 2.2 (b). When $s = s_0 = 1.0 \times 10^{-6}$, the distribution of the ion density is uniform. An absolute value of ν_+, however, is not equal to s_0 but to 8.6×10^{-7}. The result shows that recombination loss which is neglected in Boag's formula amounts to 14 % of initial production. Such X-ray field are often found at the vicinity of a target bombarded by accelerated particles and near apparatus for fusion experiments. The dosimetry of high-exposure-rate X-rays is carried out in the succeeding chapter.

Figure 2.2 (c) corresponds to the case where the ionization chamber is placed in an X-ray field of which pulse duration is equal to the ion transit time. The density distributions in the build-up stage ($s \leq s_0$) are shown by solid lines. The ions produced at the start of X-ray pulse should drift and some of them escaping recombination should

reach to the electrode until the pulse ceases. It is obvious that both recombination and collection during pulse is not negligible. The distributions in the decaying stage ($s > s_0$) are also shown in the figure by broken lines. They are not rectangular but nearly tangential. It means that the densities of positive and negative ions are not equal in the overlap region where the recombination takes place. The results shows that the Boag's approximation is not applicable to this case. Such fields are found around an X-ray tube for medical diagnosis or Tokamak-type apparatus for fusion experiments. The dosimetry of such X-rays will be discussed in Chap. 4.

2.4. Collection efficiency for pulsed X-rays

The collection efficiency, f-value, for pulsed X-rays is expressed by the following formula with variables defined in the previous section:

$$f = 1 - \frac{\alpha}{q_0 \tau_0 d} \int_0^d \left[\int_0^{\tau_0} n_+ n_- \, dt + \int_{\tau_0}^{\tau_0+\tau} n_+ n_- \, dt \right] dx. \quad (2.13)$$

Equation (2.13) is rewrriten with the normalized variables as follows:

$$f = 1 - \frac{M}{s_0} \int_0^1 \left[\int_0^{s_0} \nu_+ \nu_- \, ds + \int_{s_0}^{s_0+1} \nu_+ \nu_- \, ds \right] d\xi. \quad (2.14)$$

In the bracket in the second term on the right hand side, two integrals correspond to the amount of recombination loss during and after a pulse, respectively. For comparison, Boag's formula is rewritten with the normalized variables as follows:

$$f_B = 2/Ms_0 \cdot \ln(1 + Ms_0/2) . \quad (2.15)$$

The most important parameter in the equation, Ms_0, is equal to the product of the chamber constants (α, τ) and the parameters characteristic of the X-ray field (q_0, τ_0) as is clear in the following equation:

$$Ms_0 = (\alpha q_0 \tau^2)\cdot(\tau_0/\tau) = (\alpha\tau)\cdot(q_0\tau_0). \qquad (2.16)$$

The formula gives a same f-value so long as the total exposure per pulse is kept contant. However, the true f-value described by eq. (2.14) is in general a function of the respective values of M and s_0, that is, the exposure rate and the pulse duration.

The results of numerical calculations of eq. (2.14) are summerized in Fig. 2.3, which shows the dependence of the f-value on the normalized pulse duration for several Ms_0-values. Horizontal broken lines represent f_B-values. It is found from a comparison between two results that the Boag's approximation is valid only under the condition that $s_0 \lesssim 10^{-3}$ and $Ms_0 \lesssim 10.0$. With increasing the Ms_0-value, the true f-value becomes lower than the f_B-value. The discrepancy is attributed mainly to the neglect of the recombination loss during pulse as was pointed out in the previous section. The deviation from the f_B-value becomes serious as the pulse duration becomes longer at a constant Ms_0-value. This situation has already been stated in Fig. 2.2 (c).

High energy particle accelerators has easily achieved an exposure rate higher than 10^{10} R s^{-1}. Let consider an ionization chamber of which recombination coefficient is 1.0×10^{-6} cm^3s^{-1} and the ion transit time is 1.0×10^{-3} s, exposed in an X-ray field of which pulse duration is 1.0×10^{-6} s and the exposure rate is 5.0×10^{8} Rs^{-1}. Then, the relation that 1 Rs^{-1} = 2.08×10^{9} $cm^{-3}s^{-1}$ gives an M-value of 1.0×10^{6} and an s_0-value of 1.0×10^{-3}. After all, an Ms_0-value becomes 1.0×10^{3}, and it gives an f-value smaller than 0.01. Namely, 99 % of ion production disappears owing to recombination. A notice should be taken that the true f-value is smaller than the f_B-value by

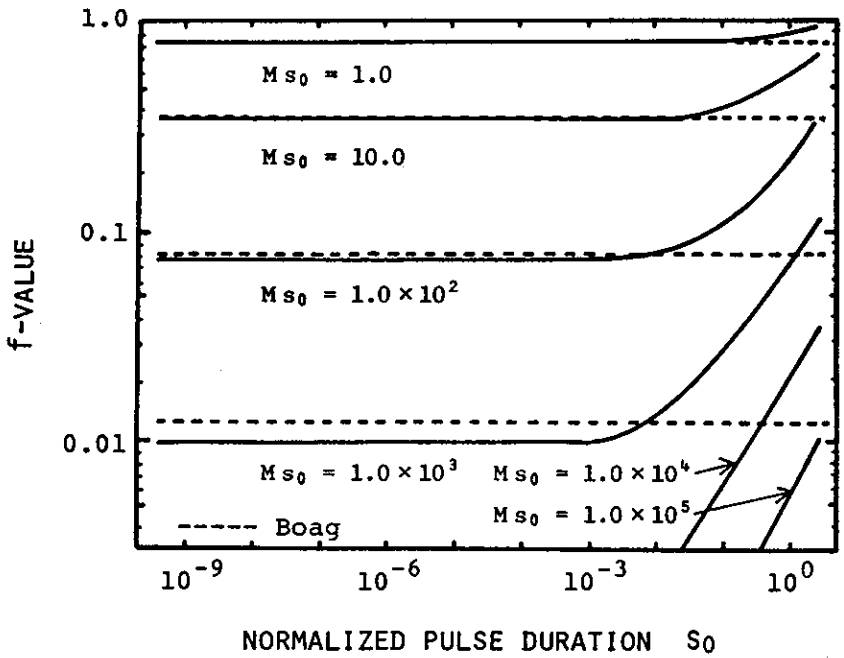

Fig. 2.3. Dependence of the collection efficiency on the normalized pulse duration. The parameter, Ms_0, corresponds to the total exposure per pulse. Boag's formula gives the values represented by broken lines.

20 % in this case. The other example is an X-ray field generated by an X-ray tube for medical diagnosis, of which pulse duration is 1.0×10^{-2} s and the total exposure is 50.0 R per pulse. The values give an Ms_0-value of 10.0 and an s_0-value of 10.0, and therefore f = 0.89. On the other hand, Boag's f-value becomes 0.35.

In order to apply the calculated f-value to actual X-ray field, errors caused by the assumptions in eq. (2.12) must be evaluated beforehand. At first is discussed the influence of a difference in mobility between positive and negative ions upon the f-value. An existance of many ion species in air has been reported.[30] According to the publications,[31-34] the average mobility of negative ions is somewhat larger than that of positive ones in air of 1 atm. Thus, the calcualtions of eq. (2.10) are performed for various η-values defined as a ratio of mobility of negative ions to that of positive ones. Figure 2.4 shows a dependence of the η-value in the case that $M = 10^3$ and $s_0 = 0.01$. The ordinate is the deviation from the f-value in Fig. 2.3 expressed by per cent. For an η-value of 1.2 for air of 1 atm, the deviation becomes about 6 %. At a constant η-value of 1.2 the deviation is shown in Fig. 2.5 as a function of the s_0-value. It is concluded from the figure that the effect due to mobility difference will not cause a significant error for practical application.

Next, the space charge effect is clarified below. The effect for continuous X-rays has been analyzed by several authors,[35,36] but few studies for pulsed X-rays exist. In order to obtain the f-value including the space charge effect, a time-consuming calculations of simultaneous equations consisting of eqs. (2.9), (2.10) and (2.11) must be carried out. An example of the results is shown in Fig. 2.6,

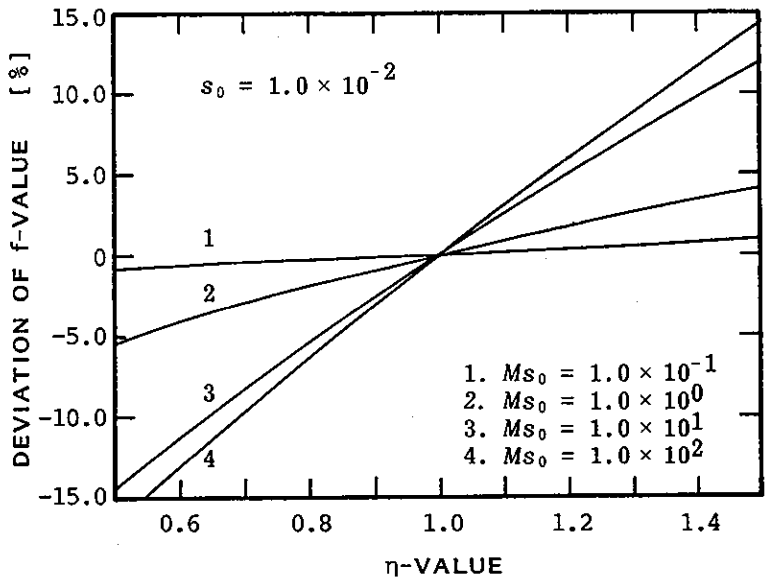

Fig. 2.4. Deviation of the f-value including the mobility effect as a function of η-value, which is defined as a ratio of the mobility of positive ions to that of negative ones. The f-values when η = 1.0 are 0.984, 0.811, 0.336 and 0.0455, respectively. For air of 1 atm η-value lies near 1.2.

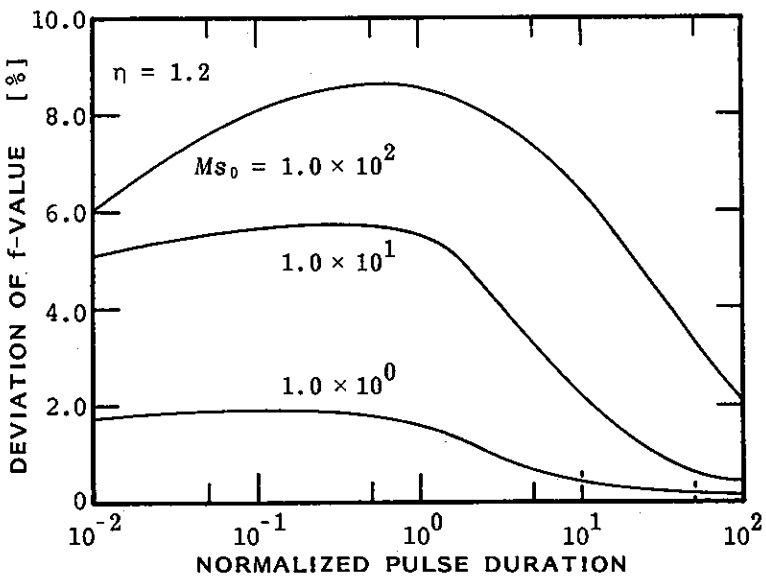

Fig. 2.5. Deviation of the f-value including the mobility effect as a function of the normalized pulse duration. The η-value is assumed to be a constant of 1.2.

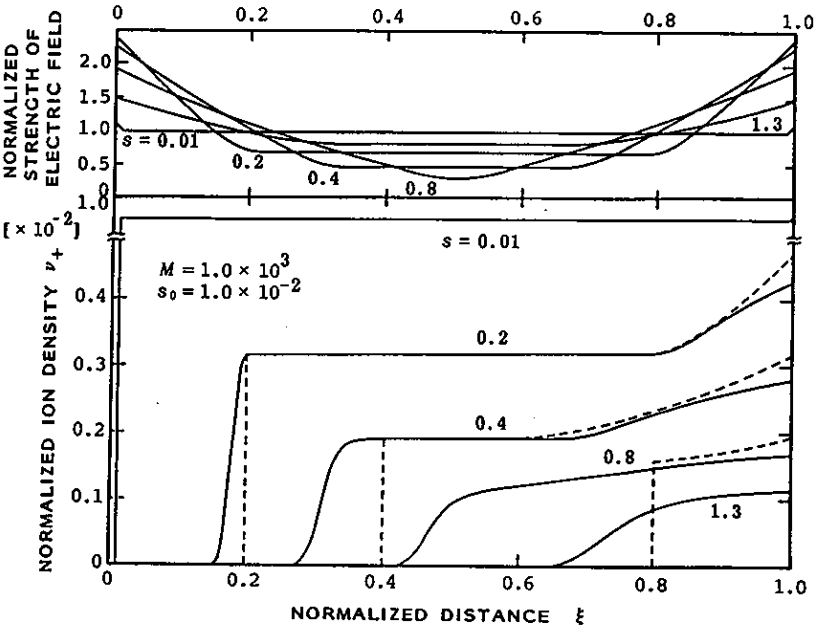

Fig. 2.6. Temporal variation of the spatial distributions of the normalized strength of electric field and the normalized ion density. The distributions in case of the neglect of the space charge effect are shown by broken lines.

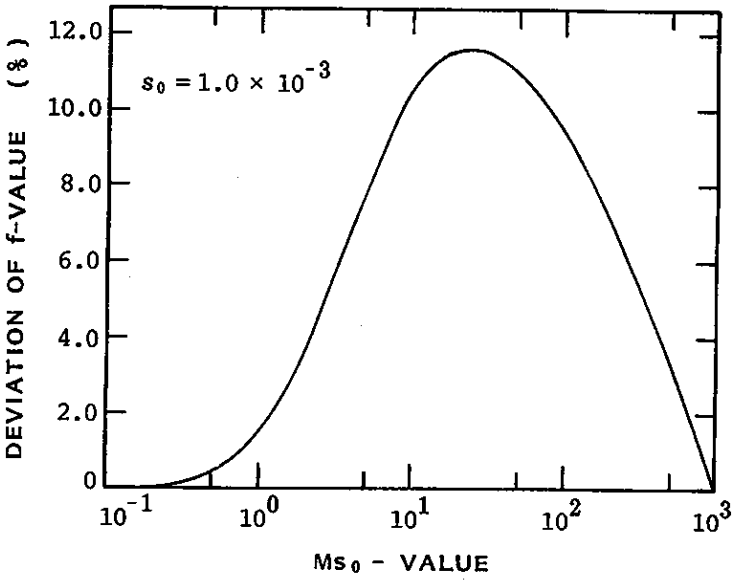

Fig. 2.7. Deviation from the approximate collection efficiency due to the space charge effect. It is shown by per cent as a function of Ms_0-value.

where $M = 1.0 \times 10^3$ and $s_0 = 0.01$. The upper curves show the temporal variations of the spatial distribution of the strength of electric field. Neglecting the effect, the curve would be a horizontal line that $c = 1.0$ independently of the time. The field strength in actual varies rapidly near both positive and negative seathes. In the overlap region, the strength is nearly constant but lower than unity, that is, the ions have a longer stay than expected in the previous calculations. It causes an increase in recombination loss. In Fig. 2.7 is shown the amount of decrease of the f-value as a function of Ms_0-value. It can be said that the space charge effect cannot be neglected especially for an Ms_0-value near 25.0, i.e. for an f-value about 0.2, when the deviation becomes about 12 %.

The pulse shape effect of the third assumptions is to be discussed in Chap. 4 in detail.

2.5. Output current of an ionization chamber

The characteristics of the response of an ionization chamber to pulsed X-rays appears as an output current shape.[22,37] The current density, $j(t)$, is expressed with the solutions of eqs. (2.6), (2.7) and (2.8) by the following general formula:

$$j(t) = eE(k_+ n_+ + k_- n_-) + \varepsilon_0 \frac{\partial E}{\partial t} . \qquad (2.17)$$

Allowing for the neglect of the space charge effect, eq. (2.17) is rewritten with the normalized variables as follows:

$$\zeta(s) = \frac{j(t)}{eq_0 d} = \frac{ed/\tau}{eq_0 d} \int_0^d [\, n_+(x,t) + n_-(x,t)] \frac{dx}{d}$$

$$= \int_0^1 [\, \nu_+(s,\xi) + \nu_-(s,\xi) \,] \, d\xi . \qquad (2.18)$$

On the other hand, the following expression is derived from eq. (2.1):

$$\zeta(s) = \begin{cases} \frac{4}{M}\ln\left(\frac{1+Ms_0 s}{1+Ms_0 s/2}\right) + \frac{2s_0(1-2s)}{1+Ms_0 s}, & 0 \lesssim s \leq 0.5 \\ \frac{4}{M}\ln\left(\frac{1+Ms_0/2}{1+Ms_0 s/2}\right), & 0.5 < s \leq 1.0 \end{cases} \tag{2.19}$$

A relation between the current form and the f-value is made clear by calculating eq. (2.18). Figure 2.8 shows the current density as a function of the normalized time, where the normalized pulse duration is assumed to be 1.0×10^{-6}. An M-value of 0 means no recombination loss, and in this case the waveform of the output current density is rectangular. The shape becomes concave with increasing the M-value, i.e. with decreasing the f-value. The f-value is implicitly shown by a ratio of the area of the current to that for an M-value of 0. It may be possible to describe quantitatively a relation between the current shape and the f-value, for example, by a curvature as a function of the f-value. A quantitative description, however, is very difficult to be applied to actual pulsed X-rays, because one cannot observe experimentally an exact peak current in the case of no recombination loss.

In Fig. 2.8 are also shown the results of calculations of eq. (2.19) by broken lines. As was pointed out in the previous sections, a difference from the exact current becomes distinctive with increasing the M-value. The same conclusion about the application limit of the Boag's formula is derived from the figure. An example of the currents for pulsed X-rays of relatively long duration is shown in Fig. 2.9, which can never be obtained from the Boag's expression. It is expected that the waveform in this case is sensitively affected by the pulse shape of X-rays. The effect on the output current shape is to be discussed in Chap. 4.

It is concluded from above discussions that an output current is

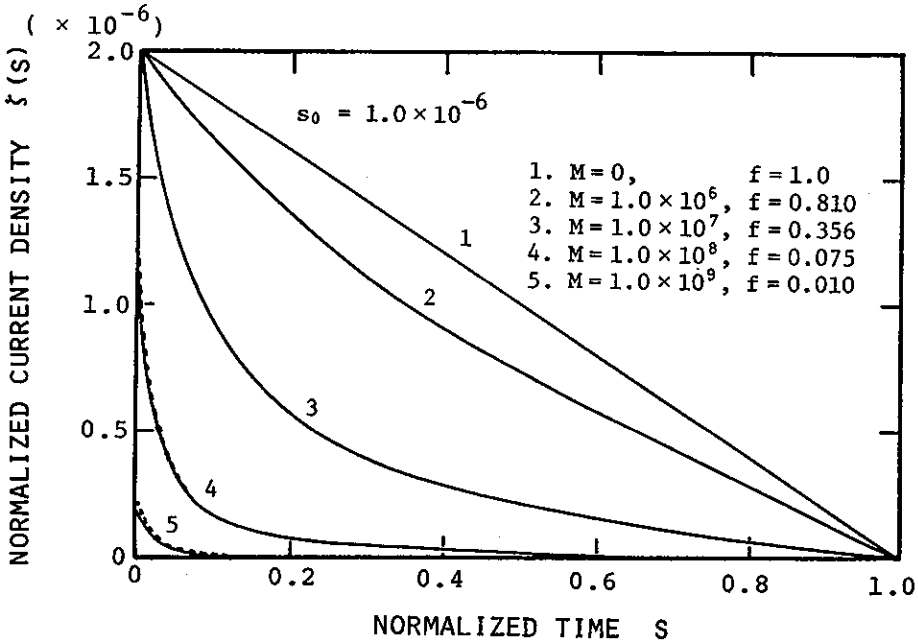

Fig. 2.8. Normalized current density for pulsed X-rays with short duration as a function of the normalized time. The current density calculated with Boag's formula is also shown by a broken line.

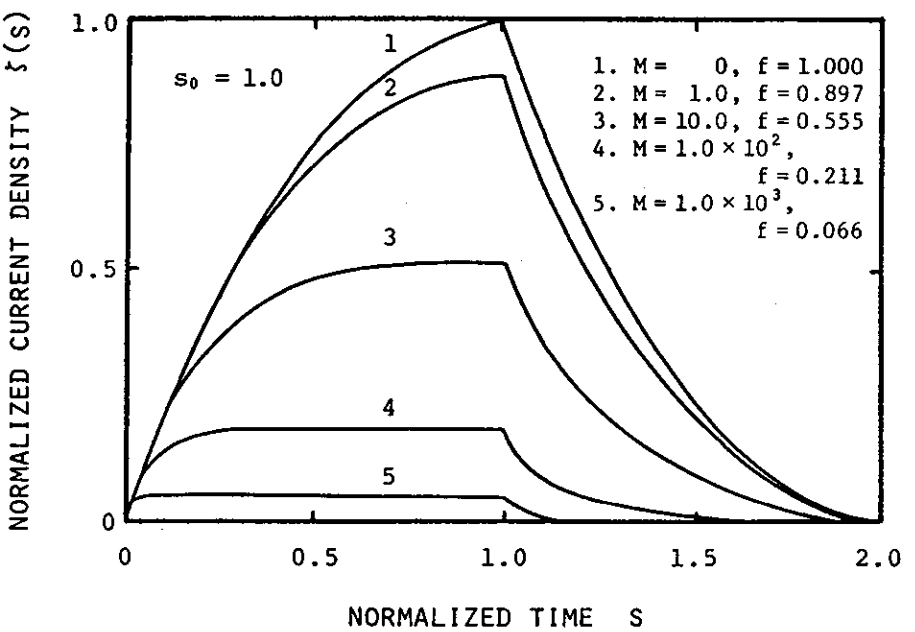

Fig. 2.9. Normalized current density for pulsed X-rays with long duration as a function of the normalized time.

regarded as a measure of the response of an ionization chamber to pulsed X-rays.

2.6. Concluding remarks

An essential problem has been discussed for absolute measurement of the exposure and the absorbed dose with an ionization chamber. The collection efficiency, which is the most important correction factor for pulsed X-rays of high exposure rate, has been numerically obtained. As a result of the calculations, the following were clarified:

(1) A description of the collection efficiency was derived which was valid beyond an application limit of the well-known Boag's formula. It was found that the collection efficiency derived by Boag was limited by the condition that the pulse duration normalized by the ion transit time was shorter than about 1.0×10^{-3} and the collection efficiency was smaller than about 0.3.

(2) The difference in mobilty between positive and negative ions was found to be caused only 6 % error of the collection efficiency for a free-air ionization chamber.

(3) It was found that the space charge effect could not be neglected for an f-value about 0.2, and in this case the deviation became the maximum of about 12 %.

(4) The output current of an ionization chamber was obtained numerically. A correlation between the current shape and the collection efficiency was confirmed.

Appendix 2.A. Numerical calculations of partial differential equations

The differential equation to be solved is written by

$$\frac{d\nu_{\pm}}{ds} = \Lambda - M\nu_{+}\nu_{-} \quad . \tag{2.A.1}$$

Let consider an N×N matrix with respect to the time, s, and the space, x, and draw characteristic lines from each point of the matrix as shown in Fig. 2.A.1. The tangent of the line, $\Delta s/\Delta \xi$, is 1 for ν_{+} and -1 for ν_{-}. Then, eq. (2.A.1) at J-th point of the time is expressed by finite differences as follows:

$$\Delta\nu_{+}(J) = [\ \Lambda(J) - M\nu_{+}(I-1,J-1)\,\nu_{-}(I-1,J-1)\ ]\,\Delta s, \tag{2.A.2}$$

$$\Delta\nu_{-}(J) = [\ \Lambda(J) - M\nu_{+}(I+1,J-1)\,\nu\ (I+1,J-1)\ ]\,\Delta s. \tag{2.A.3}$$

Both intial and boundary conditions are

$$\nu_{+}(I,0) = \nu_{-}(I,0) = 0 \qquad \text{for all } I, \tag{2.A.4}$$

$$\nu_{+}(0,J) = \nu_{-}(N,J) = 0 \qquad \text{for all } J. \tag{2.A.5}$$

The values of ν_{+} and ν_{-} at the first point of the time are calculated eqs. (2.A.2) and (2.A.3) for all points of the space. Next, those at the second point of the time are calculated by substituting the values obtained in the previous step into eqs. (2.A.2) and (2.A.3). The procedure is repeated until J becomes N.

In the case where the mobilities of positive and negative ions are different, the characteristic line of ν_{-} must change from -1 to $-\eta$. Further procedure is the same. In the case where the space charge effect is taken into account, the tangent of the characteristic lines must be varied with the time. The point of intersection of two lines for ν_{+} and ν_{-} will not always lie on a point of integer in the space. Thus, the value of each point must be found by the interpolation method with several values near the point.

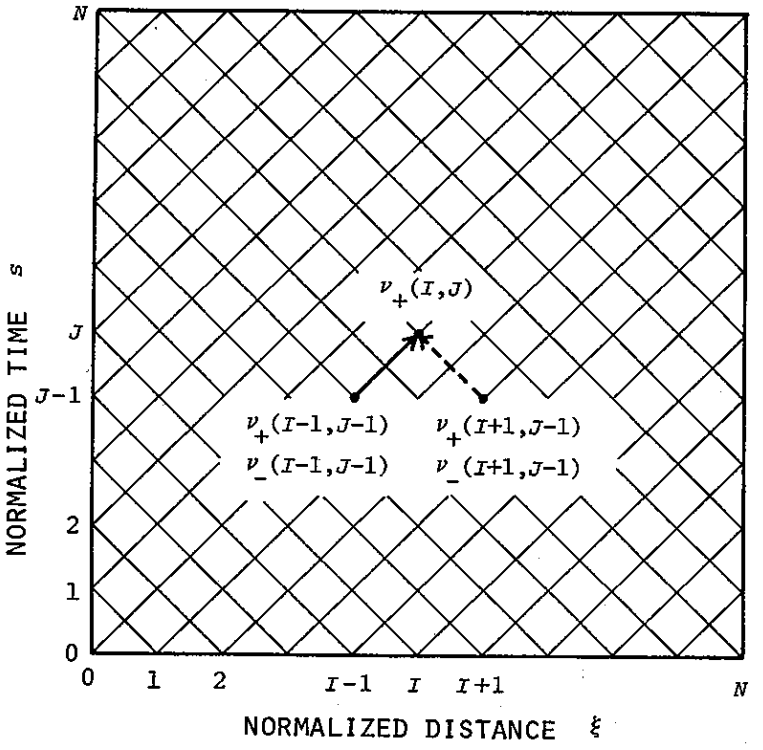

Fig. 2.A.1. Matrix of the normalized time and the normalized distance used in numerical calculations of the partial differential equations.

Appendix 2.B. Formulation of output current of ionization chamber

Allowing for Boag's approximation, the ion density, ν, becomes s_0 at the instant when the X-ray pulse ceases. After the pulse the density in the overlap region, ν_0, decreases with a rate:

$$\frac{d\nu_0}{ds'} = -M\nu_0^2 . \qquad (2.B.1)$$

Hence,

$$\nu_0(s') = s_0/(1 + Ms_0s') . \qquad (2.B.2)$$

The overlap region exists for a half of the ion transit. Thus, the current density is to be derived by dividing the time into two intervals.

(I) $0 \lesssim s \leqq 0.5$

In Fig. 2.B.1 the density distribution of negative ions at a time, s, are illustrated by a solid line and that at a time, $s/2$, by a broken line. The distribution is divided spatially into two: the ions in a region R_1 are experienced in recombination for a time past, and those in the other region R_2 are suffering from recombination. In the region R_1, the density at a point P where $\xi = 0$ is equal to that at a point P' where $\xi = s/2$. Namely,

$$\nu_-(s,0) = \nu_-(s/2, s/2) = \nu_0(s/2). \qquad (2.B.3)$$

In the same way the following relation is found:

$$\nu_-(s, s) = \nu_0(s). \qquad (2.B.4)$$

Hence the total ion density in the region, N_1, is expressed by

$$N_1 = \int_0^s \nu_-(s,\xi)\, d\xi = \int_{s/2}^s \nu_0(s')\, 2ds'$$

$$= \frac{2}{M} \ln\left(\frac{1 + Ms_0s}{1 + Ms_0s/2}\right) . \qquad (2.B.5)$$

On the other hand, the ion density in the region R_2 is $\nu_0(s)$ at any

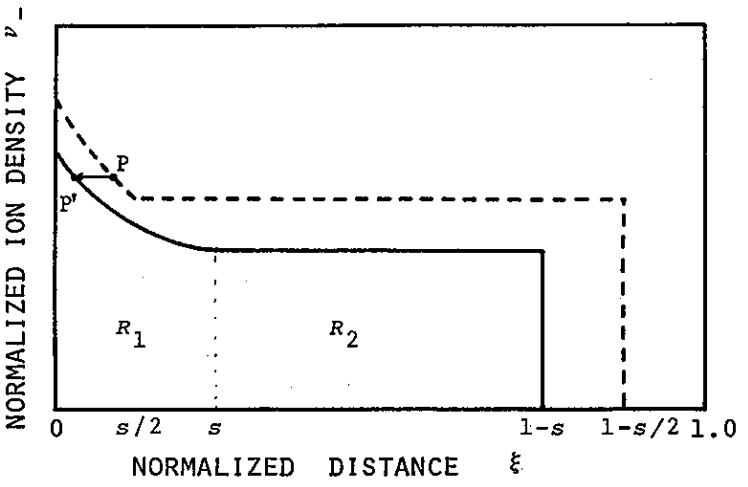

Fig. 2.B.1. Spatial distribution of the normalized density of negative ions at a normalized time between 0 and 0.5.

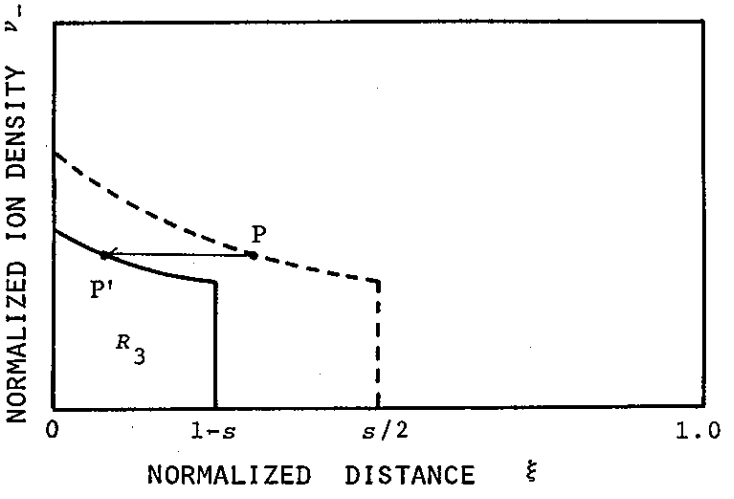

Fig. 2.B.2. Spatial distribution of the normalized density of negative ions at a normalized time between 0.5 and 1.0.

place. The width of the region is explicitly found to be $(1 - 2s)$. Then, the total density, N_2, becomes

$$N_2 = (1 - 2s)\,\nu_0(s) = (1 - 2s)\,s_0/(1 + Ms_0 s). \quad (2.B.6)$$

Accordingly, the normalized current density is expressed as follows:

$$\zeta(s) = 2\int_0^1 \nu_-(s,\xi)\,d\xi = 2(N_1 + N_2)$$

$$= \frac{4}{M}\ln\left(\frac{1 + Ms_0 s}{1 + Ms_0 s/2}\right) + \frac{2s_0(1 - 2s)}{1 + Ms_0 s} \quad (2.B.7)$$

(II) $0.5 < s \lesssim 1.0$

When the time longer than 0.5 elapsed, no recombination would take place. In Fig. 2.B.2 the distribution at a time, s, is illustrated by a solid line and that at a time of 0.5 by a broken line. In the latter distribution, the density of ions existing between ξ and $\xi + d\xi$ is expressed by

$$\nu_-(0.5,\ \xi)\,d\xi = \nu_0(0.25 + \xi/2)\,2ds'. \quad (2.B.8)$$

The latter slides as the time passes, and becomes the former at a time of s. As shown in the figure, the density at a point P is equal to that at a point P'. Namely,

$$\nu_-(s,\xi) = \nu_-(0.5,\ \xi + s - 0.5). \quad (2.B.9)$$

In other words, the distribution at a time of s from a point 0 to $(1 - s)$ is quite equal to that at a time of 0.5 from $(s - 0.5)$ to 0.5. The total ion density, N_3, is written by

$$N_3 = \int_0^{1-s} \nu_-(s,\xi)\,d\xi = \int_0^{1-s} \nu_-(0.5, \xi + s - 0.5)\,d\xi$$

$$= \int_{s-0.5}^{0.5} \nu_-(0.5,\xi)\,d\xi = \int_{s/2}^{0.5} \nu_0(s')\,2ds'. \quad (2.B.10)$$

Accordingly, the current density is expressed as follows:

$$\zeta(s) = 2N_3 = \frac{4}{M}\ln\left(\frac{1 + Ms_0/2}{1 + Ms_0 s/2}\right). \quad (2.B.11)$$

REFERENCES

1) ICRU Report 6 (1954).

2) ICRU Report 19 (1971)

3) Y.Moriuchi, A.Katoh, T.Tanaka, R.Tanaka and N.Tamura: IAEA-SM-222/44 (1978) 1.

4) J.J.Thomson and E.Ratherford: Phil. Mg. 42 (1896) 392.

5) J.J.Thomson: Phil. Mg. 47 (1899) 253.

6) G.Mie: Ann. Physik 13 (1904) 857.

7) J.W.Boag and T.Wilson: Brit. J. Appl. Phys. 3 (1952) 222.

8) J.W.Boag: Brit. J. Radiol. 25 (1952) 649.

9) V.H.Rits and F.H.Attix: Rad. Res. 16 (1962) 401.

10) P.B.Scott and J.R.Greening: Phys. Med. Biol. 8 (1963) 1.

11) J.R.Greening: Phys. Med. Biol. 9 (1964) 143.

12) W.Armstrong and P.A.Tate: Phys. Med. Biol. 10 (1965) 229.

13) Y.Moriuchi: Oyo Butsuri 34 (1965) 6, [in Japanese].

14) Y.Moriuchi: Oyo Butsuri 35 (1966) 2, [in Japanese].

15) E,A.Sprinkle and P.A.Tate: Phys. Med. Biol. 11 (1966) 31.

16) N.T.Niatel: Phys. Med. Biol. 12 (1967) 555.

17) J.W.Boag: Int. J. Rad, Phys. Chem. 1 (1969) 267.

18) R.Rosen and E.P.George: Phys. Med. Biol. 20 (1975) 990.

19) J.Bohm: Phys. Med. Biol. 21 (1976) 754.

20) F.Hajnal and J.Pane: IEEE Trans. Nucl. Sci. NS-25 (1978) 550.

21) J.W.Boag: Brit. J. Radiol. 23 (1950) 601.

22) P.M.Livingstone: J. Appl. Phys. 35 (1964) 2341.

23) R.E.Ellis and L.R.Read: Phys. Med. Biol. 14 (1969) 293.

24) R.E.Ellis and L.R.Read: Phys. Med. Biol. 14 (1969) 411.

25) J.W.Boag: *Radiation Dosimetry, vol. II*, eds. F.H.Attix and W.C.

Roesch (Acedemic, New York, 1966) Chap.1.

26) T.Yamamoto: *Proc. 1st KEK symp. Radiation Dosimetry, Tsukuba, 1978,* KEK-78-18 R (1978) 110.

27) P.A.Tata: Phys. Med. Biol. 11 (1966) 521.

28) T.Yamamoto, K.Oda, H.Kobayashi and M.Kawanishi: *Proc. 2nd KEK Symp. Radiation Dosimetry, Tsukuba, 1978,* KEK-79-19 R (1979) 129.

29) H.Kobayashi: Master Thesis (Osaka University, 1980).

30) M.Takebe: Jpn. J. Appl. Phys. 13 (1974) 207.

31) N.E.Bradbury: Phys. Rev. 40 (1932) 508.

32) G.Sinnot: Phys. Rev. 136 (1964) 370.

33) R.E.Voshall, J.L.Pack and A.V.Phelps: J. Chem. Phys. 43 (1965) 1990.

34) G.Sinnot, D.E.Golden and R.N.Varney: Phys. Rev. 170 (1968) 272.

35) A.C.Lapsley: Rev. Sci. Instrum. 24 (1953) 602.

36) J.A.Morrison and D.E.Edelson: J. Appl. Phys. 33 (1962) 1714.

37) H.Dinter and K.Tesch: Nucl. Instrum. & Methods 120 (1974) 113.

CHAPTER 3. DOSIMETRY OF PULSED X-RAYS OF HIGH EXPOSURE RATE*

—— ELECTRON LINEAR ACCELERATOR (I) ——

3.1. Introduction

The exposure rate of X-rays in the vicinity of the beam target of high-energy particle accelerators is extremely high. In such an X-ray field, almost all detectors will suffer the high-dose-rate effects.[1,2] One of the effects on an ionization chamber appears as the underestimate of the number of ion pairs due mainly to the recombination. It is the most important problem in the dosimetry of high-exposure-rate X-rays to determine the collection efficiency, f-value, which is a correction factor for the effect. The problem becomes more serious for single burst X-rays.

In the previous chapter, saturation characteristics of a parallel-plate ionization chamber was clarified by numerical calculations of the f-value. The dependence of the f-value was also obtained quantitatively upon various parameters, i.e. the exposure rate, the pulse duration and the chamber constants. In this chapter, a method based on the calculated results is proposed for determining the f-value in an unknown pulsed X-ray field. The method is practically applied to a field generated by an electron linear accelerator installed at the Institute of Scientific and Industrial Research, Osaka University. The saturation curves and output currents of an ionization chamber are also observed

---

The main part of this work is published in J. Nucl. Sci. Technol. 19 (1982) 89 *and* Nucl. Instrum. & Methods 196 (1982) 469.

in the field. It is the purpose to establish the dosimetry of pulsed X-rays of high exposure rate with an ionization chamber.

3.2. Experimental determination of collection efficiency in an unknown pulsed X-ray field

3.2.1. Normalized saturation curve

The ionic charge generated per X-ray pulse, Q_0, cannot be collected without recombination loss. The collected charge, Q, is then f-times amount of the generated charge. Namely,

$$Q = f \cdot Q_0 . \tag{3.1}$$

As was pointed out in the previous chapter, the f-value depends on not only the characteristic parameters of the X-ray field (ion production rate, q_0, and the pulse duration, τ_0) but also the chamber constants (the recombination coefficient, α, the ion mobility, k, the gap distance between the electrodes, d, and the applied voltage, V). The calculated results are shown in Fig. 3.1 in a different form from the previous. Normalized variables are defined as follows:

$$s_0 = \tau_0 / \tau , \tag{3.2}$$

$$Ms_0 = (\alpha\tau) \cdot (q_0\tau_0), \tag{3.3}$$

where τ is the transit time of ions and equal to kV/d^2. The broken line represents the f-value calculated with Boag's formula.[3,4]

The Ms_0-dependence of the f-value implies that the f-value of an ionization chamber varies by adjusting the chamber constants even at a fixed place in a X-ray field. Among the constants, applied voltage is most convenient for variation. Thus, the f-value is regarded as a function only of the applied voltage provided that the remaining parameters are fixed. Namely,

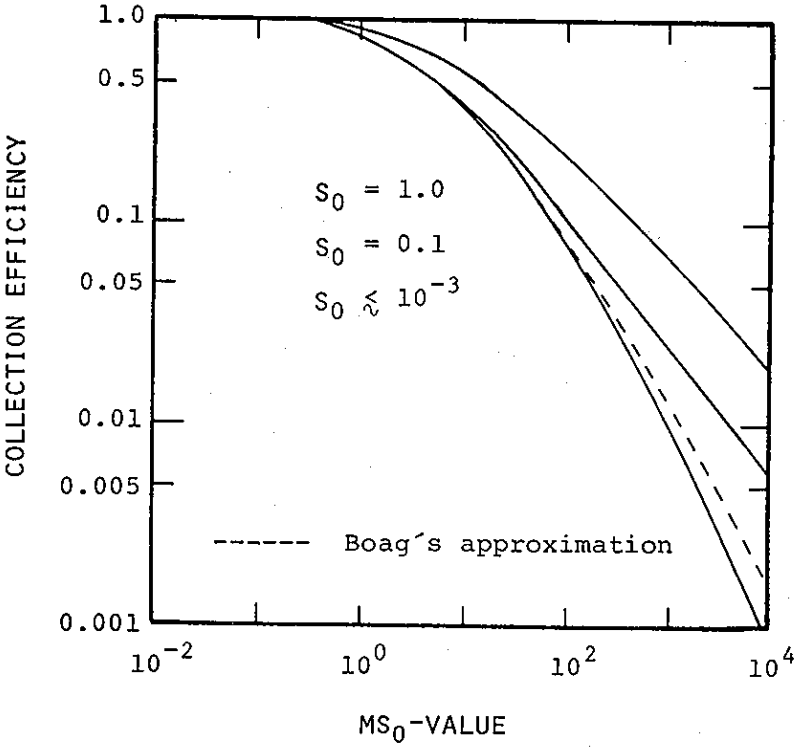

Fig. 3.1. Collection efficiency as a function of Ms_0-value, which is proportional to the total exposure per pulse. The calculated results of Fig. 2.3 are shown in a different form.

$$f = f(V). \tag{3.5}$$

Before a method for determining the f-value is proposed, it is shown that a so-called saturation curve can be obtained theoretically by use of the f-value as a function of the applied voltage.

Assuming that both s_0- and Ms_0-values at a voltage V_r, $(s_0)_r$ and $(Ms_0)_r$, are given, then the values at a different voltage, V_i, are easily calculated by the following relation:

$$(s_0)_i = (s_0)_r \cdot V_i / V_r , \tag{3.6}$$

$$(Ms_0)_i = (Ms_0)_r \cdot V_r / V_i , \tag{3.7}$$

where the suffix represents i-th applied voltage. A pair of s_0- and Ms_0-values gives an f-value, $f(V_i)$, respectively. In other words, the f-value at any applied voltage can be estimated if only the f-value at a reference applied voltage is given. Plotting the f-value against the applied voltage, a so-called saturation curve is uniquely drawn. Figure 3.2 shows typical curves for several values of $f(V_r)$. The reciprocal of the relative Ms_0-value on the abscissa is equal to the ratio of the applied voltage, as is clear from eq. (3.7). In order to generalize the saturation curve, the f-values on the ordinate of Fig. 3.2 are normalized by the value of $f(V_r)$. The normalized f-value is equal to the ratio of the collected charge, since

$$\begin{aligned} Q(V_i)/Q(V_r) &= [f(V_i)\cdot Q_0]/[f(V_r)\cdot Q_0] \\ &= f(V_i)/f(V_r) \end{aligned} \tag{3.8}$$

The normalized saturation curves are shown in Fig. 3.3. It is seen that the radius of the curvature becomes shorter with decreasing the f-value. This result implies that the f-value may be determined by finding a theoretical curve fit well to a measured one.

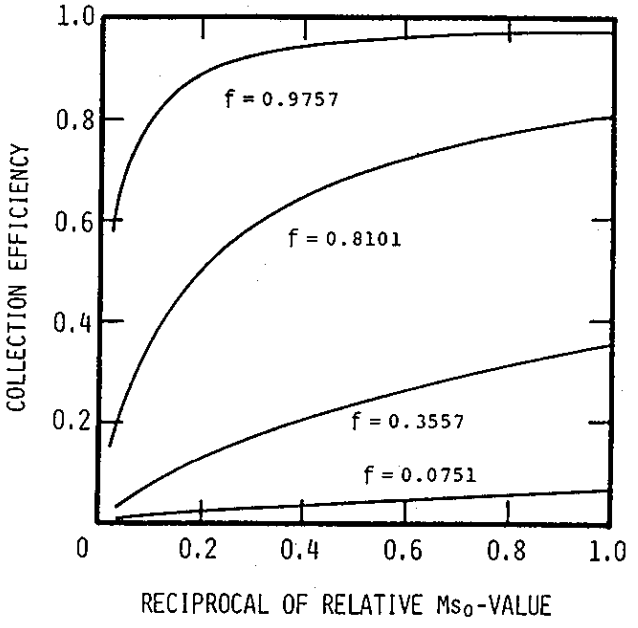

Fig. 3.2. Saturation curves for several f-values at a reference applied voltage. The abscissa is equal to the ratio of the applied voltage.

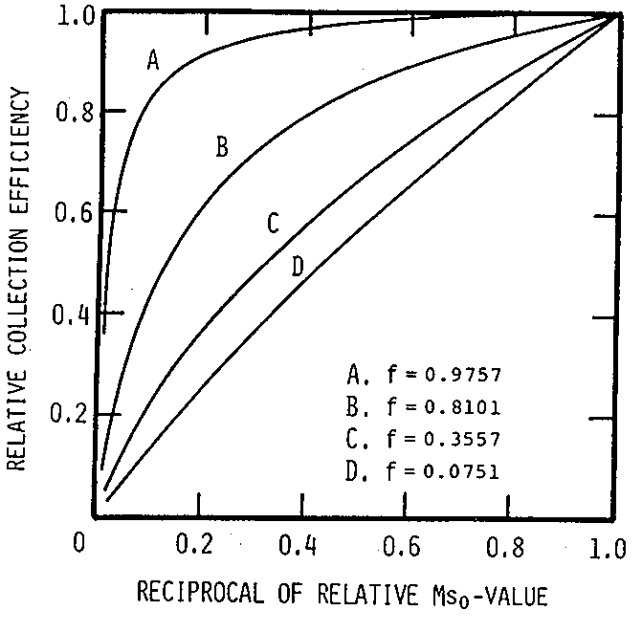

Fig. 3.3. Normalized saturation curves. The ordinate is equal to the ratio of the collected charge. A correlation between the f-values and the curvature is confirmed.

3.2.2. Determination of collection efficiency

It is assumed at first that the pulse duration of the X-ray field is measured by some detector. It will not be so difficult to measure the duration with a scintillator or streak camera. Then, the ionic charges are collected with an ionization chamber by varying the applied voltage, if the X-ray pulse is reproducibly repeated. The voltages and the collected charges are normalized by those at a reference voltage defined arbitrary, and then several points is plotted on the graph shown in Fig. 3.3. The co-ordinates of i-th point is $(V_i/V_r,\ f(V_i)/f(V_r))$. A theoretical saturation curve for a true f-value must pass all the points. In most cases, however, such a curve cannot be found because all the points have an error due to a fluctuation of the X-ray field or a poor accuracy of measuring instruments. Thus, we find a best fit of theoretical curves to all the experimental values. It is noticeable in this procedure that the best fit curve does not necessarily pass a point of (1.0, 1.0) because the collected charge at a reference voltage also have an experimental error. Hence, the computation of the fitting by, for example, the least square method must be performed by altering the relative f-value at a reference voltage as well as the absolute value of $f(V_r)$.

Next, we consider a special case that only two points are given on the normalized saturation curve. The co-ordinates are (1.0, 1.0) and $(V_i/V_r,\ f(V_i)/f(V_r))$. A theoretical curve for a true f-value should pass these points under the condition of no experimental error. Namely, the true f-value corresponds uniquely to the ratio of collected charge, $f(V_i)/f(V_r)$. Figure 3.4 shows a dependence of the f-value on the value of $f(V_i)/f(V_r)$, where the ratio of the applied voltage is

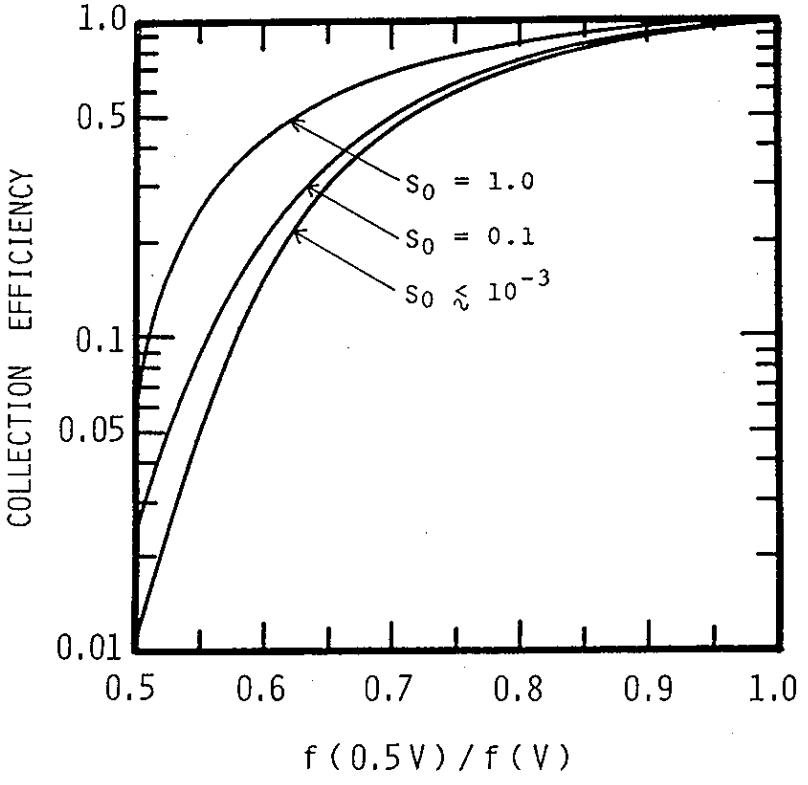

Fig. 3.4. Relation between a true f-value and the ratio of f-values for two different applied voltages. The parameter, s_0, represents the pulse duration normalized by the ion transit time of ionization chamber. Combining the figure with an abreast-type ionization chamber, an f-value can be determined for single pulse of X-rays.

assumed to be 0.5 as an example.

The X-ray pulse generated by apparatus for fusion experiments can hardly be repeated. In such a field, the measurement of collected charges must be performed from a single waveform of output currents of an ionization chamber. The author designed and constructed an abreast-type chamber for the simultaneous measurement of ionization currents at two different voltages. It has two active volumes and two pairs of the electrodes, and thereby two different currents can be observed with a dual-beam oscilloscope. The ionic charges are obtained by integrating the currents, and the s_0-value is also estimated approximately from the waveforms.

The method combining an abreast-type ionization chamber with the calculated results shown in Fig. 3.4 is also applicable to a repetitively pulsed X-ray field. However, the experimental errors in measuring the charges will directly cause a deviation from the true f-value. From a standpoint of accuracy, the generalized method is preferable because the errors are averaged statistically owing to the fitting.

In summery, the f-value in a pulsed X-ray field is evaluated in the following procedure:

(1) The pulse duration is measured with some detector.

(2) Ionization currents are observed for two or more applied voltages. For single-burst X-rays an abreast-type ionization chamber is required.

(3) The ratio of collected charge is plotted against the ratio of applied voltage.

(4) The f-value is obtained by fitting a theoretical saturation curve

to the measured points in the case of three or more points, and by finding a curve passing the points in the case of two.

3.3. Experimental apparatus

Experiments on the response of a parallel-plate ionization chamber to pulsed X-rays of high exposure rate have been carried out with the 35 MeV electron linear accelerator installed at the Institute of Scientific and Industrial Research, Osaka University.[5,6] The apparatus and experimental set-up are shown in Fig. 3.5 and Photo 3.1. A marked characteristics of the machine lies in that it can deliver singly bunched electrons more than 15 nC with a pulse duration of less than 20 ps in "single" mode. An electron beam with peak current of 10 A and duration of 10 ns can be obtained under the operating condition of "transient" mode, and that of 600 mA and 1 μs in "steady" mode. When such pulsed electrons from the machine bombard a tungsten target of 20 mm in diameter and 5 mm in thickness, bremsstrahlung X-rays are emitted there. Owing to a relatively high current of pulsed electrons, the exposure rate is very high enough for direct measurement of the output current shape of an ionization chamber with an oscilloscope.

The duration of pulsed X-rays in this experiment is adjustable in a region between 50 ps and 1.5 μs. The exposure rate of the X-ray field is variable with the current of electron beam or the distance between a target and an ionization chamber. The beam energy is fixed at 22 MeV in the experiment. A repetition rate of X-ray pulsed is adjusted to be constant of 10 pps so that ion currents of the ionization chamber may not be duplicated.

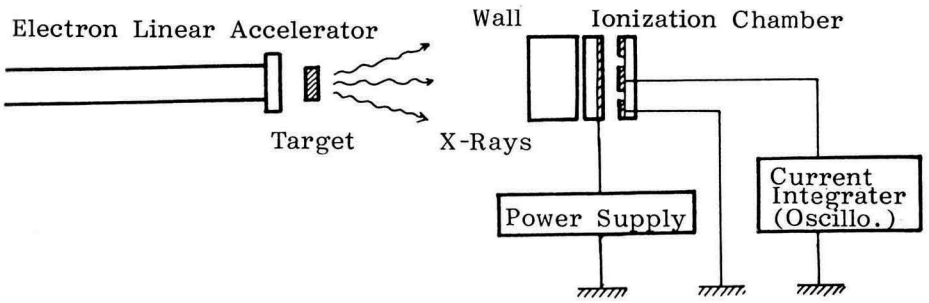

Fig. 3.5. Schematic diagram of experimental apparatus and set-up. An extremely high exposure rate higher than 10^{10} R s^{-1} can be attained.

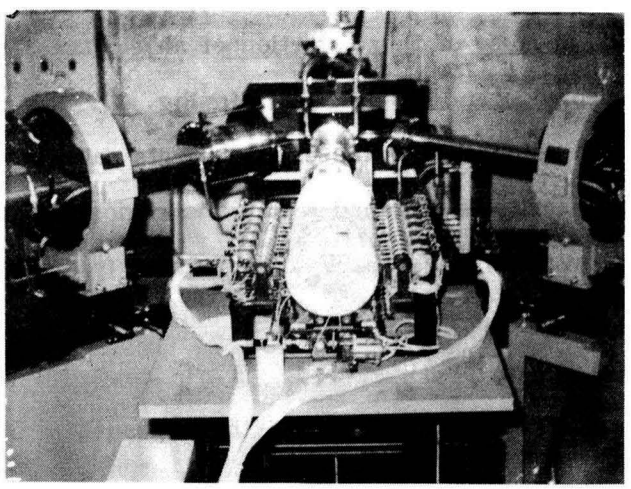

Photo 3.1. Photorgaph of the experimental apparatus.

An abreast-type ionization chamber is designed for determination of the f-value in a single-burst X-ray field as shown in Fig. 3.6. The chamber wall is made of polyethylene which is approximately equivalent to air. As shown in Fig. 3.6 and Photo 3.2, two active volumes are closely aligned in parallel and two different voltages can be applied to each pair of electrodes. Thus, two different ionization currents can be observed simultaneously with a dual-beam oscilloscope. Photo 3.3 shows an example of the output current shape of the ionization chamber exposed to pulsed X-rays. The difference in the applied voltage appears in the photograph as a difference in the ion transit time and the curvature of the current shape.

As a preliminary experiment, an active volume of the chamber is calibrated in ^{60}Co γ-ray field. In general, an active volume is somewhat larger than the product of the area of collecting electrode and the gap distance because of the distortion of an electric field between the collecting electrode and guard ring. In Fig. 3.7 is shown the ionization current as a function of the exposure rate calibrated beforehand. A good linearity is obtained within the region shown in the figure. Then, the active volume, V_a, is obtained from the relation that

$$I_i = 3.3 \times 10^{-10} X / V_a \ , \qquad (3.9)$$

where I_i is the saturation current and X the exposure rate.

3.4. Experimental results and discussions

3.4.1. Output currents

It is necessary to acertain the ion transit time of the ionization chamber, which is an important parameter for the method for

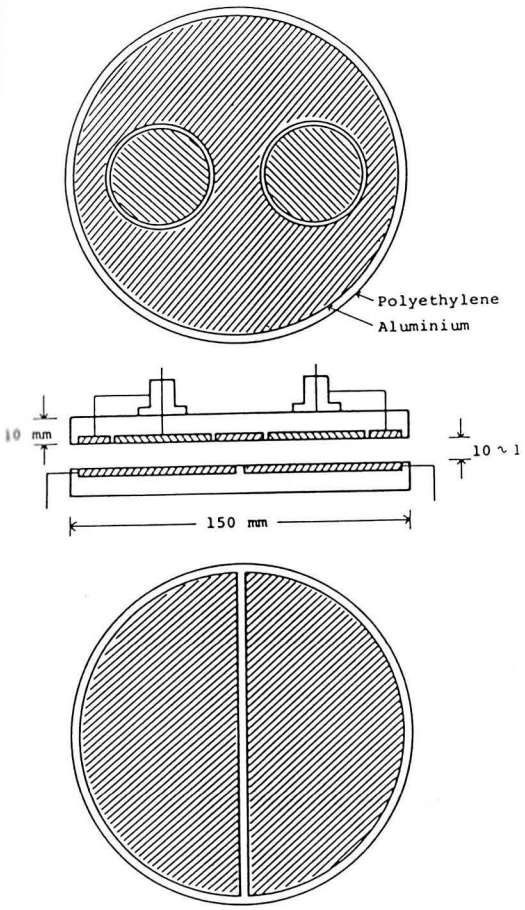

Fig. 3.6. Abreast-type ionization chamber. Two active volumes are closely aligned in parallel and different voltages can be applied to each pair of electrodes. A hatched part is made of aluminium, and the rest is made of polyethylene except connectors.

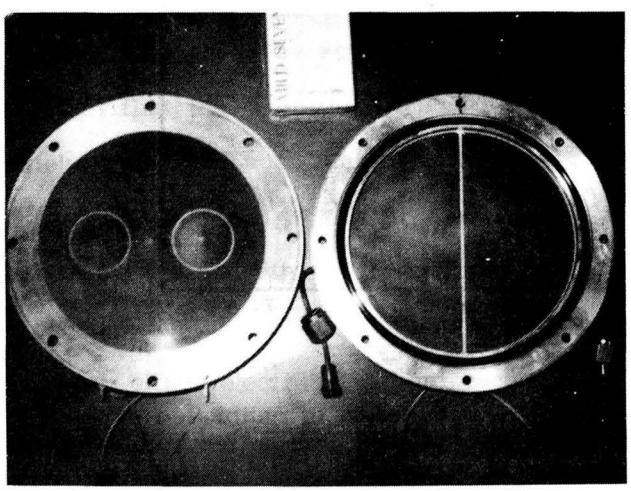

Photo 3.2. An abreast-type ionization chamber.

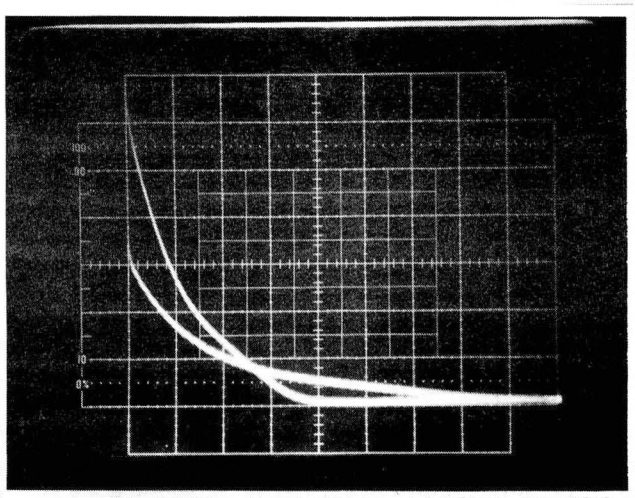

Photo 3.3. An example of the output currents of the abreast-type ionization chamber observed with a dual-beam oscilloscope. The signal of the longer tail corresponds to an applied voltage of 500 V and the other to 1000 V. Electron energy: 22 MeV, electron peak current: 8 A, pulse duration: 10 ns, wall thickness: 56 mm, distance from W-target: 65 cm. Abscissa: 0.2 ms/div., ordinate: 1.5 μA/div.

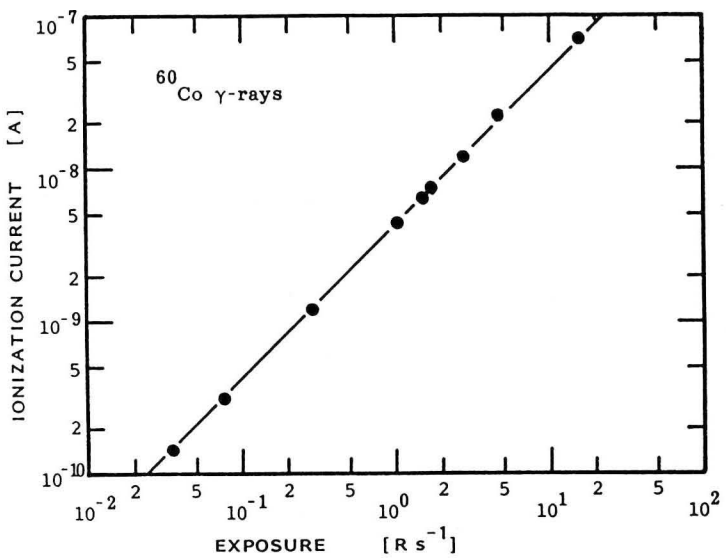

Fig. 3.7. An ionization current as a function of calibrated exposure rate, which is measured in ^{60}Co γ-ray field. The active volume of the ionization chamber is found to be 12.7 cm^3.

determining the f-value stated in the previous section. The ionization currents was observed under the condition of the pulse duration of 10 ns, the gap distance of 10 mm or 15 mm, and the applied voltage between 100 and 1000 V. The traces of waveforms on the oscilloscope are shown in Fig. 3.8 for several applied voltages. As the time constant of detecting circuit is adjusted to be less than 10 μs, the figure represents exact ion currents. Furthermore, the build-up stage of the ionic currents cannot be found because of so short duration of 10 ns. It is seen in the figure that the transit time becomes shorter with increasing the applied voltage. In Fig. 3.9 the ion transit time is plotted against the applied voltage in a full-log scale. It is experimentally confirmed that the ion transit time is inversely proportional to the applied voltage, i.e. the following relation is correct:

$$\tau = d/kE = d^2/kV \ , \qquad (3.10)$$

where τ is the transit time, d the gap distance between the electrodes, k the ion mobility, E the strength of an electric field, and V the applied voltage. The relation and the experimental result shown in Fig. 3.9 give an ion mobility of 1.34 $cm^2 s^{-1} V^{-1}$, which is reasonable value comparing with those by several authors.[7-10] Figure 3.8 implies another fact that the mobilities of positive and negative ions are approximately equal. If not, the current shape could be divided into distinctive three parts. In the first part, both ions drift in opposit directions by the collecting field and the recombination takes place in the overlap region. The second part would continue till all the faster ions reach either electrode without recombination. In the last part only the slower ions are drawn to the opposit electrode. However, only two parts exist in Fig. 3.8. The result means that the assumption of

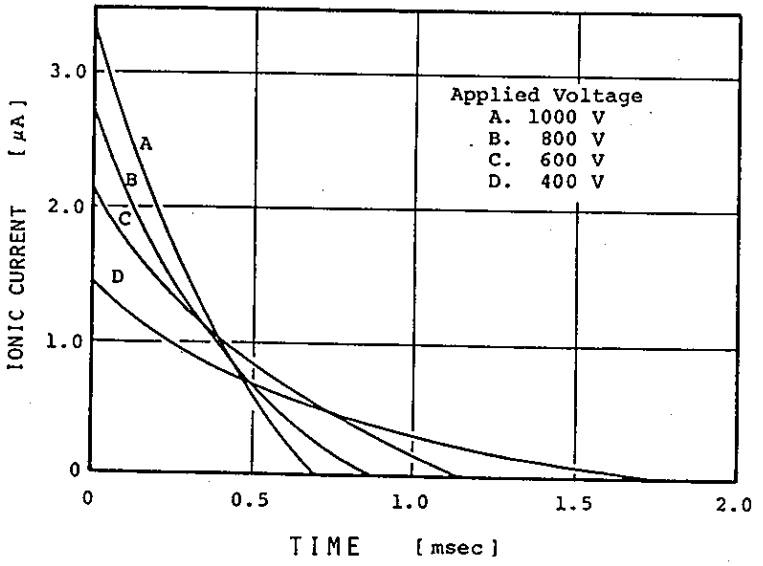

Fig. 3.8. The traces of waveforms of the output currents for several applied voltages. The gap distance between the electrodes is fixed to be 10 mm. Electron energy: 22 MeV, electron peak current: 7 A, pulse duration: 10 ns, wall thickness: 56 mm, distance from W-target: 100 cm.

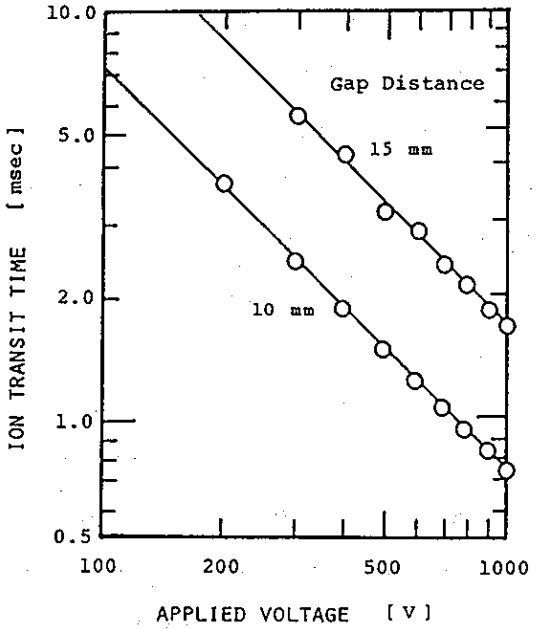

Fig. 3.9. The ion transit time is plotted against the applied voltage for two gap distances. Inverse proportionality gives a constant ion mobility of 1.34 $cm^2 s^{-1} V^{-1}$.

the equality in mobility is satisfactory in this experiment, i.e. the mobility effect stated in the previous chapter is negligible.

Next, the ion currents were observed by varying the distance between the target and the ionization chamber in order to investigate the dependence on the total exposure per pulse. Photograph 3.4 shows an example of the results under a fixed condition of the linear accelerator and the chamber constants. Namely, the energy of electrons is 22 MeV, the peak current 8 A, the pulse duration 10 ns, the gap distance of the ionization chamber 10 mm, the wall thickness 10 mm, and the applied voltage 1000 V. The sweep rate in each photograph is 0.2 ms per division, but the scale of the currents is not unified. In Fig. 3.10 are shown the ionic currents by normalizing the peak current to unity for several distances from the W-target. The time scale is also normalized by the ion transit time of 0.746 ms. Without recombination, the current shape would be triangular. It can be clearly seen that the shape changes a triangle to a concave shape with increasing the exposure rate. Figure 3.11 shows theoretical current shapes calculated under the condition of an s_0-value of 1.34×10^{-5} and M-values of 3.35×10^4, 1.00×10^5, 2.00×10^5 and 8.08×10^5, respectively. There is found a good agreement between the results shown in Figs. 3.10 and 3.11. It implies that a some assumptions made in calculations would be valid in this case.

A merit of measuring the output current shape is that the f-value can be roughly estimated from the observed shape. In the case that the exposure rate of the X-ray field is not so high and the pulse duration is sufficiently short, the ratio of the area under the observed waveform to that under the triangular correspons approximately to

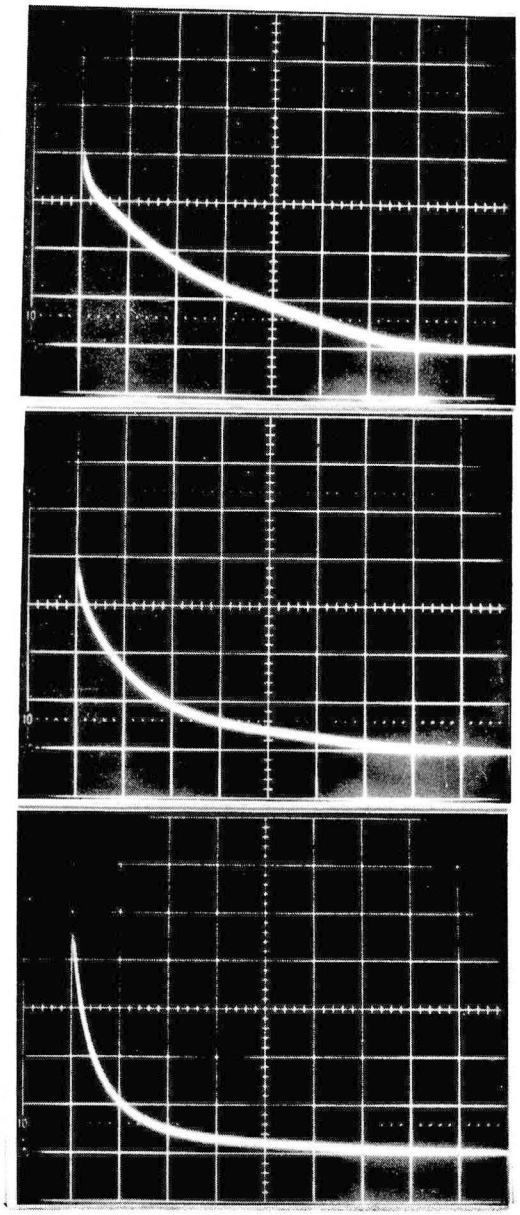

(a) D = 87 cm
f = 0.832
0.1 ms/div.
1.5 μA/div.

(b) D = 38 cm
f = 0.566
0.1 ms/div.
6.0 μA/div.

(c) D = 8.2 cm
f = 0.479
0.1 ms/div.
15.0 μA/div.

Photo 3.4. The ionic currents for three distances between W-target and chamber. (a) 87 cm, (b) 38 cm and (c) 8.2 cm. Electron energy: 22 MeV, electron peak current: 8 A, pulse duration: 10 ns, wall thickness: 56 mm.

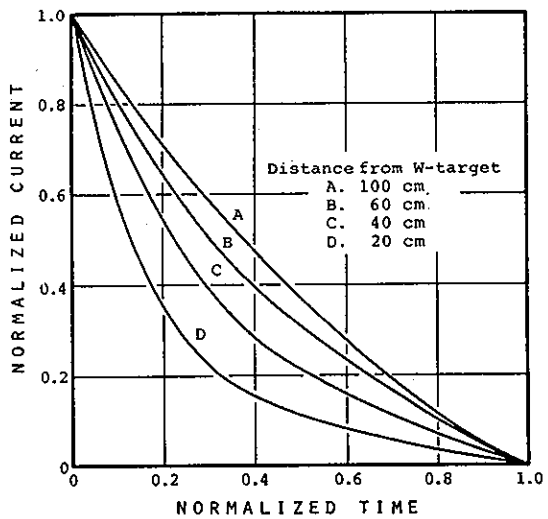

Fig. 3.10. The ionic currents normalized by the peak current for several distances from W-target. The time scale is also normalized by the ion transit time of 0.746 ms. The shape changes from a triangle to a concave shape with increasing the exposure rate. Electron energy: 22 MeV, electron peak current: 7 A, pulse duration: 10 ns, wall thickness: 56 mm, applied voltage: 1000 V.

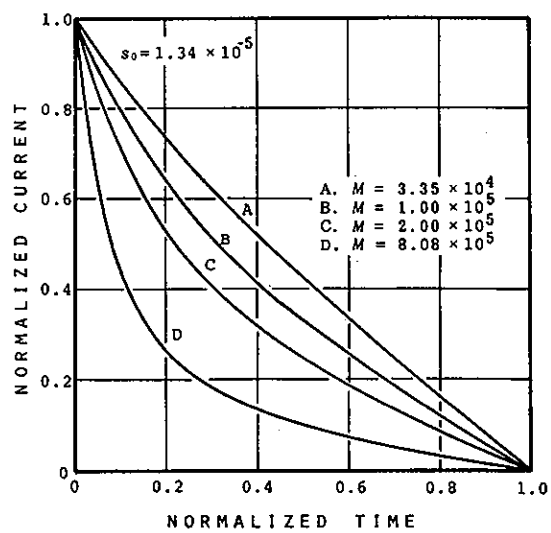

Fig. 3.11. Theoretical currents calculated under the same condition as in Fig. 3.10, i.e. s_0-value: 1.34×10^{-5}, M-values: 3.35×10^4, 1.00×10^5, 2.00×10^5 and 8.08×10^5, respectively.

the f-value. In a strict sense, the observed peak current is less than that without recombination loss, since some of the generated ions disappear through recombination in the build-up stage. The phenomena are often found in the X-ray fields of extremely high exposure rate or of relatively long duration.

3.4.2. Depth-dose curves

It is one of purposes of the X-ray dosimetry to evaluate the exposure of the field. The quantity is defined by ICRU[11,12] as follows: *Exposure of X- or γ-radiations at acertain place is a measure of the radiation that is based upon its ability to produce ionization.* The unit of the exposure is roentgen defined as follows: *The roentgen shall be the quantity of X or γ radiation such that the associated corpuscular emission per 0.001293 gram of air produced, in air, ions carrying 1 e.s.u. of quality of electricity of either sign.* According to the definition, a special attention must be paid to the ionization only by electrons produced at a point of interest, wherever the ionization takes place. It is, in actual, very difficult to separate the ionization from that by electrons produced at different points. Under a certain circumstance, however, one can directly measure the charge equivalent to that by electrons produced at a point of interest. It occurs when the energy spectrum of electrons leaving a small volume is equal to that of electrons entering into the volume. It is called a *charged particle equilibrium* (CPE) condition.

In order to attain experimentally the CPE condition, one adjust the thickness of the wall of an ionization chamber, which is, in most cases, of the order of the average range of secondary electrons. For

such high-energy X-rays as are measured in the present experiments, fundamental problems still remain about the definition and the measurement of the exposure. The kinetic energy of secondary electrons is spent mainly in radiative interactions (in generating bremsstrahlung X-rays) rather than in collisional interactions (in generating ion pairs). In this case, the range of the secondary electrons becomes comparable to the mean attenuation length of the primary X-rays. Accordingly, one must correct for attenuation of the X-rays in the chamber wall for the CPE condition. A solution for the problem has been proposed by Attix.[13] (Appendix 3.A) However, there still remains the difficulty in determining the CPE condition uniquely for X-rays distributed in wide energy region. For the present experiments, the ionic charge generated at a certain wall thickness is regarded as a measure of the field strength.

The ionic charges were measured as a function of the wall thickness at a fixed position of the chamber and applied voltage. The experimental apparatus and the controller for setting the wall are shown in Photos 3.5 and 3.6. In Fig. 3.12 is shown an example of so-called depth-dose curves in the case of the peak current of the linear accelerator of 9 A, the pulse duration of 10 ns, the distance between the W-target and the chamber of 40 cm. Both the ionic charge measured at an applied voltage of 1000 V and that corrected by the f-value are shown by dots and circles, respectively. Less charge is observed near the surface because of the non-CPE condition. The charge increases with the thickness and reaches the maximum between 30 and 40 mm of polyethylene thickness. It decreases gradually at a deeper position in the so-called *transient CPE region* because mainly of the attenuation of the

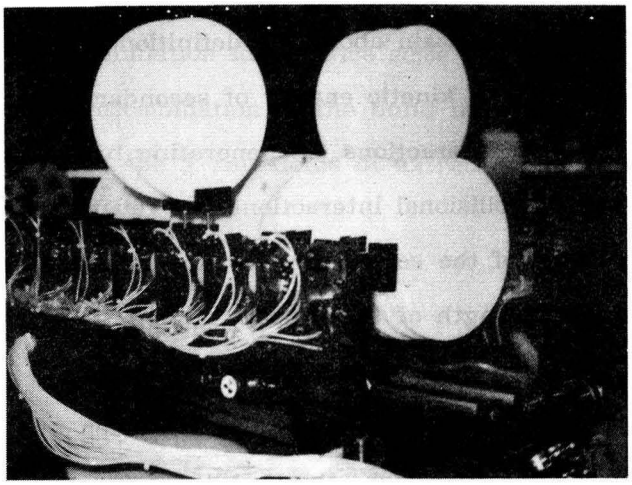

Photo 3.5. Photograph of the ionization chamber. The wall thickness is adjusted by varying the number of polyethylene disks in front of the ionization chamber.

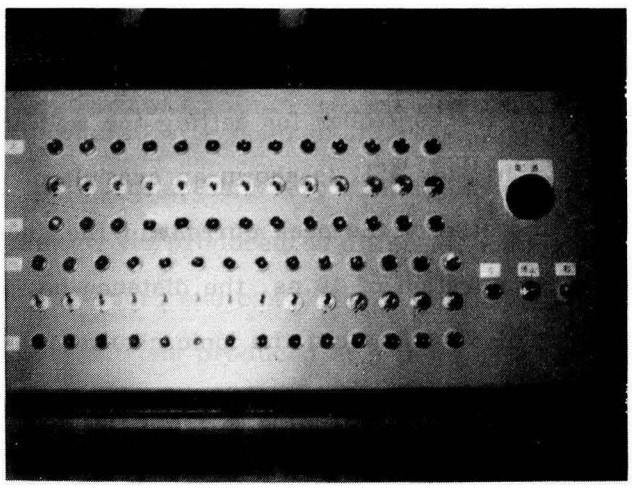

Photo 3.6. Photographic view of the remote controller for changing of the wall thickness.

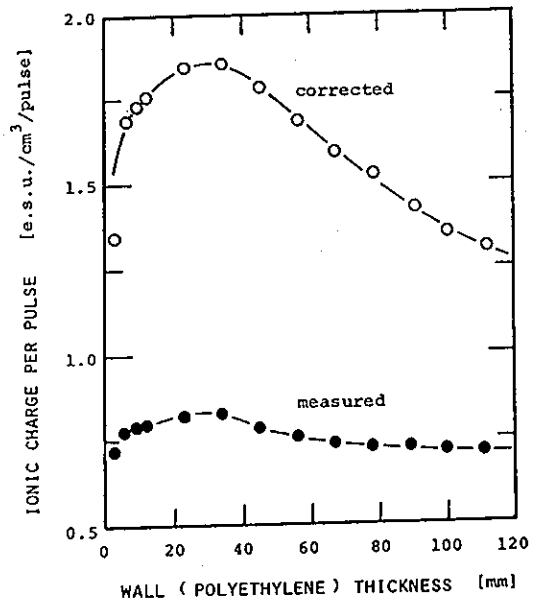

Fig. 3.12. Dependence of the ionic charge density on the wall thickness. Both the ionic charge measured at an applied voltage of 1000 V and that corrected by the f-value are shown by dots and circles, respectively. Electron energy: 22 MeV, electron peak current: 9 A, pulse duration: 10 ns, distance from W-target: 40 cm.

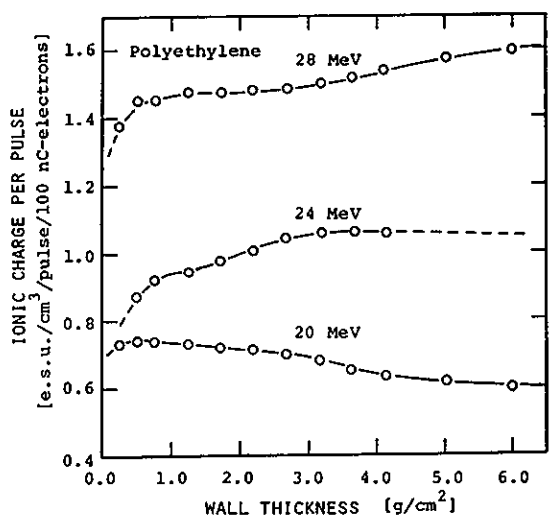

Fig. 3.13. Depth-dose curves for three electron energies of 20, 24 and 28 MeV. Pulse duration: 10 ns, distance from W-target: 52.7 cm, wall: polyethylene.

primary X-rays.

Figure 3.13 shows the depth-dose curves for several electron energies of the linear accelerator. The ionic charge density per an incident electron is plotted against the wall thickness. It is clearly seen that the thickness of the peak shifts to thicker position as the electron energy becomes high, i.e. as the average energy of X-rays becomes high. At an energy higher than 26 MeV another peak can be observed near the surface. It is attributed to neutrons produced by photo-nuclear reactions. In such a case the field should be regarded as a mixed one consisting of neutrons and X-rays rather than an X-ray one. The dosimetry of the mixed radiation field is discussed in Chap. 5.

3.4.3. Evaluation of f-value and ionic charge density

The ionic charge has been measured by varying the chamber constants under various operating conditions of the electron linear accelerator. Three typical saturation curves are shown in Fig. 3.14, where the collected charges normalized by that at a reference voltage of 1000 V are plotted against the relative value of the applied voltage. The ordinate and abscissa are equal to those of Fig. 3.3 as stated in the previous section. In the figure are also shown the respective best fits of the theoretical saturation curves by lines, which are calculated by the least square method. Then, the f-values corresponding to the best fits of the saturation curves are found to be 0.98, 0.72 and 0.054, respectively.

On the other hand, the f-values is also determined by a special of the saturation curve method, in which a ratio of the ionic charges collected at two different applied voltages is only required. In Fig. 3.15

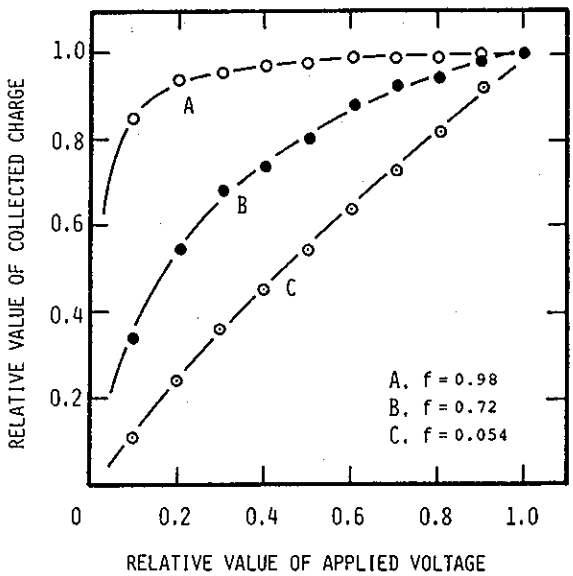

Fig. 3.14. Normalized saturation curves under three experimental conditions. The ordinate and abscissa are equal to those Fig. 3.3. The respective best fits of theoretical curves are also shown by lines. A: 28 MeV, 140 A, 50 ps, 56 mm, 95 cm, B: 20 MeV, 470 A, 50 ps, 56 mm, 9.5 cm, C: 22 MeV, 280 mA, 1 μs, 56 mm, 12 cm.

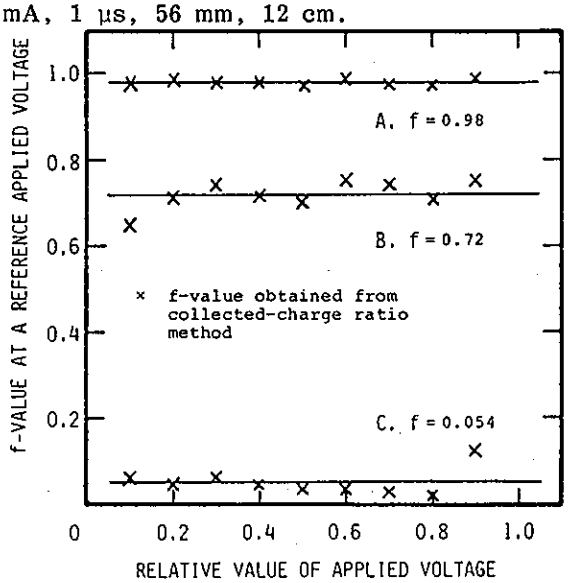

Fig. 3.15. The *f*-values determined by a special method for single burst X-rays. Horizontal lines represents the *f*-values obtained in Fig. 3.14.

the results obtained by the special method are shown by crosses and those in Fig. 3.14 by horinzontal lines. The former f-values deviate in a certain region because of experimental errors in measuring each ionic charge and the fluctuation of the beam current. For instance, the f-values of data B range from 0.64 to 0.75. From a statistical viewpoint, it is desirable to measure the charges for many applied voltages so far as the time for experiments and computation permits.

It is necessary to justify the f-value obtained by the above-mentioned method for a practical application. An ionization chamber in common use cannot be applied to such a high exposure rate X-ray field as is generated by the linear accelerator because of a very small f-value. Hence, the inverse square law is confirmed experimentally, which should be right in the present experiments because both the beam diameter and the range of 22 MeV-electrons in the target are short enough for the X-rays to be regarded as emitted from a point source.

Under the three operation modes of the linear accelerator, the ionic charge were measured and corrected by the f-value determined in the procedure stated above. Figure 3.16 (a) shows the experimental results in the case of "single" mode, where the pulse duration is 50 ps and the electronic charge is 7 nC per pulse. The "measured" values shown by dots were obtained with an applied voltage of 1000 V. The f-value was determined by the saturation curve method and is shown by crosses. The circles on the straight line on a full-log scale represent the ionic charge density corrected by the f-value. The f-value does not become less than 0.8 owing to extremely short duration although the extended exposure rate[13] exceeds 10^{10} R s^{-1}. As is clear from the figure, the corrected charge satisfies the inverse square law. Figure 3.16 (b) corres-

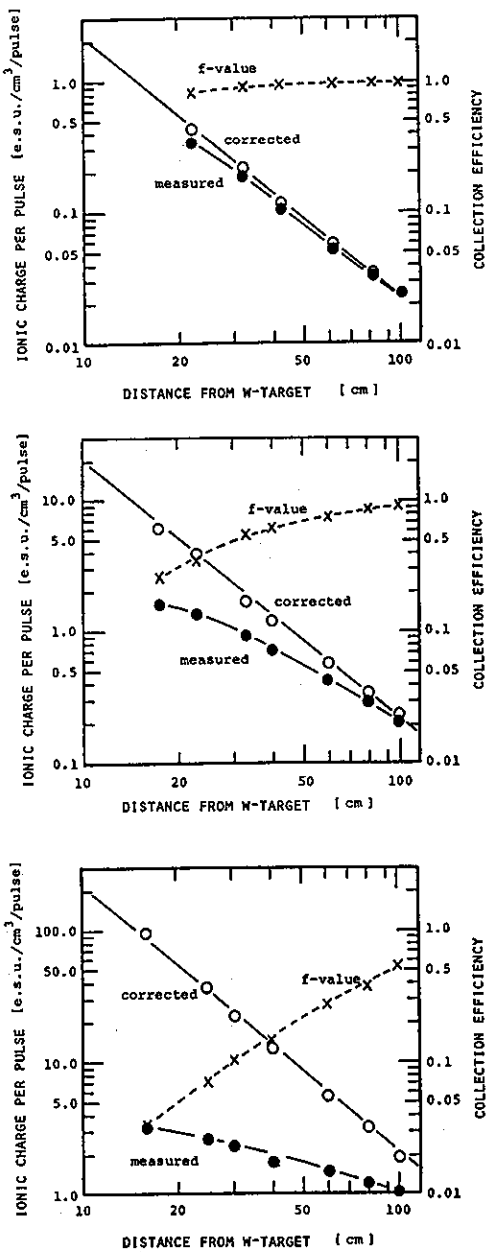

Fig. 3.16. Dependence of the ionic charge density on the distance from W-target. The "measured" values shown by dots are obtained with an applied voltage of 1000 V. (a) 22 MeV, 140 A, 50 ps, 56 mm, (b) 22 MeV, 7 A, 10 ns, 56 mm, (c) 22 MeV, 640 mA, 1 μs, 56 mm.

ponds to the case of "transient" mode, where the pulse duration is 10 ns and the peak current is 7 A. The f-value becomes less than 0.3, but the corrected values still becomes linear. In Fig. 3.16 (c) is shown the case of "steady" mode, where the pulse duration is 1 μs and the peak current is 640 mA. The f-value decreases to be less than 0.4. Namely, 96 % of initial production of ion pairs disappears owing to recombination during charge collection. In spite of such a large correction the inverse square law is still satisfied. In other words, the f-values determined by the proposed method are sufficiently accurate. It is concluded from the results shown above that the proposed method can be practically applied to pulsed X-ray fields.

3.5. Concluding remarks

A method has been proposed for determining the collection efficiency in an unknown pulsed X-ray field. The procedure is as follows:

(1) The pulse duration of the X-ray field is measured by some detector such as a scintillator, a streak camera, and so on.

(2) The ionic charge is measured as a function of the applied voltage.

(3) A reference voltage is arbitrary defined. Then, the ratio of collected charges is plotted against that of applied voltages. The curve is called a normalized saturation curve.

(4) A best fit of the normalized saturation curves to the measured one is found by numerical calculations by the least square method. What one wants to know is the f-value corresponding to the best fit.

In order to confirm an applicability of the proposed method, experiments have been carried out in a pulsed X-ray field generated by the 35 MeV electron linear acceleartor installed at ISIR, Osaka Univer-

sity. An abreast-type ionization chamber was designed and constructed for simultaneous measurement of two ionization currents and two ionic charges in a single-burst X-ray field. As a result of the experiments, the following results were obtained:

(1) Ionic currents of the ionization chamber exposed to pulsed X-rays were observed with little time delay. The waveforms agreed well with those predicted by the calculated results described in the previous chapter. It was confirmed that the assumptions made in the calculations were sufficiently valid.

(2) The ionic charge density under the CPE or transient CPE condition was regarded as a measure of the strength of the X-ray field. Its depth dependence was obtained with polyethylene walls. It was found that 40 mm-polyethylene should be required to attain the CPE condition for bremsstrahlung X-rays generated by 22 MeV electrons.

(3) In order to justify the f-value obtained by the proposed method, the ionic charge density was measured as a function of the distance between the target and the ionization chamber. It was confirmed that the corrected charge density satisfied the inverse square law and the method would be applicable to pulsed X-rays.

Appendix 3.A. Extended exposure

Attix proposed a method for determining the exposure for higher energy than the limitation of a few MeV.[13] It is called an extended exposure. In this section, a modified concept about this quantity is introduced in the following.

Let consider a small volume of air, where a photon interacts with an atomic electron, for example, through the Compton interaction as illustrated in Fig. 3.A.1. For a lower photon energy, the kinetic energy of a recoil electron is spent mainly by ionization or excitation of atomic electrons. For a higher energy, however, a considerable part of the electronic kinetic energy is spent in radiative interactions, i.e. in generating bremsstrahlung X-rays.

In Fig. 3.A.1, a photon with an energy of $h\nu$ is entering in a volume, and the scattered photon with an energy of $h\nu'$ is leaving after transferring kinetic energy of T_0 to the recoil electron. The transferred energy, ε_{tr}, is expressed by

$$\varepsilon_{tr} = h\nu - h\nu' = T_0 \ . \qquad (3.A.1)$$

The kerma, K, defined by the energy transferred from indirectly to directly ionizing particles per unit mass of the material,[14,15] is expressed as follows:

$$K = d\varepsilon_{tr}/dm \ , \qquad (3.A.2)$$

where dm is the mass of a volume element. Here, the kerma is divided into its collisional part and its radiative part. The collision kerma, K_c, in air is closely related to the exposure, X, through the following formula:

$$X = \frac{e}{W} K_c = \frac{e}{W} \cdot \frac{d(T_0 - h\nu'')}{dm} \ , \qquad (3.A.3)$$

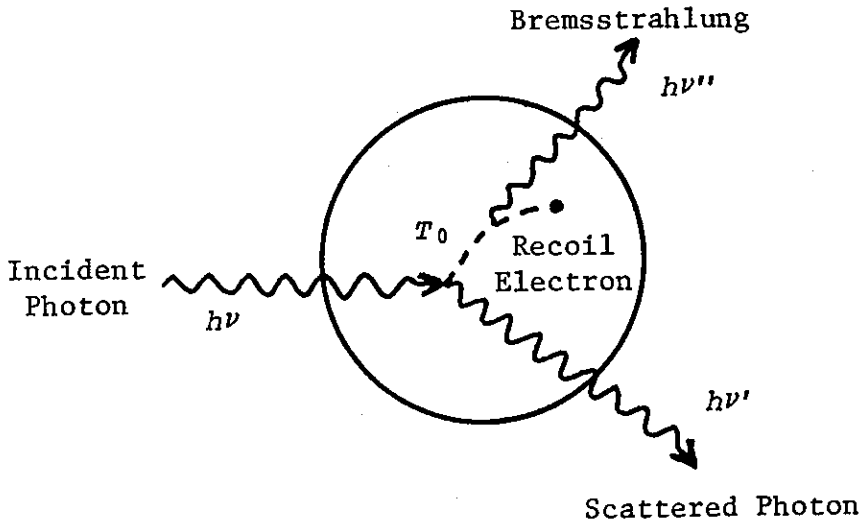

Fig. 3.A.1. Illustration of a small volume of air, where a photon interacts with an atomic electron through Compton collision.

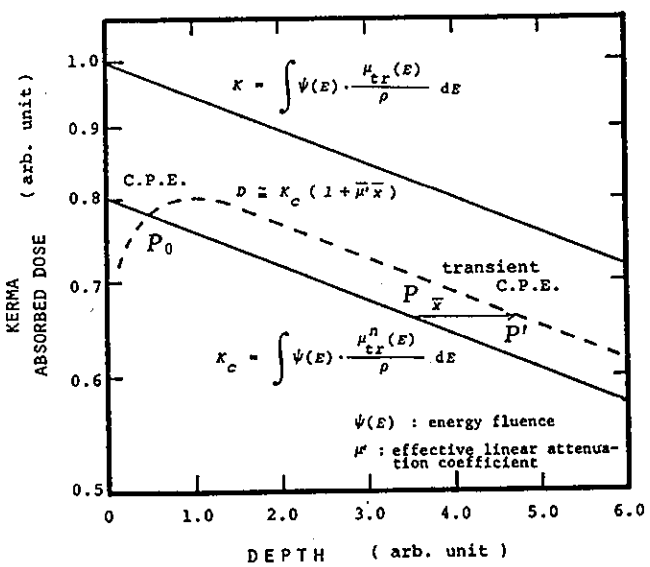

Fig. 3.A.2. Relationship of dependences of kerma, collisional kerma, absorbed dose on the depth. The CPE condition is satisfied at a point, P_0, where collisional kerma is equal to absorbed dose.

where e is the electronic charge, W the mean energy expended per ion pair formed, and $h\nu$" the energy of bremsstrahlung X-ray.

A measurable quantity, however, is not the collision kerma but the absorbed dose in the volume element of interest. In Fig. 3.A.2 are illustrated the dependence of the kerma and the absorbed dose upon the depth in air.[16] The CPE condition is satisfied only at a point where

$$D = K_c. \tag{3.A.4}$$

It is very difficult to find experimentally the point for actual X-rays distributing widely in energy, and especially for very high energy X-rays.

Let $K_c(t,E)\,dE$ be the collision kerma of photons of which energies lie between E and $E + dE$, $D(t)$ the absorbed dose at a depth of t, and $\mu(E)$ the linear attenuation coefficient. Then, in a sufficiently deep region which Attix called a transient CPE region, the energy deposited by the electron at a depth of t (point P) is absorbed at a depth of $t + \bar{x}(E)$ (point P'). Namely, the following relation exists:

$$\begin{aligned} D(t) &= \int_0^{E_{max}} K_c(t - \bar{x}(E),\, E)\, dE \\ &= \int_0^{E_{max}} K_c(0,E)\, e^{-\mu(E)\cdot(t - \bar{x}(E))}\, dE\ . \end{aligned} \tag{3.A.5}$$

Thus, the quantity to be evaluate, i.e. the collision kerma at a depth of 0, $(K_c)_0$, is written by

$$(K_c)_0 = D(t)\cdot F(t), \tag{3.A.6}$$

where

$$F(t) = \frac{\int_0^{E_{max}} K_c(0,E)\, dE}{\int_0^{E_{max}} K_c(0,E)\, e^{-\mu(E)\cdot(t - \bar{x}(E))}\, dE}\ . \tag{3.A.7}$$

The modifying factor, $F(t)$, is approximately estimated from the measured dependence of the absorbed dose upon the wall thickness. For monoenergetic X-rays, eqs. (3.A.3), (3.A.6) and (3.A.7) lead the formula that

$$X = \frac{e}{W} D(t)\ e^{-\mu(E)\cdot(t - x(E))}. \qquad (3.A.8)$$

The values of $\mu(E)$ and $x(E)$ are tabulated in the literature,[14] and thereby the exposure can be determined.

REFERENCES

1) S.Okabe: *High-Dose-Rate Effect Caused by Ionizing Radiations*, (At. Energy Soc. Japan, 1980), p. 1, [in Japanese].

2) D.K.Nochols: IEEE Trans. Nucl. Sci. NS-23 (1980) 1016.

3) J.W.Boag: Phys. Med. Biol. 23 (1950) 601.

4) J.W.Boag: *Radiation Dosimetry, vol. II*, eds. F.H.Attix and W.C. Roesch, (academic, New York, 1966) Chap. 9.

5) K.Tsumori, N.Kimura, T.Yamamoto, T.Hori, S.Takada, J.Okuma, T.Sawai, M.Kawanishi, H.Sakurai and K.Hayashi: *Proc. 3rd Symp. Accelerator Science & Technology, Osaka, 1980*, p.49.

6) H.Sakurai, M.Kawanishi, K.Hayashi, T.Okada, K.Tsumori, S.Takeda, N.Kimura, T.Yamamoto, T.Hori, J.Ohkuma and T.Sawai: Mem. Inst. Sci. Ind. Res., Osaka Univ. 39 (1982) 21.

7) N.E.Bradbury: Phys. Rev. 40 (1932) 508.

8) G.Sinnot: Phys. Rev. 136 (1964) 370.

9) R.E.Voshall, J.L.Pack and A.V.Phelps: J. Chem. Phys. 43 (1965) 1990.

10) G.Sinnot, D.E.Golden and R.N.Vorney: Phys. Rev. 170 (1968) 272.

11) ICRU Report 8 ; Radiology 29 (1937) 634.

12) ICRU Report 5 ; Natl. Bur. Std. Handbook 62 (1956).

13) F.H.Attix: Health Phys. 36 (1979) 347.

14) W,C,Roesch: Rad. Res. 9 (1958) 399.

15) ICRU Report 19 (1971).

16) F.H.Attix: Health Phys. 15 (1968) 49.

CHAPTER 4. DOSIMETRY OF PULSED X-RAYS OF RELATIVELY LONG DURATION*

—— X-RAY TUBE FOR MEDICAL DIAGNOSIS ——

4.1. Introduction

It is the most important work for radiation protection to evaluate absolutely the absorbed dose in human body irradiated in diagnostic or therapeutic X-rays.[1,2] For the measurement of the dose are often used thermolumunescence dosimeters and film badges as a personal monitor. The dosimeters must be calibrated beforehend by standard dosimeters such as an ionization chamber.

In recent years, much effort in decreasing the absorbed dose has been made by optimizing the energy spectrum of diagnostic X-rays and by improvement of radiographic imaging systems.[3-7] On the other hand, the pulse duration of X-ray sources has been shortening to be of the order of ms in order that the image of the subjects may not be blurred. In inverse proportion, the exposure rate becomes higher. Thus, an important problem has ocurred in dose-evaluation with an ionization chamber. The ion transit time of the chamber in common use lies in the region of ms, which is comparable to the pulse duration of diagnostic X-rays. This is just the case where Boag's formula for collection efficiency[8,9] becomes invalid, as already pointed out in Chap. 2.

In the analysis of the collection efficiency for pulsed X-rays in Chap. 2, three assumptions were made about the space charge effect,

---

*This work is published in Hoken Butsuri 17 (1982) 143.

the mobilty difference and the pulse shape. The effects on the collection efficiency caused by the first two assumptions have already been discussed. It is the purpose of this chapter to clarify the effect caused by the third assumption. The output currents of a parallel-plate ionization chamber are observed and the saturation curves are also obtained with an X-ray tube in practical use at the Hospital attached to the Research Institute for Microbial Diseases, Osaka University. These experimental results are compared with the numerical calculations, and the pulse shape effect on the output current and the collection efficiency are discussed in detail.

4.2. Pulse shape effect on f-value and output currents

In the numerical calculations in Chap. 2, the shape of X-ray pulses was assumed to be a rectangle for simplicity. In most cases, however, the shape of pulsed X-rays emitted from an X-ray tube for medical diagnosis is far from rectangular.

In order to obtain the f-value for an arbitrary pulse shape, the normalized production rate, $\Lambda(s)$, is introduced in eq. (2.12) as a function of the normalized time under the condition for normalization that

$$\int_0^{s_0} \Lambda(s)\, ds = s_0 \qquad (4.1)$$

where s_0 is the pulse duration normalized by the ion transit time of an ionization chamber. Figure 4.1 shows typical normalized production rates used in succeeding calculations. A dotted and broken line represents the production rate for rectangular pulses, a broken line that for triangular pulses, and a solid line that for typical X-rays emitted

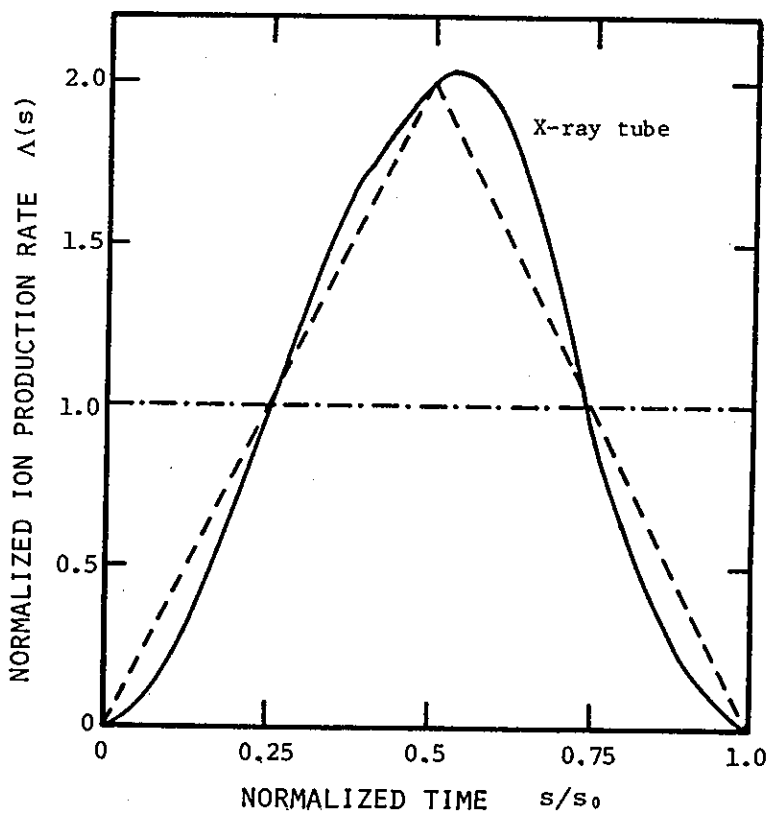

Fig. 4.1. Normalized production rates as a function of the normalized time for three pulse shapes of a rectangle, triangle and the shape of typical X-rays emitted from an X-ray tube in practical use for medical diagnosis.

from an X-ray tube in practical use. The normalized time, s/s_0, on the abscissa is equal to the time normalized by the pulse duration of X-rays. Namely,

$$\frac{s}{s_0} = \frac{t/\tau}{\tau_0/\tau} = \frac{t}{\tau_0} . \tag{4.1}$$

For rectangular pulses, the normalized production rate is expressed in a functional form as follows:

$$\Lambda(s) = \begin{cases} 1 & 0 \leqq s \leqq s_0 \\ 0 & s_0 < s \leqq 1+s_0 \end{cases} , \tag{4.2}$$

and for triangular pulses,

$$\Lambda(s) = \begin{cases} 4\,s/s_0 & 0 \leqq s \leqq s_0/2 \\ 4 - 4\,s/s_0 & s_0/2 < s \leqq s_0 \\ 0 & s_0 < s \leqq 1+s_0 \end{cases} . \tag{4.3}$$

At first, the temporal variations of spatial distribution of the ion density are calculated for two types of pulse shapes. The normalized pulse duration is assumed to be 1.0 as an example. Figure 4.2 (a) and (b) correspond to the case where $M = 0$, i.e. no recombination between positive and negative ions takes place. The ions distribute in a triangle form at the instant when an X-ray pulse ceases, because the drift by a collecting field occurs simultaneously with the ion production during the pulse. If the pulse duration is very short compared with the transit time, the drift is negligible and the ions distribute uniformly in the ionization chamber. Such a case has already been discussed in Chaps. 2 and 3. Temporal variation of the density distribution for a triangular pulse is shown in Fig. 4.2 (b). The time-variant ion production brings about a curved distribution. A distinctive difference is found between Figs. 4.2 (a) and (b). The cases that $M = 10.0$ are shown in Figs. 4.3 (a) and (b) for rectangular and triangular pulses,

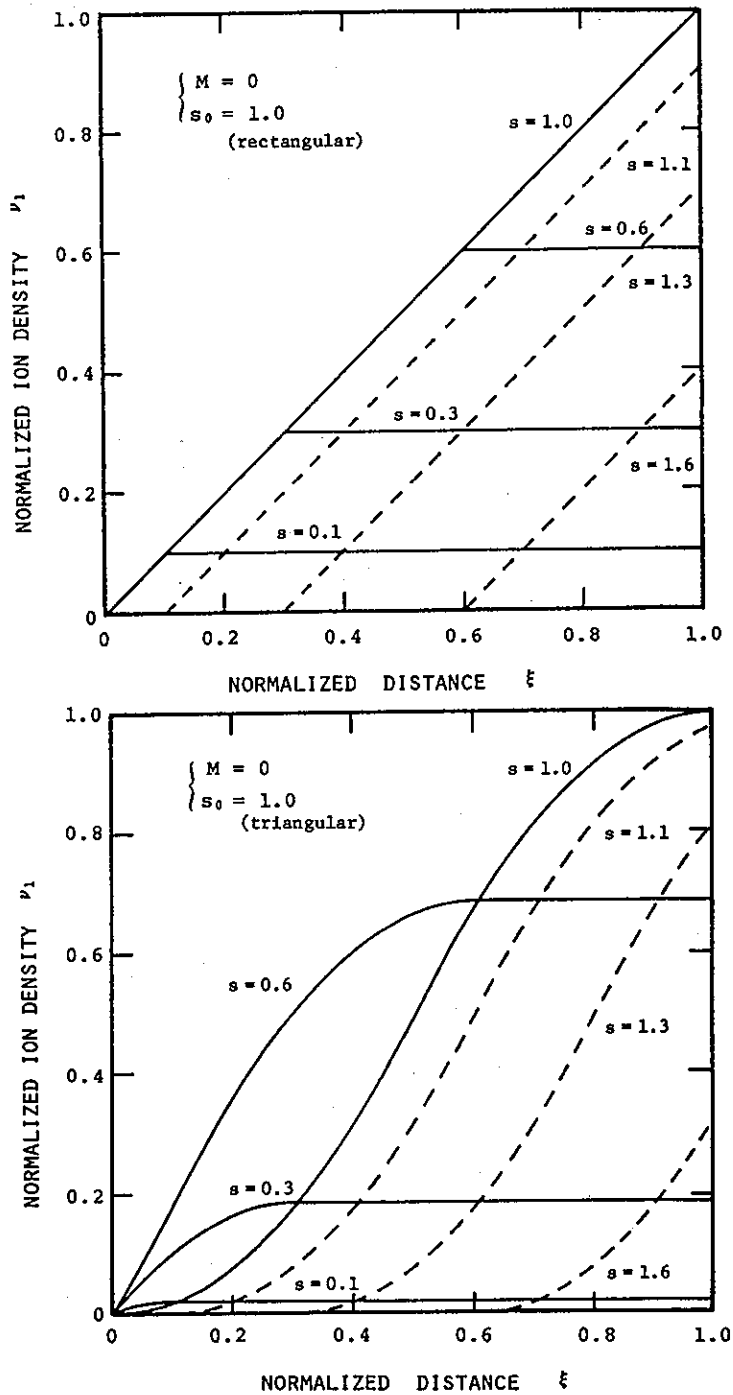

Fig. 4.2. Temporal variation of the spatial distribution of the normalized ion density for pulsed X-rays of which duration is equal to the ion transit time. No recombination takes place. (a) rectangular pulse, (b) triangular pulse.

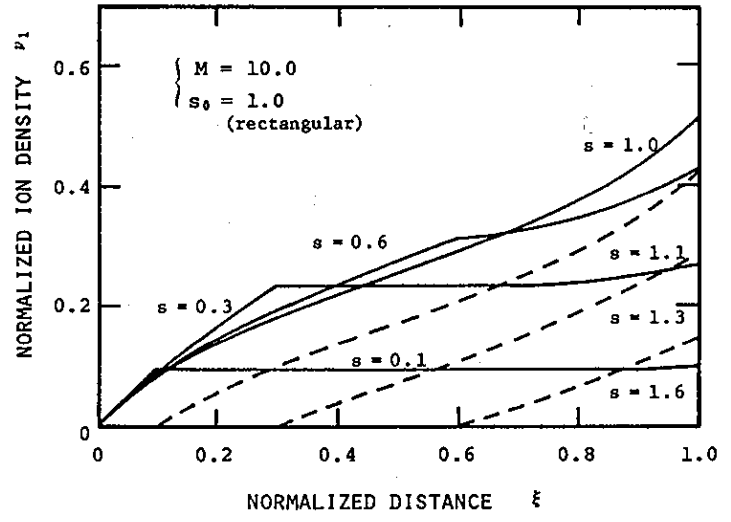

(a)

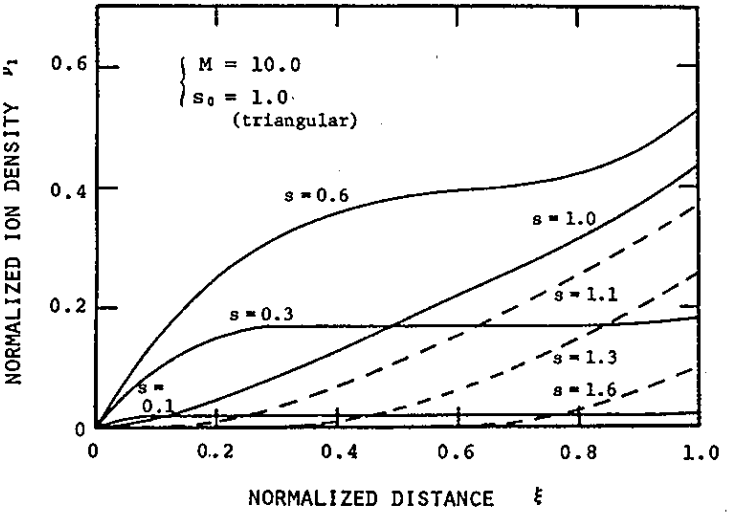

(b)

Fig. 4.3. Temporal variation of the spatial distribution of the normalized ion density for pulsed X-rays of which duration is equal to the ion transit time. Owing to recombination the distribution changes to a tangential curve. (a) rectangular pulse, (b) triangular pulse.

respectively. An s_0-value of 1.0 and M-value of 10.0 correspond nearly to the pulse duration of 1.0 ms and the exposure rate of 5.0×10^3 R s^{-1} provided that the transit time of an ionization chamber is 1.0 ms and the recombination coefficient is 1.0×10^{-6} $cm^3 s^{-1}$. Owing to recombination the density distribution changes from a triangular or a sine curve to a tangential one. It can be expected that such a difference in the distribution between two pulse shapes should affect the output current shape and the f-value.

The waveform of the output currents of an ionization chamber have been derived theoretically by a few authors,[10,11] but they had neglected the pulse shape effect. The normalized current density, $\zeta(s)$, is given here by eq. (2.18). For pulsed X-rays of relatively long duration, the current density cannot be derived from Boag's formula, because the drift of ions during pulse is neglected in the assumptions. Figure 4.4 shows the results of numerical calculations of eq. (2.18) in the case that $s_0 = 1.0$ and $M = 10.0$. The normalized current density for a rectangular pulse is shown by a solid line, which is similar to that obtained by Livingstone.[10] A broken line in the figure shows the current density for a triangular pulse. It is clearly seen that the output current shape is affected sensitively by the shape of X-rays.

Numerical calculations of the f-value has been performed under various conditions. An example is shown in Fig. 4.5, where the f-values for a rectangular and a triangular pulse are represented by a solid and a broken line, respectively, as a function of Ms_0-value corresponding to the total exposure per pulse. The Boag's f-value is also shown by a dotted-broken line. In the region where the pulse dura-

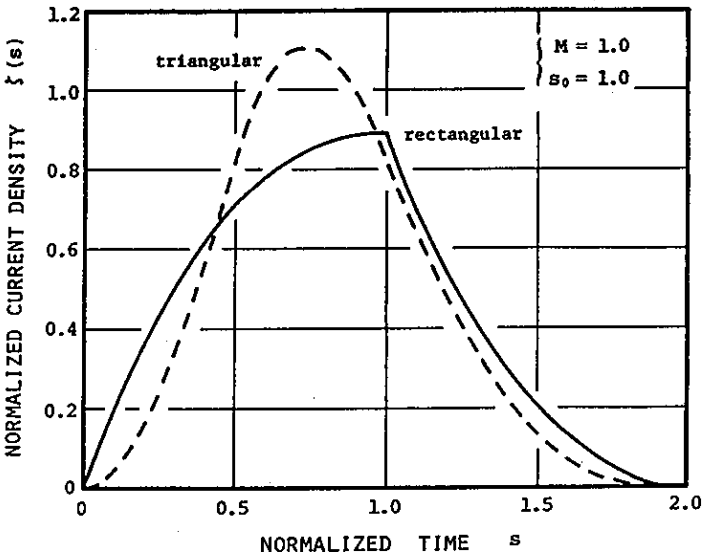

Fig. 4.4. Normalized current densities as a function of the normalized time for both rectangular and triangular pulses. The difference between them is clearly seen.

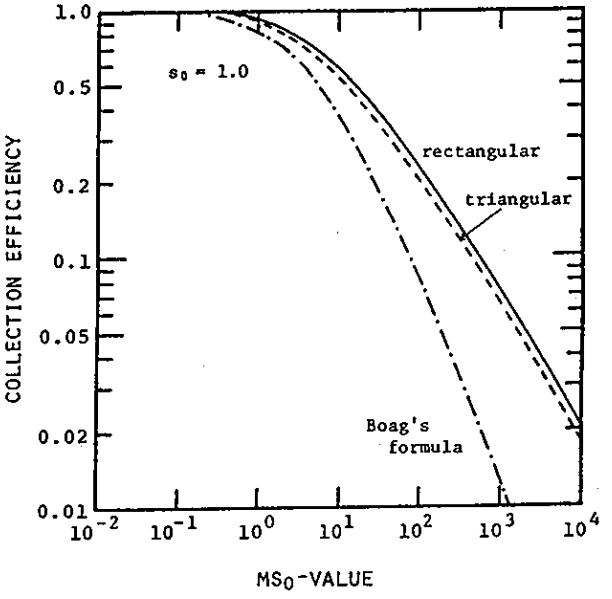

Fig. 4.5. Dependence of the collection efficiency on Ms_0-value, which corresponds to the total exposure per pulse. For a relatively long pulse, the f-value deviates distinctively from the Boag's formula.

tion is comparable to the ion transit time, the true f-value deviates from the Boag's formula as already stated. The pulse shape effect in question acts on the f-value so as to decrease it, i.e. to increase the recombination loss. Figure 4.6 shows the f-value as a function of the normalized pulse duration, which lies between about 0.5 and 5.0 for diagnostic X-rays. In Fig. 4.7 is shown the deviation of the f-value for a triangular pulse from that for a rectangular pulse. It is found that the deviation reaches the maximum of about 10 % near an s_0-value of 1.0. Namely, the pulse shape effect becomes most significant for pulsed X-rays in the diagnostic region. In the figure is also shown the deviation of the f-value for X-rays emitted from an X-ray tube, of which shape was shown in Fig. 4.1. Another notice should be taken that the pulse shape for the X-ray tube may be approximated by a triangle within a few per cent error. It is concluded that both pulse duration and pulse shape must be measured in evaluating the f-value acuurately for pulsed X-rays in the diagnostic region.

4.3. Experimental results and discussion

4.3.1. Experimental apparatus

The pulsed X-rays in this experiment were generated by an X-ray tube (Type: Circlex 1/2 P38C) installed at the Hospital of the Research Institute for Microbial Diseases, Osaka University. The tube was operated under the condition of the tube voltage of 60 kV and the beam current of 500 mA. The total filtration was 1.2 mm-Al equivalent. Three typical X-ray energy specra are shown in Fig. 4.8. In Photo 4.1 is shown a typical output signal of a plastic scintillator exposed to the pulsed X-rays. The time delay can be neglected because the res-

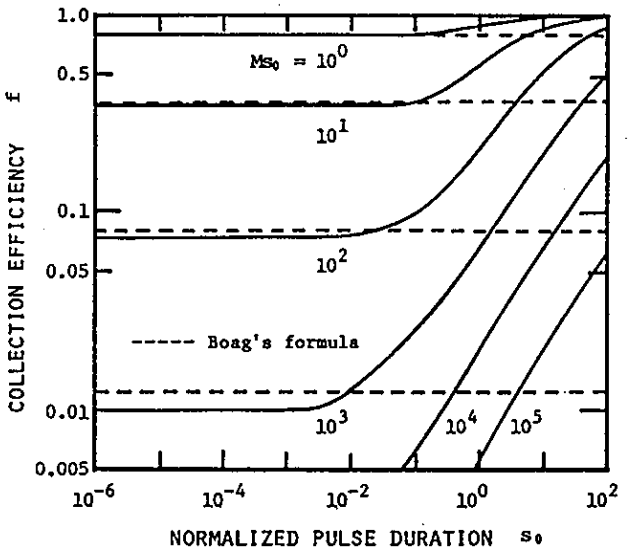

Fig. 4.6. Dependence of the collection efficiency on the normalized pulse duration. The values obtained with the Boag's formula are shown by broken lines. For an usual X-ray tube, the normalized pulse duration lies between about 0.5 and 5.0.

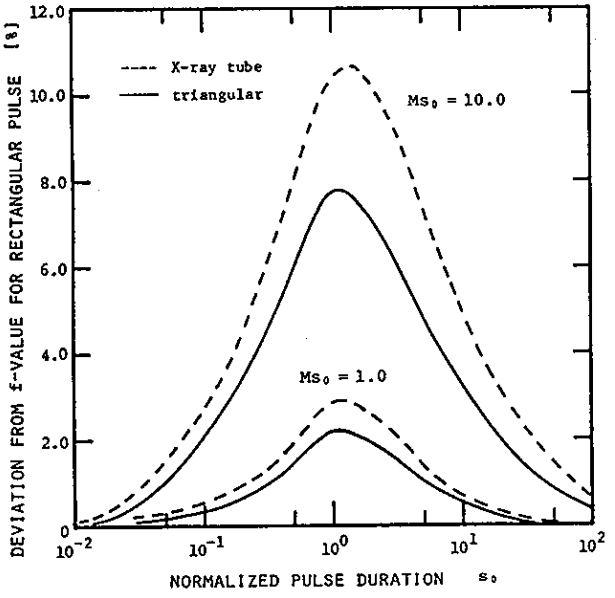

Fig. 4.7. Deviation of the f-value for two pulse shapes from that for a rectangular pulse shown in Fig. 4.6. The pulse shape effect is most serious at an s_0-value of about 1.0.

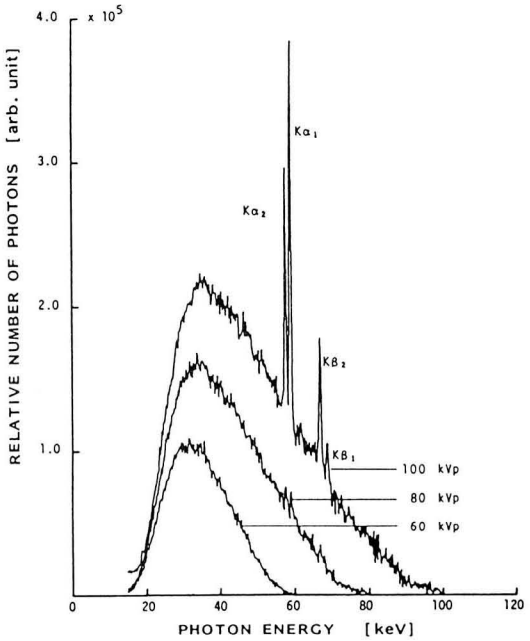

Fig. 4.8. Typical X-ray energy spectra. The X-ray tube was operated under the condition that the tube voltages were 60, 80 and 100 kV, and the total filtration was equivalent to aluminium of 1.2 mm thickness. [after H. Terada]

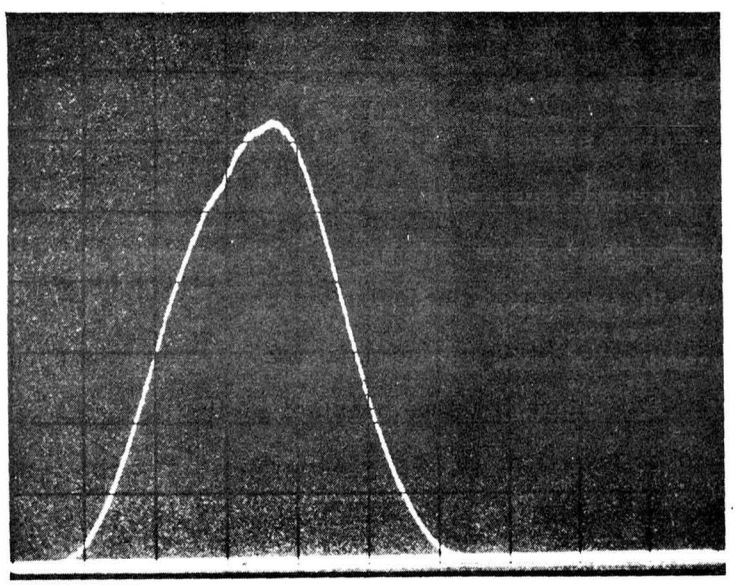

Photo 4.1. Waveform of pulsed X-rays emitted from the X-ray tube. It was observed with a plastic scintillator. Sweep rate: 1 ms/div.

ponse time of the scintillator and a photomultiplier is shorter than several ns. In actual, the energy dependence of the scintillation efficiency reflects on the output signal, but approximately the signal corresponds to the exposure rate. Accordingly, a significant error would not be caused if we take the waveform shown in the photograph as that of the pulsed X-rays. Then, the pulse duration is found to be 5.46 ms.

An air-equivalent ionization chamber of parallel plate was used in this experiment. The chamber was made of polyethylene, which is nearly equivalent to air, except the connectors and the conducting materials in order not to disturb the X-ray field. The wall was a thin polyethylene sheet of 200 μm thickness to attain the CPE condition. The polyethylene sheet and disks were coated with a thin film of aluminium by use of a vacuum evaporation method. The gap distance between the electrodes was 10.0 mm, and the active volume was 12.7 cm^3. The ion mobilty in air has already been estimated to be 1.34 $cm^2 s^{-1} V^{-1}$ from the experiment described in Chap. 3. Accordingly, the ion transit time at an applied voltage, V, is expressed as

$$\tau = 0.746/V. \qquad (4.5)$$

4.3.2. Output currents

The output currents of the ionization chamber were observed with a memory oscilloscope through a co-axial cable. The shunt impedance was 10 kΩ, and therefore the time constant of the detecting circuit can be adjusted to be less than 10 μs. Photograph 4.2 shows typical waveforms of the currents of the ionization chamber, which was placed at a distance of 26.2 cm from the target of the X-ray tube. To the chamber were applied the voltages of (a) 300 V, (b) 200 V and (c) 100 V,

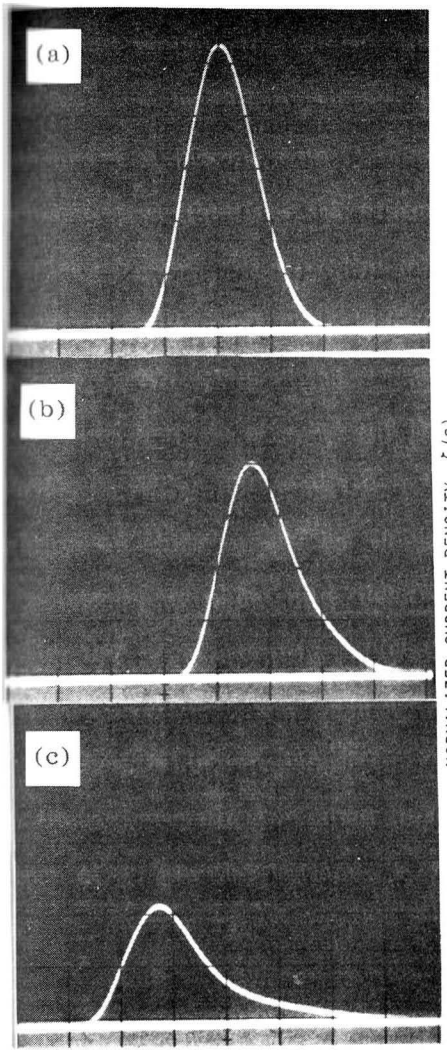

Photo 4.2. Output current shapes of a parallel-plate ionization chamber exposed to pulsed X-rays shown in Photo 4.1. To the chamber were applied the voltages of (a) 300 V, (b) 200 V and (c) 100 V. Sweep rate: 2 ms/div.

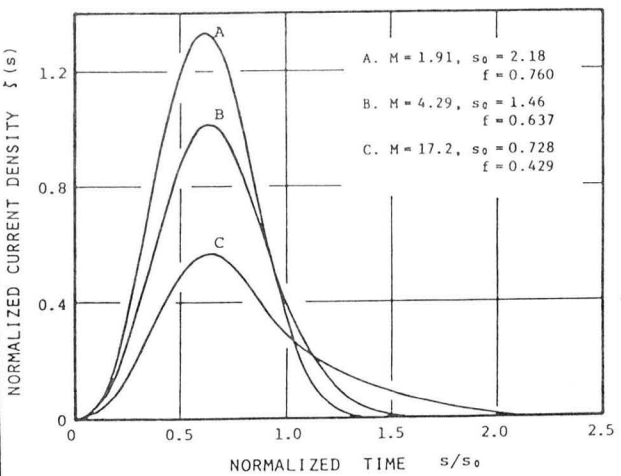

Fig. 4.9. Output current shapes calculated under the same conditions as in Photo 4.2. The symbols, A, B and C, correspond to Photo 4.2 (a), (b) and (c), respectively. A good agreement with the photographs is found.

respectively. The normalized pulse duration, therefore, are 2.20, 1.46 and 0.73, respectively. It is seen that as the applied voltage becomes lower the peak current decreases and the tail becomes longer. Furthermore, the change of the current shape is clearly seen in the photographs. In the case of a high applied voltage, that is, a long normalized duration, the output current follows immediately the primary X-rays and the ion current after the X-ray pulse is hardly seen. In the case of a short normalized duration, the ion current after the pulse is distinctively seen as shown in Photo 4.3 (c). For a much shorter duration, the current after pulse is only observed as described in Chap. 2.

In order to obtain the currents theoretically, the calculations are carried out by putting the waveform of pulsed X-rays into eq. (2.18). The results are shown in Fig. 4. 9 , which represents the normalized current densities as a function of the time normalized by the pulse duration, i.e. $s/s_0 = t/\tau_0 = 183t$. The symbols, A, B and C, correspond to Photo 4.3 (a), (b) and (c), respectively. The M-values of 1.91, 4.29 and 17.2 used in the calculation will be evaluated in the succeeding subsection. There is found a good agreement between calculated and experimental results. This means that some assumptions made in the calculation are valid and therefore our calculations is applicable to pulsed X-rays of relatively long duration with an arbitrary pulse shape.

4.3.3. Saturation curves

It was pointed out in the previous chapter that the f-value in an unknown pulsed X-ray field could be determined from a characteristics

of saturation curve. The proposed method[12,13] is applied to the X-ray field in this experiment.

The normalized saturation curve is obtained theoretically from the f-Ms_0 curve. In the case of very short pulse duration, the f-Ms_0 curve can be regarded as a single curve for various applied voltages. However, in this case where the normalized pulse duration lies between about 0.73 and 7.3, the curves for applied voltages are no longer the same. Figure 4.10 shows the f-Ms_0 curves for four s_0-values. The s_0-values of 0.728, 1.46, 3.64 and 7.28 correspond to the applied voltages of 100, 200, 500 and 1000 V. Let a reference voltage be 1000 V and choose the f-value, $f_{1.0}$, arbitrarily on the uppermost curve. The corresponding Ms_0-value is represented in the figure by $(Ms_0)_{1.0}$. The Ms_0-value multiplied by a factor of 1000/500 corresponds to $(Ms_0)_{0.5}$. Then the value of $f_{0.5}$ is found on the second curve as shown in the figure. The f-values for all the applied voltages can be determined in the same procedure. Plotting the values normalized by that at a reference voltage against the applied voltage, the so-called saturation curve is obtained.

The saturation curves were measured by varying the distance between the X-ray source and the ionization chamber. In Fig. 4.11 is shown an example at a distance of 26.2 cm by dots. The three theoretical curves are also shown in the figure. There is found no curve fit to all measured points among the curves predicted by Boag's formula. Two of them are shown by broken lines. The upper curve agrees well with the points at applied voltages higher than 600 V, but deviates from the rest. The lower does not pass the points except for two at the voltages of 100 and 1000 V. On the other hand, according

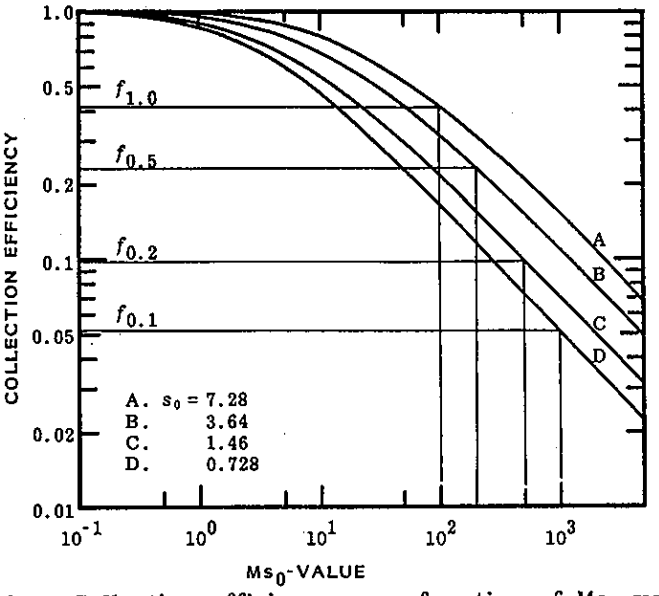

Fig. 4.10. Collection efficiency as a function of Ms_0-value for several normalized pulse durations. Four s_0-values of 0.728, 1.46, 3.64 and 7.28 correspond to the voltages of 100, 200, 500 and 1000 V applied to the ionization chamber. The procedure for obtaining a saturation curve is also shown.

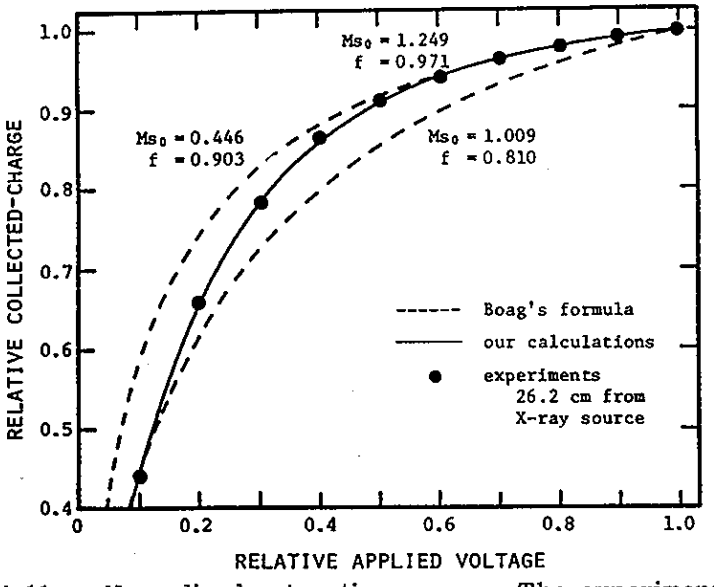

Fig. 4.11. Normalized saturation curve. The experimental results are shown by dots, and the theoretical curves are also shown by solid and broken lines. Only our calculations fit well to all the measured points.

to the calculations a best fit of the saturation curves to all the points is found as shown in the figure by a solid line. This curve gives a true f-value of 0.971 at a voltage of 1000 V. In general, Boag's formula brings about the underestimate of the f-value, that is, 0.81 or 0.90 in this case.

Figure 4.12 shows the measured and corrected values of the ionic charge density (exposure) as a function of the distance from the X-ray source. The measurement was performed by adjusting the beam current as reproducible as possible. The radius of the electron beam of the X-ray tube was so small that X-rays are considered to be emitted from a point source. Furthermore, the absorption of the X-rays in air can be neglected, since the mean energy is about 28 keV and the total absorption at a distance of 80 cm from the filter of the tube is 4 % at most.[14-16] Accordingly, the exposure should satisfy the inverse square law about the distance. As shown in Fig. 4.12, the exposure corrected by the method lies near a straight line on a full-log scale, whereas that corrected by Boag's formula deviates near the source. It is concluded from the result that the f-value in the X-ray field of relatively long duration can be accurately evaluated by our method.

4.4. Concluding remarks

The collection efficiency of a parallel-plate ionization chamber has been discussed for pulsed X-rays of which duration is of the order of the ion transit time of the chamber. The following results were obtained by the numerical calculations of the f-value including the pulse shape effect.

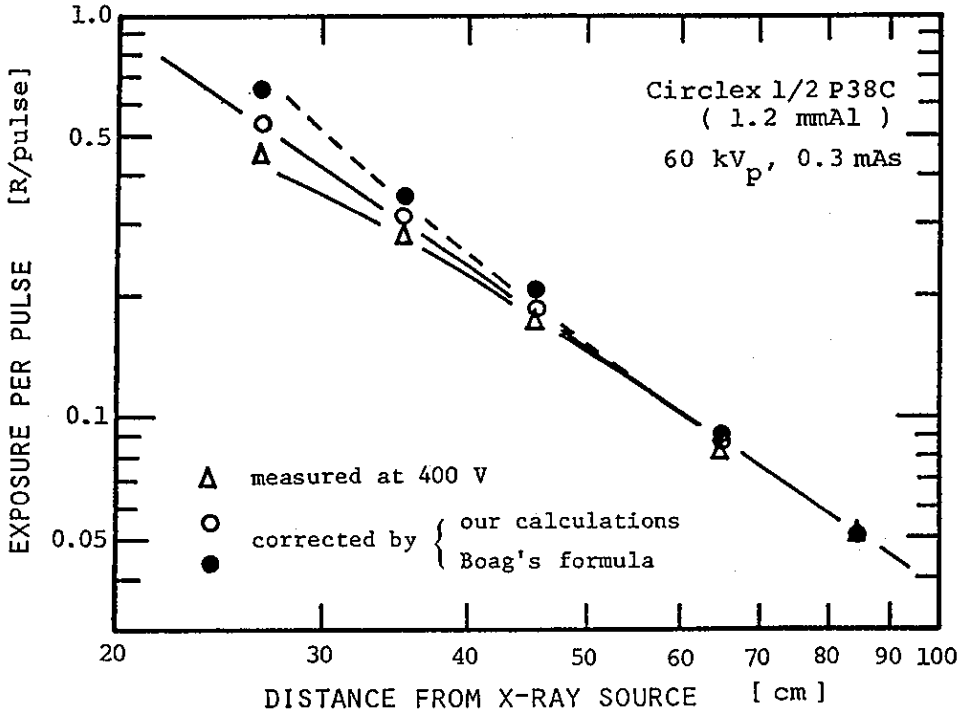

Fig. 4.12. Dependence of the ionic charge density or the exposure on the distance from the X-ray source. The exposure corrected by our method follows the inverse square law, whereas that corrected by Boag's formula becomes much larger near the source.

(1) A distinctive difference in the spatial distribution of the ion density was found between a rectangular and a triangular pulse. Especially, the output current shape of the ionization chamber was affected sensitively by the pulse shape of X-rays.

(2) It was found that the pulse shape effect on the f-value should appear as the underestimate of the recombination loss. The effect was most significant in the case that the pulse duration was comparable to the ion transit time.

(3) The pulse shape of the X-rays in the diagnostic region could be approximated by a triangle within a few per cent error.

In order to confirm experimentally that the method proposed in Chap. 3 should be applicable to pulsed X-rays of relatively long duration with an arbitrary pulse shape, the experiments were carried out by using an X-ray tube for medical diagnosis installed at the Hospital of the Research Institute for Microbial Diseases, Osaka University. The following results were obtained.

(4) The observed currents of the ionization chamber agreed well with the results calculated in cosideration of the pulse shape effect.

(5) The saturation curves were measured by varying the distance between the X-ray source and the chamber. There was found no curve among those predicted by Boag's formula, but a best fit of the curve to all the measured points could be found by our calculations.

(6) The exposure corrected by the f-value satisfied the inverse square law. The result showed that the method for determining the f-value could be applied to pulsed X-rays for medical diagnosis as well as high-exposure-rate X-rays generated by particle accelerators.

REFERENCES

1) ICRU Report 17 (1970).

2) ICRU Report 24 (1976).

3) M.Ter-Pogassian: Acta Radiol. 45 (1956) 313.

4) B.Jacobson and R.S.Mackay: Adv. Biol. Med. Phys. 6 (1958) 201.

5) G.T.Barnes and I.A.Brezovich: Radiology 126 (1978) 243.

6) N.Abe, T.Yamamoto and M.Kawanishi: Hoken Butsuri 13 (1978) 287.

7) T.Nishikawa: Master Thesis (Osaka University, 1981).

8) J.W.Boag: Brit. J. Radiol. 23 (1950) 601.

9) J.W.Boag: *Radiation Dosimetry, vol. II,* eds. F.H.Attix and W.C. Roesch (Academic, New York, 1966) Chap.9.

10) P.M.Livingstone: J. Appl. Phys. 35 (1964) 2341.

11) H.Dinter and K.Tesch: Nucl. Instrum. & Methods 120 (1974) 113.

12) T.Yamamoto, K.Oda, H.Kobayashi and M.Kawanishi: Nucl. Instrum. & Mehtods 172 (1980) 447.

13) K.Oda, H.Kobayashi, T.Yamamoto and M.Kawanishi: J. Nucl. Sci. Technol. 19 (1982) 89.

14) R.D.Evans: *Atomic Nucleus,* (McGraw-Hill, New York, 1955).

15) R.D.Evans: *Radiation Dosimetry, vol. I,* eds. F.H.Attix and W.C. Roesch (Academic, New York, 1968) Chap.3.

16) R.Birch and M.Marshall: *Catalogue of Special Data for Diagnostic X-Rays,* (Hospital Physists' Association, London, 1979) Chap.3.

CHAPTER 5. DOSIMETRY OF MIXED RADIATIONS CONSISTING OF X-RAYS AND NEUTRONS*

—— ELECTRON LINEAR ACCELERATOR (II) ——

5.1. Introduction

Radiations emitted from particle accelerator and other sources do not consist only of X-rays, but in most cases they involve neutrons, electrons, protons, and so on. It is the purpose of dosimetry of such a mixed radiation field to evaluate the radiation effect on irradiatied materials. The effects is represented, for example, by displacement per atom in solid state physics and RBE (relative biological effect) dose in biology. Especially for radiation protection purpose are defined the dose equivalent (DE). According to its definition,[1-3] DE is proportional to the absorbed dose in human body and a proportional constant is called quality factor (QF). The QF, in general, depends on species and energy of the radiation. The ICRU recommended QF as a function of the collision stopping power (LET).[3] Alternative expression is accepted of a product of the particle fluence and the conversion factor (CF).[4,5] Both factors of QF and CF connot be measured directly as physical quantities because of complicated functions of the particle energy. Thus various techniques for estimating the factors have been developed and improved, but there still remain some problems in each technique at present.

In this chapter is discussed the dosimetry of mixed radiations

---

*The main part of this work is presented in KEK-80-1 R (1980) 75 and Nucl. Instrum. & Methods 202 (1982) 481.

consisting of X-rays and neutrons generated by high temperature plasmas and high energy particles accelerators. Placing a matter in a mixed field consisting of such indirectly ionizing radiations, the secondary radiation field consisting of directly ionizing particles (electrons and protons) is formed in the matter. Such recoil particles ionize the atoms and their kinetic energy is eventually absorbed in the matter. A characteristic feature of the ionization in a mixed radiation field lies in a non-homogeneous distribution of the density of ion pairs, which caused by the difference in physical property between electrons and protons.

The author tried to evaluate DE in a mixed radiation field with an ionization chamber. A merit in using an ionization chamber is that the total absorbed dose due to both neutrons and X-rays can be obtained according to its definition if only the number of ion pairs generated is determined. Thus the DE evaluation depends on how one estimates QF. It is considered that the nonuniform distribution of the ion density is the key to estimate QF. Two methods are proposed in this chapter. They are compared with other methods, i.e. theoretical calculations of energy spectra, measurement of LET spectrum, and separate measurement of absorbed doses with two ionization chambers, and then, the applicability of two proposed methods is confirmed.

5.2. Basic concept of mixed field dosimetry

The purpose of the mixed field dosimetry is focused on DE evaluation in the present chapter. The various methods have been developed and they may be roughly classified into three categories according to the radiation quantity to be measured, as shown in Fig. 5.1. Namely,

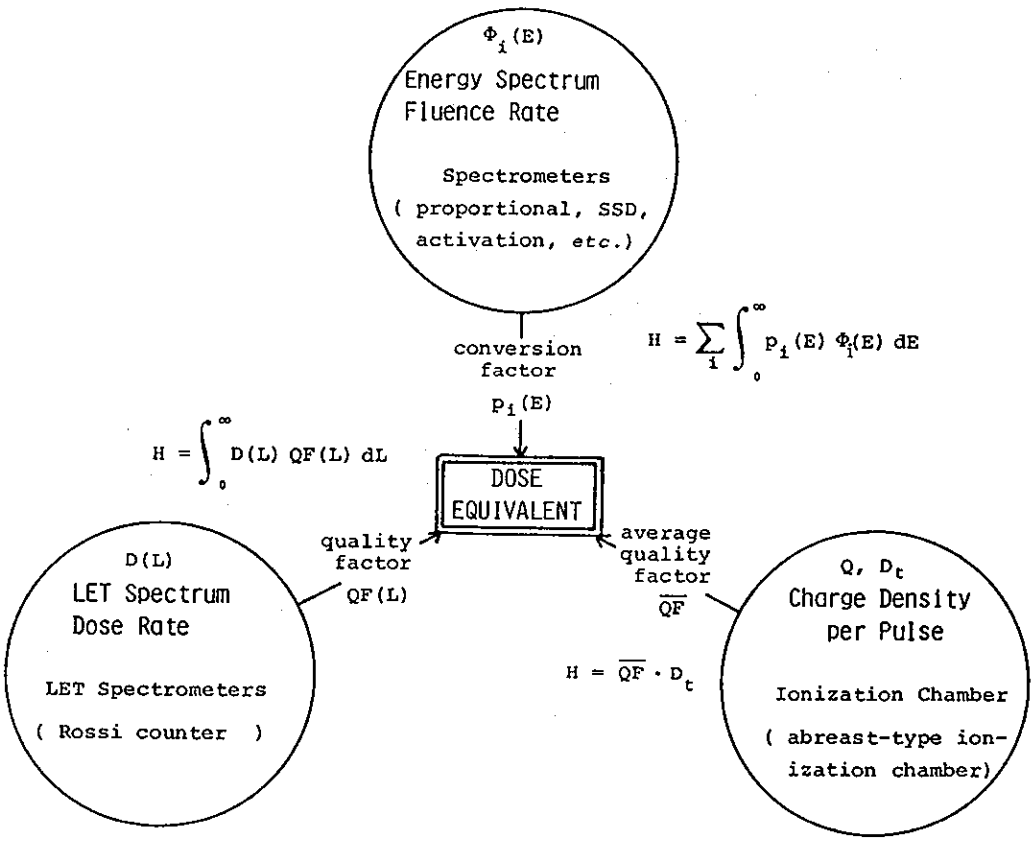

Fig. 5.1. Classification of methods for evaluating the dose equivalent in a mixed radiation field.

		HIGH ENERGY	MIXED FIELD	HIGH FLUENCE RATE	SINGLE BURST
ENERGY SPECTRA	spectrometers	△	×	×	×
	activation	○	○	○	○
LET SPECTRUM	Rossi counter	○	○	×	×
IONIZATION CHAMBER	recombination	○	△	×	×
	abreast-type	○	○	○	○

Table 5.1. Comparison among three methods for DE evaluation. Applicability to single burst, high energy, high fluence rate and mixed radiation field is summerized.

(1) Measurement the energy spectrum and the fluence rate of every species constituting a mixed field.

(2) Measurement of the LET spectrum of absorbed dose and the dose rate.

(3) Measurement of the total absorbed energy or the charge generated by all the species.

The applicability of the methods to various radiation field is summerized in Table 5.1, which is discussed in detail below.

5.2.1. Energy spectrum

In the case that the fluence rate of the i-th species is known, the DE, H, is obtained by the following formula:

$$H = \sum_i \int_0^{\tau_i} \int_0^{\infty} p_i(E)\, \phi_i(E,t)\, dE\, dt, \qquad (5.1)$$

where $\phi_i(E,t)\, dE$ is a fluence rate of particles with energies between E and $E + dE$ at a time t, $p_i(E)$ is the fluence-to-DE conversion factor given by ICRP[4,5] as shown in Fig. 5.2, and τ_i is the pulse duration

An X-ray spectrum can be measured with a solid state detector, a proportional counter, etc. and a neutron spectrum with a BF_3 counter, a He^3 counter, etc. in most cases. However, there remain some problems described below in applying the detector to a single burst, high-fluence-rate and mixed radiation field.

(1) measurement in high-fluence-rate field

The detectors, in general, are operated in a way where a radiation pulse is processed one by one. If the detectors are placed in such an intensive field, plural pulses would be superposed to make a single output pulse. It is necessary to improve the electronic circuit such

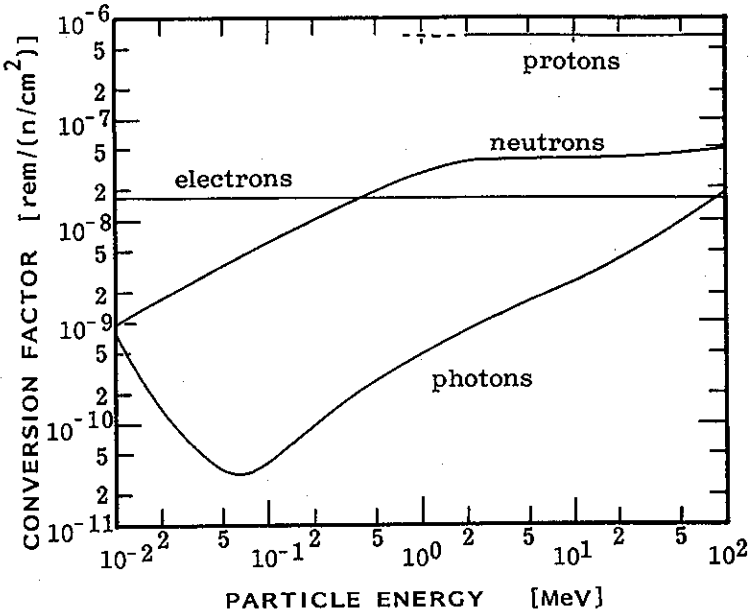

Fig. 5.2. Conversion factors for particle fluence to dose equivalent index for protons, neutrons, electrons and photons. [ref. 5]

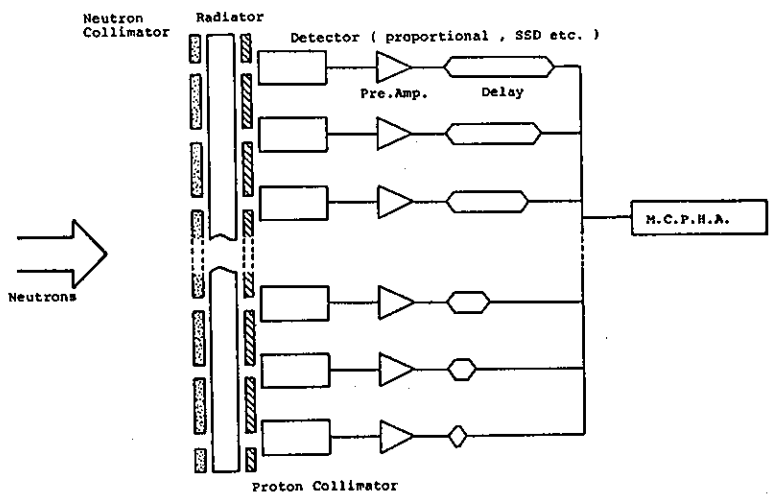

Fig. 5.3. Conceptual design of burst radiation spectrometer. Output sugnals from plural detectors aligned a matrix should be accumulated by a PHA through a circuit with each time delay.

as a pre-amplifier, AD converter, etc to make the response time much shorter.

(2) measurement in a single-burst field

Because the maximum counting rate is of the order of several hundred kHz, a time resolution of microseconds or less can not be attained. A method with a multi-channel detector may be possible of improving the time resolution. A conceptual block diagram of such a system is shown in Fig. 5.3. It is based on the principle that temporally averaged spectrum is equivalent to spatially averaged one in a certain region. The output signal of each element of the detectors is accumulated in a pulse height analyzer through a circuit with each different time delay.

(3) measurement in a mixed field

All the detectors sensitive to X-rays have some sensitivity to neutrons. It is very difficult to distinguish the pulses due to X-rays from those due to neutrons. An attempt has been done to separate the pulses according to the pulse shape and delay time.

(4) direct measurement of extremely high energy particles

From particle accelerators are emitted X-rays of extremely high energy from several tens of MeV to GeV. High energy bremsstrahlung X-rays are also generated at a limiter of Tokamak-type apparatus which is bombarded by run-away electrons in high-temperature plasmas. In order to measure directly such energetic X-rays, a huge crystal of scintillator will be required in spite of a complexity in correction.

5.2.2. LET spectrum

Idetification of i-th species indispensable for above method is not always necessary. The energy-deposition rate, instead of the particle fluence rate, is measured as a function of the collision stopping power (LET) in human body. The, DE is expressed alternatively as follows:

$$H = \int_0^{\tau_0} \int_0^{\infty} QF(L)\, L\, \psi(L,t)\, dL\, dt$$

$$= \int_0^{\tau_0} \int_0^{\infty} QF(L)\, D(L,t)\, dL\, dt\ , \qquad (5.2)$$

where $\psi(L,t)\, dL$ denotes the fluence rate of mixed species of which LET lies between L and $L + dL$ at a time t, and $D(L,t)$ the absorbed dose per unit LET. The QF as a function of LET, $QF(L)$, is defined by ICRP[6] as shown in Fig. 5.4. Pulse durations of all apecies are assumed to be equal and denoted by τ_0.

It is unnecessary in this method to identify each species. The LET of charged particles is analyzed with a spherical tissue-equivalent (TE) proportional counter developed by Rossi.[7-11] The characteristics of the counter as follows:

(1) The counter can be used for mixed radiations consisting of high energy particles.

(2) It has the same difficulty in measurement in a high-fluence-rate or single-burst field as the spectrometers for energy distribution.

(3) Some errors occur when an observed pulse height spectrum is converted into Y-spectrum and eventually into LET spectrum.

5.2.3. Ionic charge density

Equation (5.2) is transformed as

$$H = D_t\, \overline{QF}\ , \qquad (5.3)$$

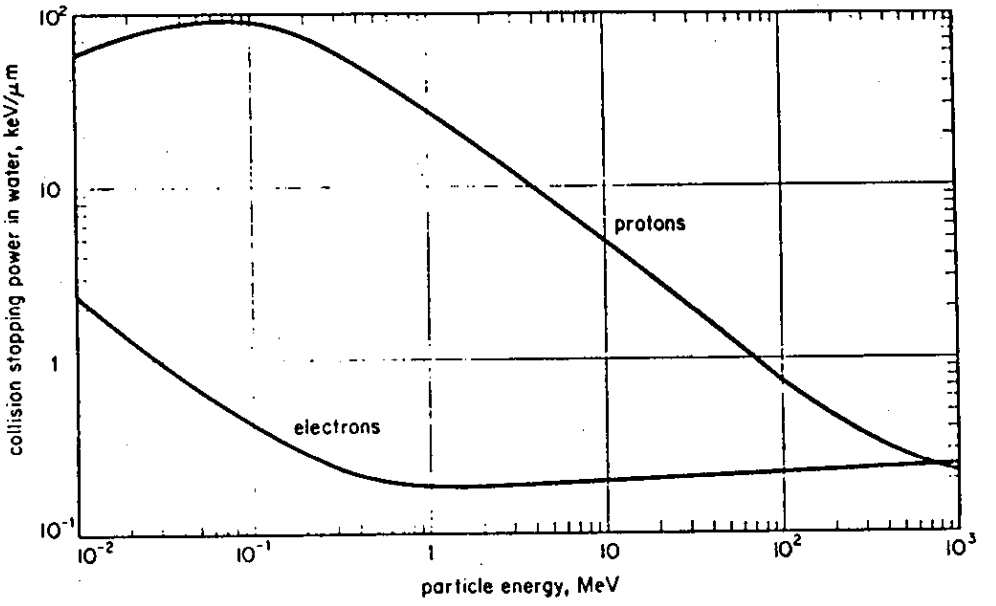

Fig. 5.4. Dependence of collision stopping power in water upon kinetic energy. [ICRP 21 (1971)]

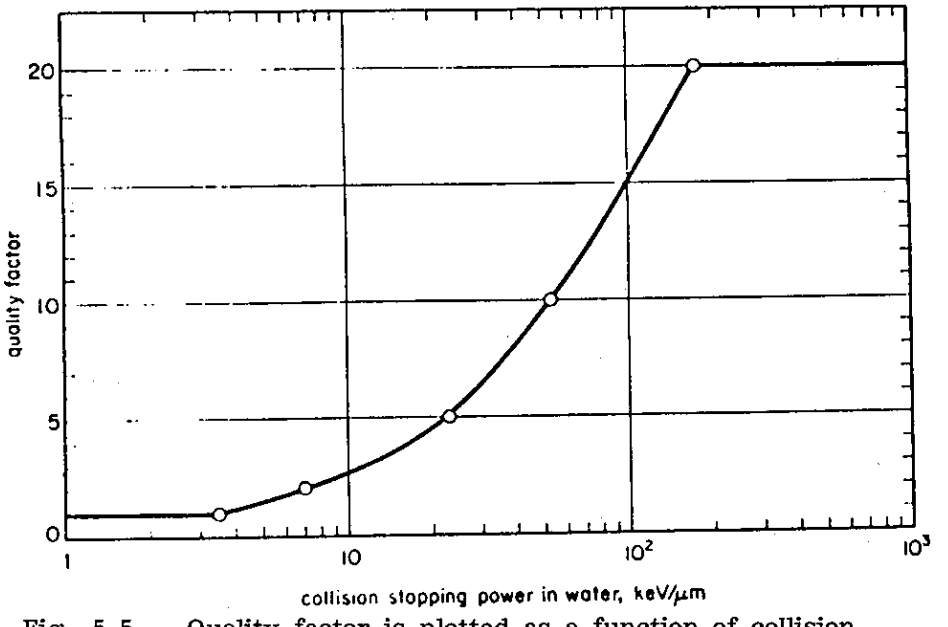

Fig. 5.5. Quality factor is plotted as a function of collision stopping power in water. [ICRP 26 (1977)]

where D_t is the total absorbed dose and $\overline{QF}$ the dose-averaged QF. Namely,

$$D_t = \int_0^{\tau_0} \int_0^{\infty} D(L,t)\ dL\ dt\ , \tag{5.4}$$

$$\overline{QF} = \frac{\int_0^{\tau_0} \int_0^{\infty} QF(L)\ D(L,t)\ dL\ dt}{\int_0^{\tau_0} \int_0^{\infty} D(L,t)\ dL\ dt} \tag{5.5}$$

It is considered in physical concept of interactions of radiations with matter that radiations transfer their kinetic energy into matter eventually by ionization or excitation. Thus, the total absorbed dose is proportional to the number of ion pairs liberated in matter, as expressed by the following formula:

$$D_t = \frac{1}{\rho} \int_0^{\tau_0} \int_0^{\infty} L\ \psi(L,t)\ dL\ dt = \frac{WN_0}{\rho}\ , \tag{5.6}$$

where ρ is the density, N_0 the number of ion pairs, and W the mean energy per ion pair formed, which is assumed to be independent of the radiation quality.

It is most covenient to use an ionization chamber for measuring the number of ion pairs. A major correction factor, collection efficiency, can be determined by such a method as stated in Chaps. 3 and 4. Then, a remaining problem is how the average QF is estimated. Thus, this method with an ionization chamber has the following characteristics:

(1) The total absorbed dose per pulse, in principle, can be measured with a TE ionization chamber in any radiation field.

(2) The techniques for estimating the average QF have not been established in all cases.

It is considered from comparison among three methods that only

the third method described in this subsection have the possibility of applying to all the radiation fields.

5.3. Estimation of average quality factor with ionization chambers

5.3.1. Review of prevailing techniques

An attempt to determine the average QF experimentally has been made by several authors intensively in 1960's.

Pszona[12,13] and Zel'chinskii[14-16] proposed the instruments composed of two detectors: one is a TE ionization chamber for determining the absorbed dose, and the other is a detector having an appropriate response to LET. They assumed that QF is approximately expressed by a function of $aL/(1+bL)$, and proposed to use a detector of which response to LET is expressed as the similar function to QF. Then, the output signal of the detector is a linear function of QF. As such a detector are practically used plastic scintillators, organic scintillators, ionization chambers filled with a liquid dielectric, recombination chambers, which are gaseous chambers operated under unsaturation region.

Sullivan and Baarli[16] took notice of a saturation characteristics of a TE ionization chamber exposed to mixed radiations. This is based on experimental results that the average QF depends on the recombination index, which is defined as the slope of the saturation curve on a full-log scale.

Few methods, however, have been established for pulsed radiations and especially for single burst ones at present. Two methods for evaluating DE in a pulsed radiation field will be proposed in the following.

5.3.2. Effective stopping power

A difference in radiation effects between an X-ray field and a mixed radiation field is ascribed to that in the density of ion pairs liberated by secondary radiations of electrons and protons. In other words, it is ascribed to LET of the charged particles. It is desirable, if possible, to know the distribution of the charged particle fluence in LET in all cases. The measurable quantity with the ionization chamber, however, is only ionic charge density, Q, which is related with the LET as follows:

$$Q = eL\Psi/W \ , \tag{5.7}$$

where e is the electronic charge, and Ψ the total fluence. Actually, eq. (5.7) must be rewritten with the fluence as a function of LET. Then,

$$Q = \frac{e}{W}\int_0^\infty L\,\psi(L)\,dL \ , \tag{5.8}$$

Here, an effective stopping power is defined as the LET averaged over the fluence, that is,

$$\bar{L} = \int_0^\infty L\,\psi(L)\,dL \ / \int_0^\infty \psi(L)\,dL \ . \tag{5.9}$$

Substituting eq. (5.8) into eq. (5.9),

$$\bar{L} = WQ/e\Psi \ . \tag{5.10}$$

where W and e are the constants, Q is determined experimentally, and Ψ will be estimated from a current to be observed with no voltage applied to an electrode of the ionization chamber. Then, the effective LET becomes a measurable quantity. Furthermore, a rough approximation is made, apart from its mathematical meaning:

$$\overline{QF} \ \tilde{=} \ QF(\bar{L}). \tag{5.11}$$

Allowing for the assumption, one can finally estimate DE in mixed fields

from the eqution that

$$H = \overline{QF}\, D \simeq QF(\bar{L})\, D. \qquad (5.12)$$

In Fig. 5.6 is shown a flow-chart to obtain DE experimentally in a way based on the absove assumptions. In the first step, output currents of an abreast-type ionization chamber are observed and the f-value is determined by such a method as was stated in Chap. 3. The ionic charge density corrected by the f-value is converted into the total absorbed dose according to the cavity chamber theory. Next, a current is measured without applying an electric voltage to the chamber. Then, one can determine the total charged particle fluence provided that a cintribution of proton current can be neglected. Finally, multiplying the total absorbed dose by QF corresponding to the effective LET, DE can be obtained.

But, there remain some ambiguities in the flow-chart, that is, measurement of charged particle fluence with the ionization chamber, and assumption that $\overline{QF} \simeq QF(\bar{L})$. It is necessary to discuss validity of the assumptions for practical application.

measurement of charged particle fluence

A current without applying a voltage to an ionization chamber, in general, is due to not only a particle stream in an active volume but also a stream in a gap except for the chamber, i.e. a lead wire, connectors, co-axial cables, and so on. The latter is called a stem current.

Firstly, experiments are carried out in ^{60}Co γ-ray field with a parallel-plate ionization chamber in order to confirm whether charged charged particle fluence is really measurable. The details of the ex-

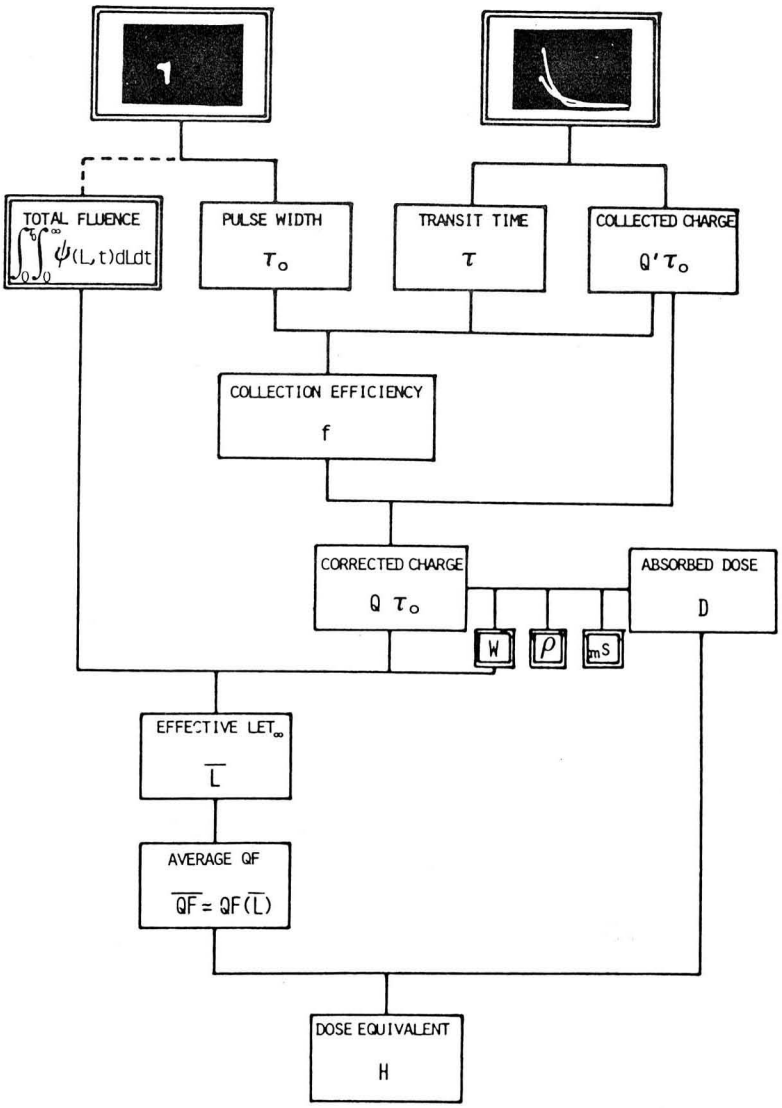

Fig. 5.6. Flow-chart to estimate DE in a single-burst mixed field with an abreast-type ionization chamber.

periments are left to Appendix 5.A. The results obtained are as follows:

(1) A current with no applied voltage, I_0, is independent of the gas pressure in an active volume of the chamber.

(2) The current, I_0, is nearly equal to the mean of positive saturation current and negative one, that is, $I_0 \triangleq \frac{1}{2}(I_{s+} + I_{s-})$. In other words, the mean of absolute values of positive and negative saturation currents gives a true saturation current, that is, $I_s = \frac{1}{2}(I_{s+} - I_{s-})$.

(3) When we cut a lead between electrodes and connectors, a negative current of several per cent of I_0 is still observed. It is probably a stem current (I_{stem}).

(4) The effective LET determined experimentally, $\bar{L}_{exp}$, is larger than theoretical one by about 30 %. About 70 % of this value is ascribed to angular dependence of Compton scattering.

It is concluded that the effective LET can be estimated within about 30 % error in the X-ray energy region higher than several tens of keV.

Another problem is measurement of $\bar{L}$ in a mixed radiation field consisting of X-rays and neutrons. In this case, two species of secondary charged particles have opposite sign to each other. If the fluences of both charged particles are the same, an observed current must be zero. In such a field, however, most part of the absorbed dose is due to protons. In other words, the field can be regarded as a neutron field rather than mixed one. This problem is closely related with the succeeding and the details is discussed below.

approximation that $\overline{QF} \triangleq QF(\bar{L})$

The average QF is expressed by the following formula:

$$\overline{QF} = \int_0^\infty QF(L)\, L\, \psi(L)\, dL \;/\; \int_0^\infty L\, \psi(L)\, dL. \qquad (5.12)$$

For greater simplicity, it is assumed that a secondary radiation field consists of mono-LET electrons and protons. Moreover is introduced a parameter, F_p, which denotes the ratio of proton dose to the total:

$$F_p = L_p \Psi_p / (L_p \Psi_p + L_e \Psi_e) = D_p / D_t, \qquad (5.13)$$

where Ψ is fluence per pulse, D the absorbed dose per pulse, and suffixes e, p and t represents electrons, protons and total, respectively. Then, eqs. (5.9) and (5.11) give

$$\overline{QF} = 1 + [QF(L_p) - 1]\, F_p . \qquad (5.14)$$

From eqs. (5.9) and (5.13) is obtained a relation that

$$\bar{L} = (L_e \Psi_e + L_p \Psi_p)/(\Psi_e + \Psi_p) = L_e L_p / (L_p - F_p L_p + F_p L_e). \qquad (5.15)$$

In Fig. 5.7 are shown the calculated values of $\overline{QF}$ and $QF(\bar{L})$ as a function of the fractional proton dose, where L_e = 0.2 keV/μm and L_p = 10.0 keV/μm. It is seen that $QF(\bar{L})$-value is in general smaller than the average QF. This may be attributed to that an increase in the effective LET contributes little to increase in the corresponding QF because of non-linear function of $QF(L)$. A difference between $\overline{QF}$- and $QF(\bar{L})$-values causes a danger of underestimating DE.

However, it is fortunate that a difference between a true $\overline{QF}$ and a experimentally obtained QF is reduced owing to overestimate of the effective LET in measurement. Namely, a current without voltage applied is not equal to total fluence of secondary electrons and protons but to a difference between electron fluence and proton one. The effective LET obtained experimentally, $\bar{L}_{exp}$, is then expressed by

$$\bar{L}_{exp} = (L_e \Psi_e + L_p \Psi_p) / |\Psi_e - \Psi_p|$$

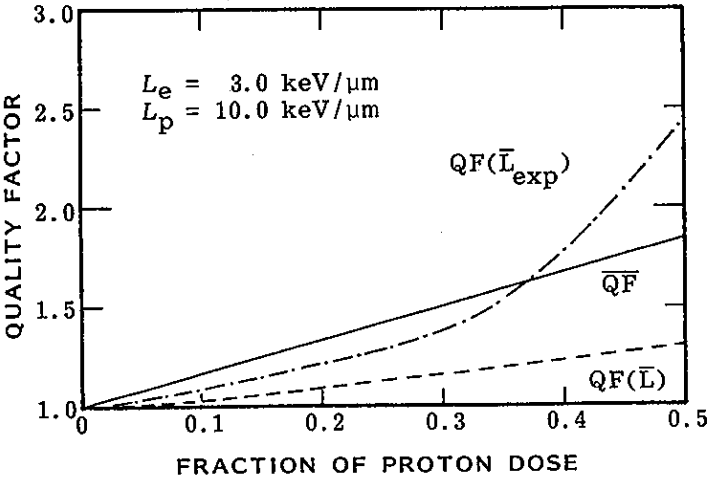

Fig. 5.7. Average QF and the QF corresponding to effective LET as a function of the fraction of proton dose. The LET's are assumed to be 3.0 and 10.0 keV/μm for electrons and protons, respectively.

$$= L_e L_p / |L_p - F_p L_p - F_p L_e| \ . \qquad (5.16)$$

A corresponding QF is shown in Fig. 5.7 by a broken line. As is clear in the figure, $QF(\bar{L}_{exp})$-value approaches to the average QF and it can be said that two values is nearly the same within 10 % deviation for a D_p/D_t-value smaller than 0.44.

5.3.3. Average recombination coefficient

A most distinctive difference between X-rays and mixed radiations lies in LET of secondary charged particles. From a standpoint of irradiated materials, the difference appears as a spatial distribution of the density of ion pairs liberated. In an ionization chamber, the distribution of the ion density is nearly uniform in an X-ray field, whereas it is nonuniform in a mixed radiation field. The nonuniformity of the ion density will cause a spatial vatiation of the recombination loss which is proportional to the product of densities of positive and negative ions. In this section, a relation between the recombination loss in an ionization chamber exposed to mixed radiations and the average QF is discussed in detail, and furthermore a convenient method for estimating the average QF is discussed according to the following steps:

(1) The average recombination coefficient in a mixed radiation field is defined.

(2) A relation between the average recombination coefficient and the average QF is clarified.

(3) A method for estimating the average QF is proposed.

<u>average recombination coefficient</u>

In an ionization chamber exposed to mixed radiations consisting of

X-rays and neutrons, the gas in the active volume is ionized mainly by secondary electrons and recoil ions which are ejected from the wall as a result of collisions between primary radiations and the wall materials. Some of the ions libearted by the secondary radiations will disappear on the way to the collecting electrodes owing to recombination. The recombination processes are in general divided into columnar and volume recombinations:

(1) columnar (initial) recombination

The recombination occurs between positive negative ions formed in the track of a single ionizing particles such as protons, α-particles and heavy ions. Jaffé derived an excellent theoretical formula for the f-value.[17,18]

(2) volume (general) recombination

The recombination occurs between ions formed in the track of different ionizing particles such as electrons. An approximate formula for the f-value was given by Boag,[19] and an exact f-value was calculated in Chap. 2.[20]

Their original forms, however, cannot be applied to a mixed field where both columnar and volume recombinations take place.

In this situation, the following assumptions are made for simplicity:

(1) Ion pairs liberated by secondary electrons are uniformly distributed in the active volume.

(2) The LET of recoil protons is constant along the tracks, namely, the linear ion density along the track is constant.

(3) Ion pairs around the proton track are uniformly distributed within a radius of several microns.

(4) The proton tracks are approximately parallel to the collecting electric field applied to a parallel-plate ionization chamber.

(5) The diffusion loss is dominated by the ion loss due to the drift by the electric field and the recombination.

(6) The recombination coefficient itself is independent of the ion density.

A distribution of ions in a parallel-plate ionization chamber is illustrated in Fig. 5.8 . Allowing for the assumptions, the density of ions liberated by the secondary electrons, n_e, and the density of ions around the proton track, n_p, are expressed as follows:

$$n_e = L_e \Psi_e / W \text{ , and } n_p = L_p / (WS), \tag{5.17}$$

where L denotes LET, Ψ the fluence per radiation pulse, S the cross-sectional area of spurs around the proton track, W the mean energy expended per ion pair formed, and the suffixes e and p represent electrons and protons, respectively. The assumtion (1) means that the density, n_e, is constant at any place in the active volume. The assumtions (2) and (3) mean that the density, n_p, is superposed on n_e in the proton spurs. Then, the active volume is divided into two regions. One is the region where the ion density is the sum of n_e and n_p, and the relative volume is the product of the proton fluence and the area of the spurs. In the other region the ion density is n_e and the relative volume is $(1-\Psi_p S)$. Furthermore, it is permitted to apply the f-value for volume recombination to each region owing to the assumtions (4) and (5).

Then, a nonuniformity of the ion density causes a spatial difference of the f-value, which is a function of the ion density as stated in Chap. 2. Thus, an average recombination coefficient in a mixed field

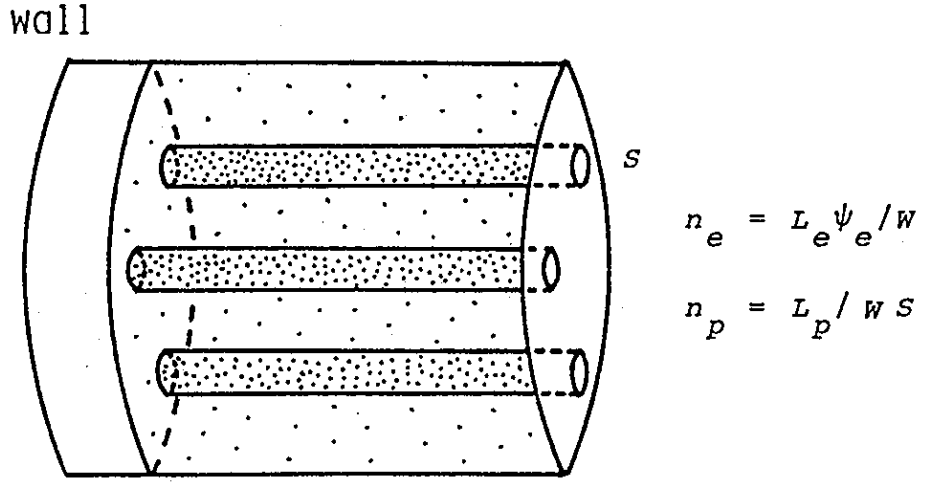

Fig. 5.8. Illustration of ion distribution in a parallel-plate ionization chamber exposed to mixed radiations consisting of neutrons and X-rays. The gas is ionized directly by recoil protons and secondary electrons.

is introduced as follows:

$$\bar{\alpha} = \frac{\text{(recombination loss in the volume)}}{\text{(number of ions generated in the volume)}^2} . \quad (5.18)$$

The amount of recombination loss is expressed by the density of generated ions multiplied by a factor of (1–f), as is clear from the definition of the f-value. Let the f-value in two regions be f_1 and f_2, respectively, and eq. (5.18) becomes

$$\bar{\alpha} = \frac{(n_e + n_p)(1-f_1)\Psi_p S + n_e(1-f_2)(1-\Psi_p S)}{(n_e + n_p \Psi_p S)^2} . \quad (5.19)$$

It is anticipated from the equation that the $\bar{\alpha}$-value will vary with the fluence and LET of the secondary charged particles even though the total ion density is constant. In other words, the $\bar{\alpha}$-value depends on the fractional dose by the recoil protons even though the the total absorbed dose is constant. Figure 5.9 shows the dependence of the relative value of $\bar{\alpha}$ on the fractional dose by the protons. It is assumed in the calculations that L_e and L_p are 0.2 and 10.0 keV/μm in water, respectively, the gas density is 1.0×10^{-3} g cm^{-3}, the gap distance between the electrodes 1.0 cm, the ion mobility in the gas 1.34 cm^{2}s^{-1}V^{-1}, the applied voltage 1000 V, and the cross-sectional area of the spurs 1.0×10^{-5} cm^2. The f-value calculated in Chap. 2 are used. As is clear in the figure, the $\bar{\alpha}$-value is 1.0 when the proton dose is 0, and increases monotonously with the proton dose.

For greater simplicity, it is assumed that the expression of recombination loss of $n(1-f)$ can be replaced by αn^2. Then, eq. (5.19) is rewritten by the following formula:

$$\frac{\bar{\alpha}}{\alpha} = 1 + \left(\frac{L_p \Psi_p}{L_e \Psi_e + L_p \Psi_p}\right)^2 \left(\frac{1 - \Psi_p S}{\Psi_p S}\right) . \quad (5.20)$$

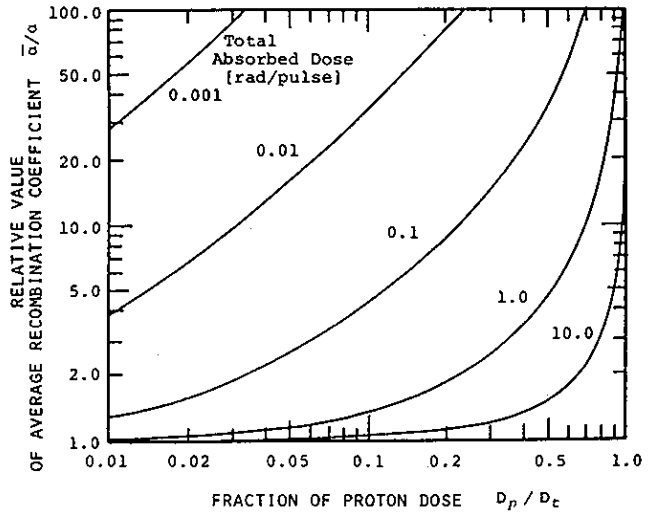

Fig. 5.9. The relative value of the average recombination coefficient as a function of the fractional dose by protons. The average recombination coefficient increases monotonously with the proton dose. Proton LET: 10.0 keV/μm, electron LET: 0.2 keV/μm, gas density: 1.0×10^{-3} g cm^{-3}, ion transit time: 7.5×10^{-4} s, cross-sectional area of proton spurs: 1.0×10^{-5} cm^2.

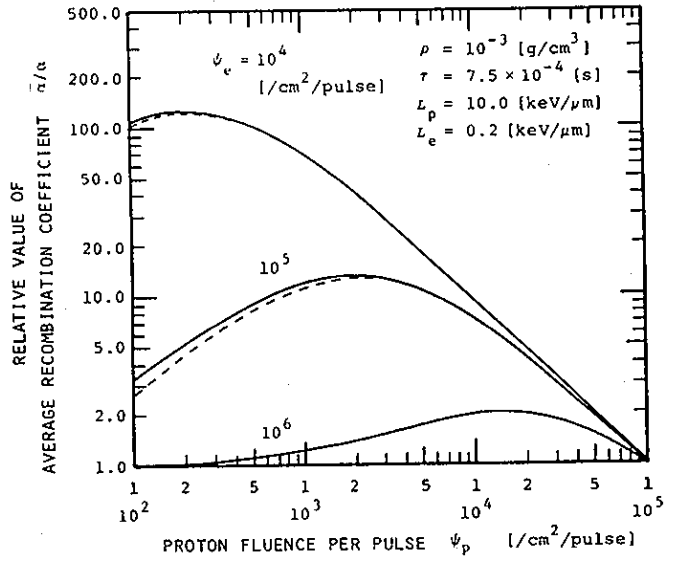

Fig. 5.10. The dependence of the $\bar{\alpha}/\alpha$-value on the proton fluence for constant values of L_p, L_e and ψ_e. Solid lines represent the results obtained with eq. (5.20), and broken lines those obtained with eq. (5.19). There is no significant difference between two results.

In order to ascertain the validity of the assumption, the results of the calculations of eqs. (5.19) and (5.20) are compared in Fig. 5. 10, where the $\bar{\alpha}/\alpha$-value is shown as a function of the proton fluence for constant values of L_e, L_p and Ψ_e. It is found that the simplified formula of eq. (5.20) will not cause a significant error for practical use.

Equation (5.20) implied that the $\bar{\alpha}$-value is determined by two parameters: one is $L_p\Psi_p/(L_e\Psi_e + L_p\Psi_p)$ which is equal to the fractional dose by the protons, and the other is $\Psi_p S$ which expresses the fractional volume of the proton spurs. Namely, the $\bar{\alpha}$-value is closely related with the absorbed dose and LET of the recoil protons. From this result, it is considered that the $\bar{\alpha}$-value can be regarded as a parameter characteristic of the mixed radiation field.

relation between $\overline{QF}$ and $\bar{\alpha}$

Eliminating L_e and Ψ_e, eq. (5.20) becomes

$$\bar{\alpha}/\alpha = 1 + [(1-\Psi_p S)L_p^2\Psi_p/S]/(D_t C)^2 , \qquad (5.21)$$

where D_t is the total absorbed dose and C is the dose-to-energy conversion factor. The equation has three constants (α, S, C) and two quantities to be determined experimentally (D_t, $\bar{\alpha}$). The experimental and theoretical values of α have been published by several authors, and they lie between 1.1×10^{-6} and 1.8×10^{-6} $cm^3 s^{-1}$ in 1 atm air. Concerning the S-value, it is considered to be of the order of 10^{-6} or 10^{-5} cm^2. The constant C includes the gas density and the ratio of the mass stopping power in tissue to that in gas material. Dividing the density of generated ions by the C-value, the total absorbed dose in tissue can be obtained according to the cavity chamber theory.[21] The $\bar{\alpha}$-value can also be determined experimentally with eq. (5.18),

where the recombination loss is evaluated from the ionic charges collected by the ionization chamber and the f-value determined in such a way as described in Chap. 3.

Thus, the unknown parameters remaining in eq. (5.21) are only L_p and Ψ_p. Both values, of course, can never be determined mathematically from eq. (5.21) only, but they must satisfy the following physical conditions:

(1) The solutions of L_p and Ψ_p are real numbers.

(2) $L_p < 91$ keV/μm.

(3) $D_p = L_p \Psi_p / C \leq D_t$.

The condition (1) or (3) gives a lower limit of the L_p-value and condition (2) an upper limit. Then, the average QF is calculated as a function of L_p by substituting the L_p- and Ψ_p-values into the following equation:

$$\overline{QF} = [QF(L_p)\, D_p + (D_t - D_p)]/D_t \,, \qquad (5.22)$$

where QF as a function of LET, $QF(L)$, is given by ICRP.[6] The first term of the numerator on the right hand side represents DE by the protons and the second one DE by the electrons.

The procedure mentioned above is actually followed and shown in Figs. 5.11 (a), (b) and (c), where the D_t-value is assumed to be 0.01 rad per pulse and the $\bar{\alpha}/\alpha$-value to be 10.0. Figure 5.11 (a) shows the Ψ_p-value as a function of L_p-value, which is calculated by regarding eq. (5.21) as a quadratic equation with respect to Ψ_p. The lower limit of the L_p-value determined by the condition (1) is found to be 3.75 keV/μm. The corresponding Ψ_p-value lies widely between 35.0 and 1.0×10^5 cm^{-2} per pulse. The proton dose is calculated with the formula of $L_p \Psi_p / C$ and shown in Fig. 5.11 (b) as a function of L_p-

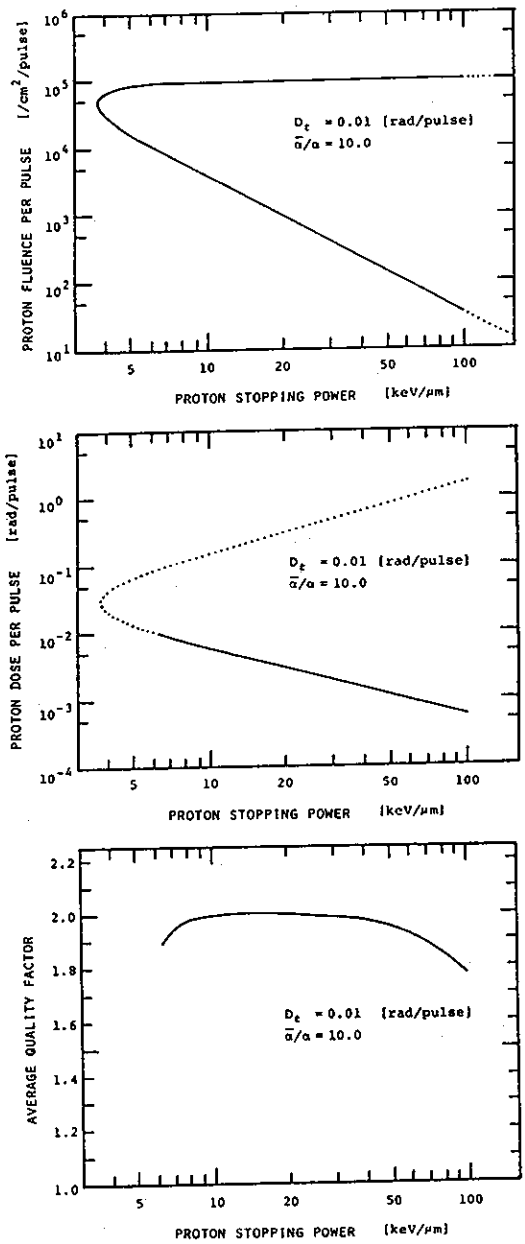

Fig. 5.11. The procedure for estimating the average QF from the total absorbed dose and the average recombination coefficient. (a) proton fluence, (b) proton dose and (c) average QF are shown as a function of proton LET.

value. The condition (3) gives a lower limit of 6.3 keV/μm. Finally, the average QF is calculated with eq. (5.22) and shown in Fig. 5.11 (c). The figure shows that the average QF lies between 1.78 and 2.01. The result shows a fact that DE can be estimated only from experimental values of D_t and $\bar{\alpha}$ with some deviation. In this case, the values of 0.01 rad and 10.0 for D_t and $\bar{\alpha}/\alpha$ give a DE of 0.019 rem per pulse with 6 % deviation.

The calculated results for several D_t- and $\bar{\alpha}/\alpha$-values are summerized in Fig. 5.12, where the average QF is shown as a function of the $\bar{\alpha}/\alpha$-value for three D_t-values of 0.01, 0.05 and 0.1 rad per pulse. The increase in the $\bar{\alpha}/\alpha$-value corresponds to that in the proton dose, as pointed out in Fig. 5. 9 . It is reflected on the increase in the average QF. It is concluded from the figure that the average QF can be estimated if only the total absorbed dose and the average recombination coefficient could be evaluated with an ionization chamber.

experimental determination of $\overline{QF}$ and DE

In Fig. 5.13 is shown the flow-chart of the experimental determination of DE with an ionization chamber. It is divided into three stages:

(1) determination of f-value

It is necessary to know beforehand the ion transit time, the recombination coefficient, the gas density and W-value. The pulse duration must be measured with a scintillator or a streak camera. The quantities to be measured with the chamber are the ionic charges collected at different applied voltages. A succeeding procedure has already been stated in Chap. 3. If the radiations are

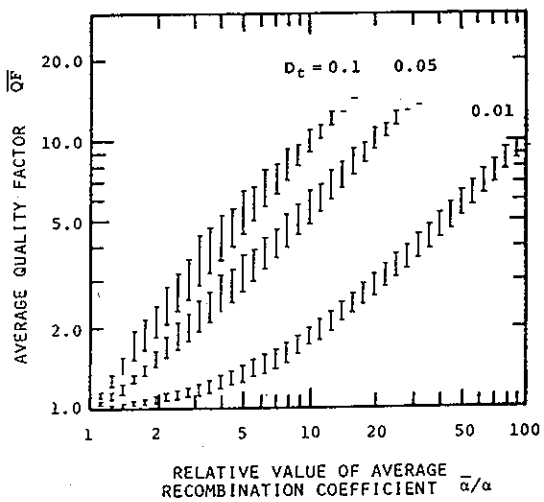

Fig. 5.12. The average QF as a function of $\bar{\alpha}/\alpha$-value for three D_t-values of 0.01, 0.05 and 0.1 rad per pulse. It is found that the average QF can be estimated if only the total absorbed dose and the average recombination coefficient could be evaluated.

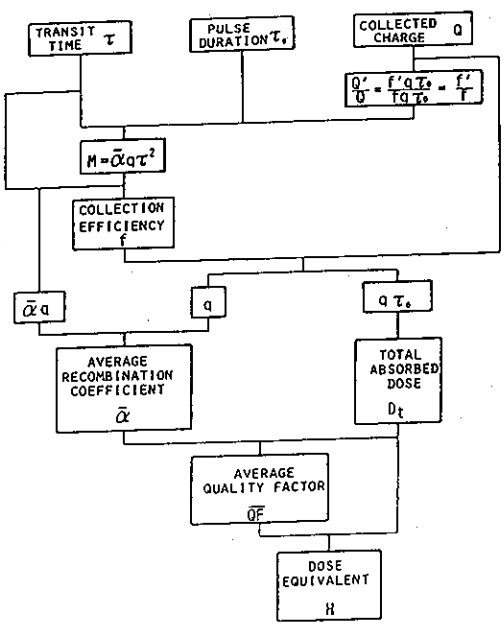

Fig. 5.13. Flow-chart of the procedure for estimating DE experimentally with an abreast-type ionization chamber. The collection efficiency is determined by the method described in Chap. 3 and the average QF is estimated in the procedure shown in Fig. 11.

singly pulsed, it is necessary to use an abreast-type ionization chamber. In addition, M-value ($M = \bar{\alpha} q_0 \tau^2$) is also obtained when the f-value is determined.

(2) evaluation of total absorbed dose and average recombination coefficient

Correcting the number of collected ions (charge) by the f-value, and the number of ions (charge) liberated in gas material is obtained. It is to be converted into the absorbed dose in tissue according to the cavity chamber theory. On the other hand, dividing the M-value obtained in the previous stage by the ion transit time and the square of the ion production rate, one obtained the average recombination coefficient.

(3) estimation of $\overline{QF}$ and DE

The average QF can be estimated in such a procedure as is mentioned above in detail. After all, DE is obtained by the product of the total absorbed dose and the average QF.

The method can be applied not only the pulsed radiations but also to continuous ones, since the quantities to be measured are only the collected charges. There exists, however, a weak point of difficulty in application to extremely high-fluence-rate neutron field, where the proton tracks in the chamber becomes superposed on each other and therefore the densities in the two regions become undistinguishable.

5.4. Experimental results and discussions

5.4.1. Experimental apparatus

The experiments on DE evaluation were carried out in a pulsed and mixed radiation field generated by the 35 MeV electron linear ac-

celerator installed at the Institute of Scientific and Industrial Research, Osaka University.[22,23] From a target bombarded by such a high energy electrons, bremsstrahlung X-rays emitted in forward direction and photo-neutrons isotropically. The fluence ratio of neutrons to X-rays varies in general with (1) energy of primary electrons, (2) angle with the electron beam, (3) atomic number of target material and (4) thickness of the target, because of energy dependence of the cross section for photo-nuclear reactions and difference in emission characteristics between X-rays and neutrons. The total absorbed dose is also a function of (5) current of primary electrons and (6) distance from the target. Main purpose of this experiment is placed on the evaluation of the average QF as a function of the angle with an electron energy fixed.

A parallel-plate ionization chamber stated in Chaps. 3 and 4 were used. An abreast-type chamber is desirable for practical use. But in the experiment where radiation pulse is repeated with satisfactory reproducibility, an ordinary chamber with single active volume was utilized in principle. Then, the f-value was obtained by the saturation curve method[24] rather than the charge ratio one.[20] The materials of chamber wall, kind of gas filling the chamber and the active volume were varied according to respective purposes.

5.4.2. Angular dependence of total absorbed dose

There is a minor factor determining the total absorbed dose such as the depth in irradiated materials as well as major factors of the beam current and distance from the target. The depth-dose curves for X-rays have already been shown in Chap. 3. The depth at which the

dose reaches to the maximum varies generally with X-ray energy. In this case, the curves will be modified by contribution of neutrons to the dose. Thus, at first the angular distribution of the depth-dose curves was measured with a graphite chamber and a polyethylene one. The experimental conditions were as follows: a target is tungsten of which diameter is 20 mm and thickness is 5 mm, the beam energy is 28 MeV and a distance from the target is 30 cm. The results are shown in Figs. 5.14 (a) and (b) where the ionic charges per 1 μC-electrons are plotted against the wall thickness in $g\,cm^{-2}$. In case of a graphite chamber, contribution of neutrons is considered to be negligible. The angular dependence of the effective X-ray energy appears as the shift of the peak of the ionic charges. In Fig. 5.14 (b) is found a distinctive increase near the surface due mainly to recoil protons. In other words, the angular dependence of the total absorbed dose is modified by the wall thickness.

5.4.3. Angular dependence of average quality factor

The average QF and DE, in general, varies with the depth in tissue as well as the total absorbed dose. The DE used in radiation protection is, in a strict sense, the dose equivalent index (DEI), which is the maximum DE in tissue of a sphere with a diameter of 30 cm. However, in this experiment the average QF and DE at a certain depth is to be measured.

At first, a method for estimating the average QF from the average recombination coefficient was applied to a mixed radiation field generated by bombarding a tungsten target with 28 MeV or 20 MeV electrons. The chamber wall consists of two thin sheets of 200 μm polyethylene

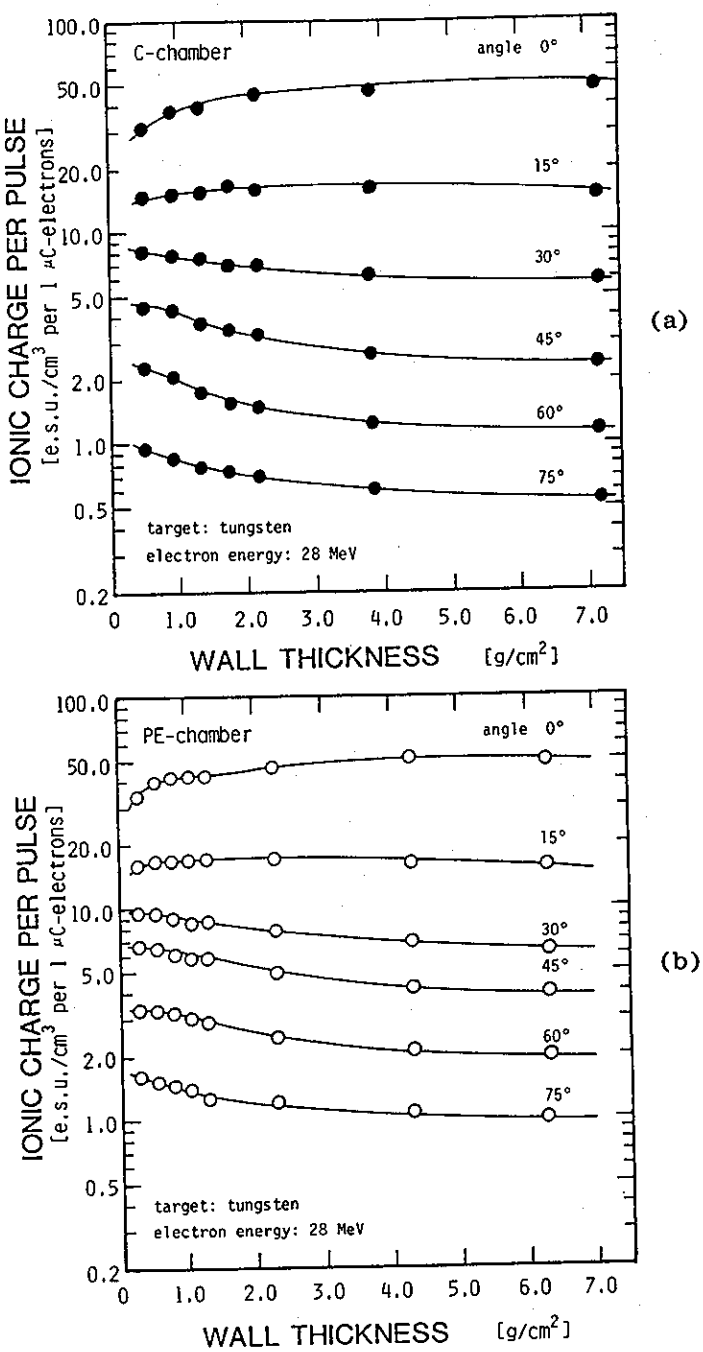

Fig. 5.14. Depth-dose curves for various angles to the electron beam. Electron energy: 28 MeV, distance from W-target: 30 cm. (a) graphite wall and (b) polyehtylene wall.

and water of 30 mm thickness. Accordingly, the field of the secondary radiations in the active volume is approximately equivalent to that in tissue at a depth of 30 mm. The results are shown in Figs. 15 (a), (b) and (c), which represent the angular dependences of the total absorbed dose, the average recombination coefficient and the average QF, respectively. All the values in the figures are evaluated according to the flow-chart shown in Fig. 5.13.

Next was applied another proposed method for estimating the average QF from the effective LET. However, it was very difficult to measure directly the current due to a stream of secondary charged particles at high angle because the current without a voltage applied becomes so low as to be comparable with the stem current. Then, the average QF could not be estimated except for low angles. The effective LET became from about 2.0 to 3.0 with increasing the angle up to 15°, but the corresponding $QF(\bar{L}_{exp})$-value remained 1.0.

In order to ascertain the validity of the proposed methods, comparison with other method in common use was carried out in the mixed radiation field.

energy specra

Energy spectra of bremsstrahlung X-rays and photo-neutrons for various electron energies and targets have been obtained experimentally and theoretically by many authors.[25-39] A typical X-ray energy spectrum in a reference[28] is shown in Fig. 5.16, which is adopted in the succeeding calculations in spite of a little error due to difference in condition of the linear accelerator operation. Concerning the photo-neutrons, we assume that both energy spectrum and the fluence rate would be independent of the angle with the electron beam. Measure-

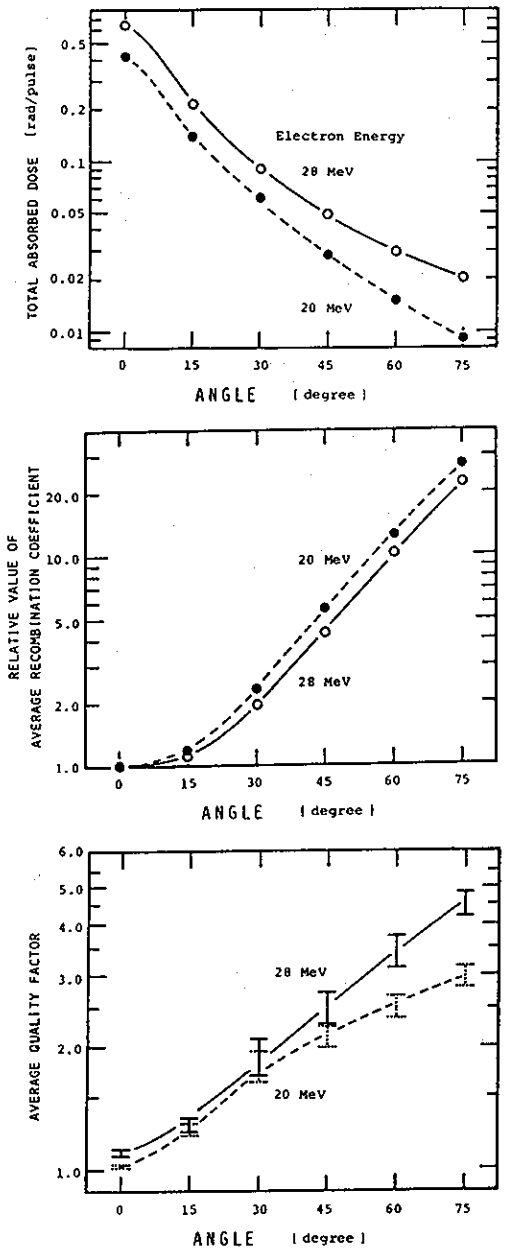

Fig. 5.15. Angular dependence of (a) total absorbed dose, (b) average recombination coefficient and (c) average quality factor. Pulse duration: 50 ps, distance from W-target: 20 cm.

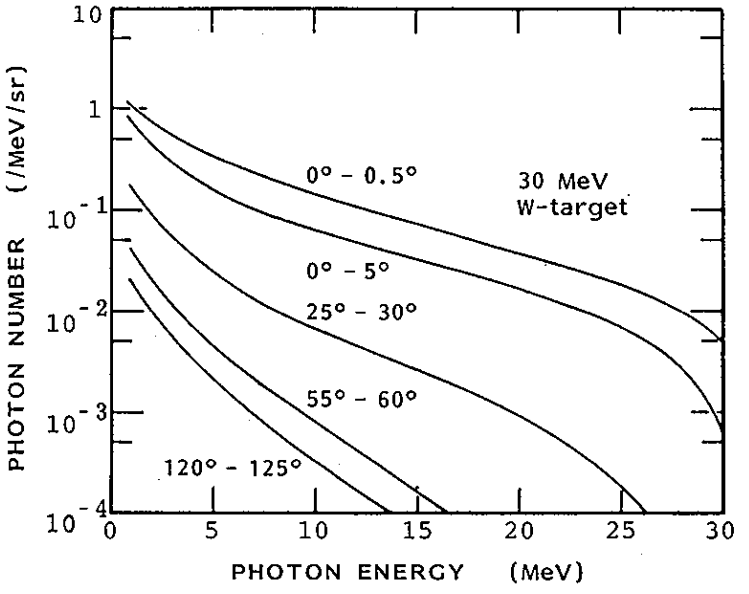

Fig. 5.16. Energy spectra of bremsstrahlung X-rays emitted from a W-target for several angles. [M.J.Berger & S.M.Seltzer: Phys. Rev. C 2 (1970) 621]

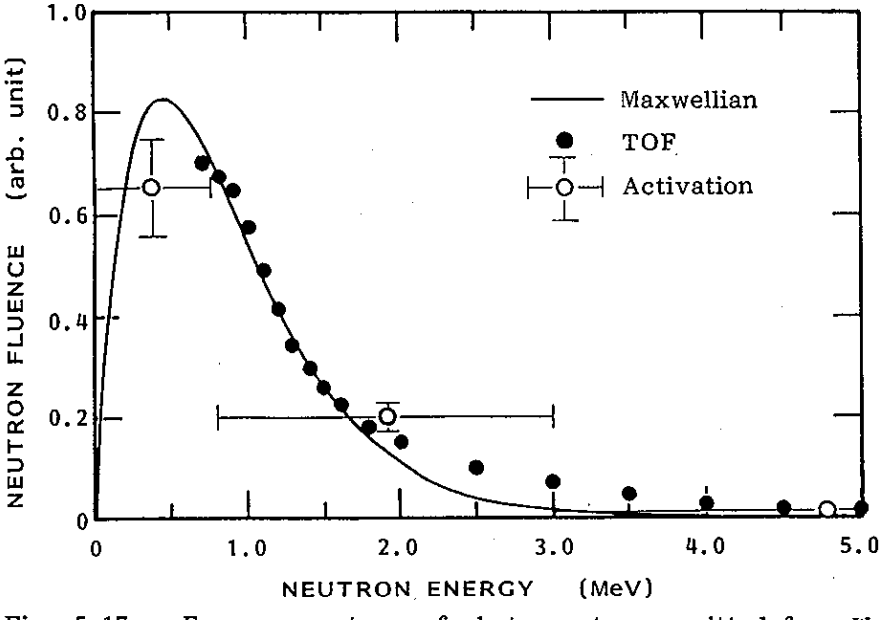

Fig. 5.17. Energy spectrum of photo-neutrons emitted from W-target bombarded by 28 MeV-electrons. Experimental results by TOF method are shown by dots, and those by activation method by circles. A Maxwellian distribution is also shown by a solid line.

ments by TOF and activation methods have been performed and the results[40] are shown in Fig. 5.17 by dots and circles, respectively. A solid line in the figure represents an energy spectrum obeying a Maxwellian distribution of which characteristic parameter of a nuclear temperature is 0.44 MeV. Let ϕ be the fluence, p' the fluence-to-dose conversion factor and p the fluence-to-DE conversion factor, the average QF can be expressed as follows:

$$\overline{QF} = \sum_i \int_0^\infty p_i(E)\,\phi_i(E)\,dE \;/\; \sum_i \int_0^\infty p'_i(E)\,\phi_i(E)\,dE$$

$$= \frac{\int_0^\infty E_x \phi_x(E_x) \frac{\mu_{en}(E_x)}{\rho}\,dE_x + \int_0^\infty p(E_n)\,\phi_n(E_n)\,dE_n}{\int_0^\infty E_x \phi_x(E_x) \frac{\mu_{en}(E_x)}{\rho}\,dE_x + \int_0^\infty p'(E_n)\phi_n(E_n)\,dE_n}, \quad (5.23)$$

where $\mu_{en}(E_x)$ is the energy absorption coefficient for X-rays, and $p(E_n)$ and $p'(E_n)$ are tabulated in the literature[5] recommended by ICRP. The results of calculations of eq. (5.23) are shown in Fig. 5.18 as a function of the angle. The first term of the numerator on the right hand side of eq. (5.23) represents the collision kerma at the surface rather than the absorbed dose at a certain depth. The experimental results of the depth-dose curves shown in Fig. 5.18 shows that the absorbed dose increases with the depth until the CPE condition is satisfied, i.e. the absorbed dose becomes equal to the collision kerma. Namely, the X-ray dose in eq. (5.23) is in general overestimated, i.e. the average QF is underestimated.

LET distribution of absorbed dose

The distribution of the absorbed dose in LET has been measured

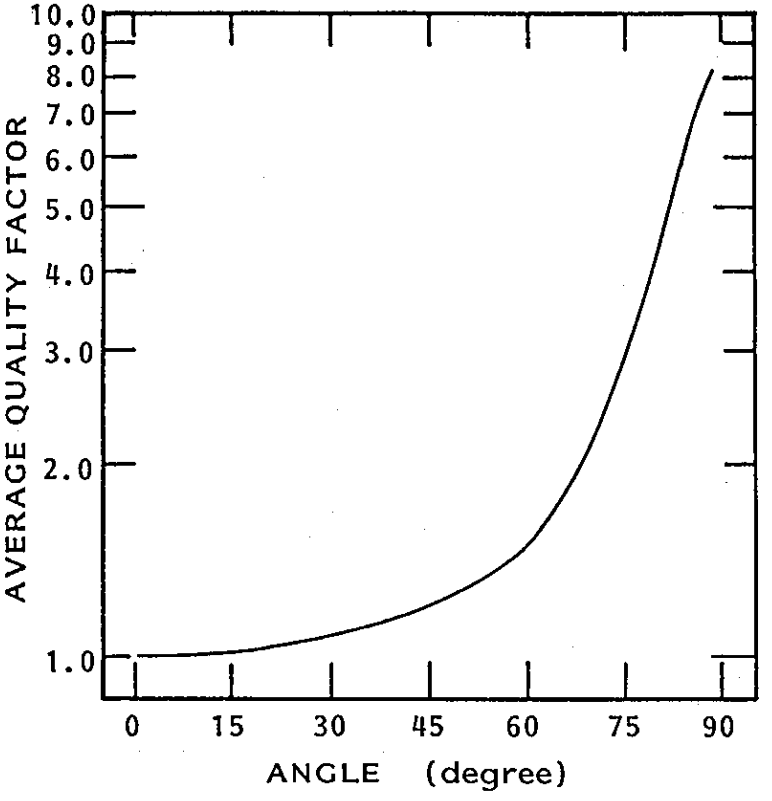

Fig. 5.18. Angular dependence of average QF evaluated from theoretical and experimental energy spectra of X-rays and neutrons.

with a so-called Rossi counter, which is a spherical TE proportional counter. (Appendix 5.B) A typical LET spectrum is shown in Fig. 5.19, where the electron energy is 28 MeV and the angle is 60°. The average QF is calculated by the following formula:

$$\overline{QF} = \int_0^\infty QF(L)\, D(L)\, dL \;/\; \int_0^\infty D(L)\, dL \;. \qquad (5.24)$$

In Fig. 5.20 is shown the angular dependence of the average QF. At an angle lower than 45°, the spectra could not be obtained because the fluence rate became so high that duplication of radiation pulses occurred in the counter.

separate measurement of absorbed doses

Both X-ray dose and neutron dose have been measured separately with two ionization chambers having different sensitivities to neutrons. (Appendix 5.C) The results are shown in Fig. 5.21, where both fractional doses due to X-rays and neutrons are plotted against the angle to the electron beam with an energy of 28 MeV. The bars in the figure is not attributed to experimental errors in measuring the ionic charges collected by a graphite and a polyethylene chamber, but to energy dependence of neutron sensitivity of the graphite chamber. Then, the average QF is obtained by

$$QF = (D_x + \overline{QF}_n D_n)/(D_x + D_n) \;, \qquad (5.25)$$

where $\overline{QF}_n$ is the average QF only for neutrons and is evaluated from the neutron energy spectrum shown in Fig. 5.17 to be 10.2. In Fig. 5.22 is shown the angular dependence of the average QF obtained by the present method.

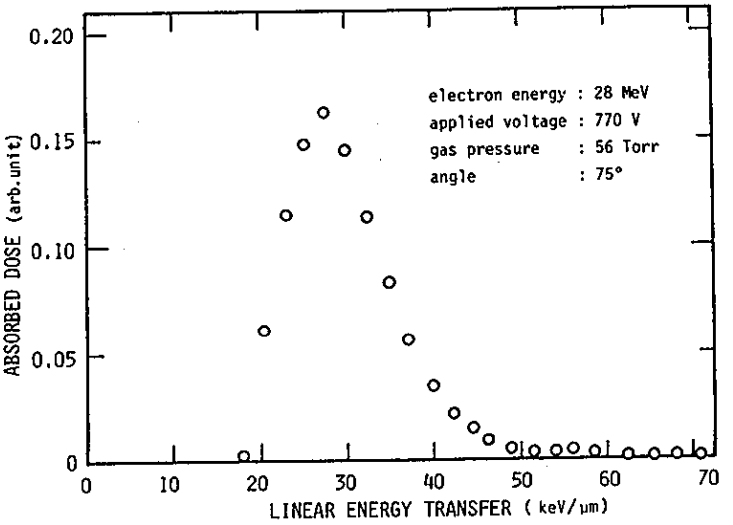

Fig. 5.19. A typical LET distribution of absorbed dose obtained with a Rossi counter. Electron energy: 28 MeV, angle: 60°. A gas pressure in the counter was adjusted to be 56 Torr in order to attain an effective diameter in tissue of 1 μm.

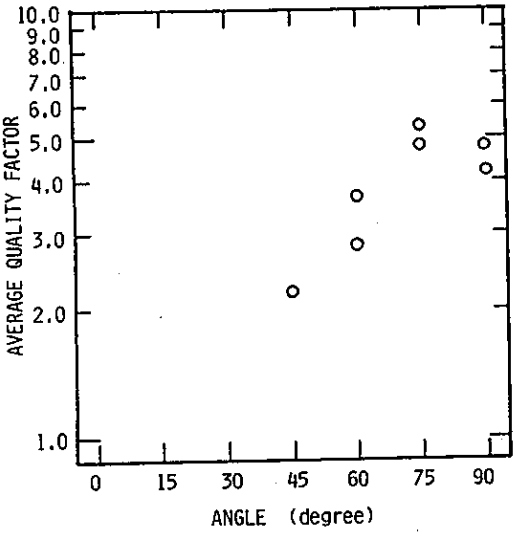

Fig. 5.20. Angular dependence of average QF evaluated from experimental results of LET distribution of absorbed dose shown in Fig. 5.21.

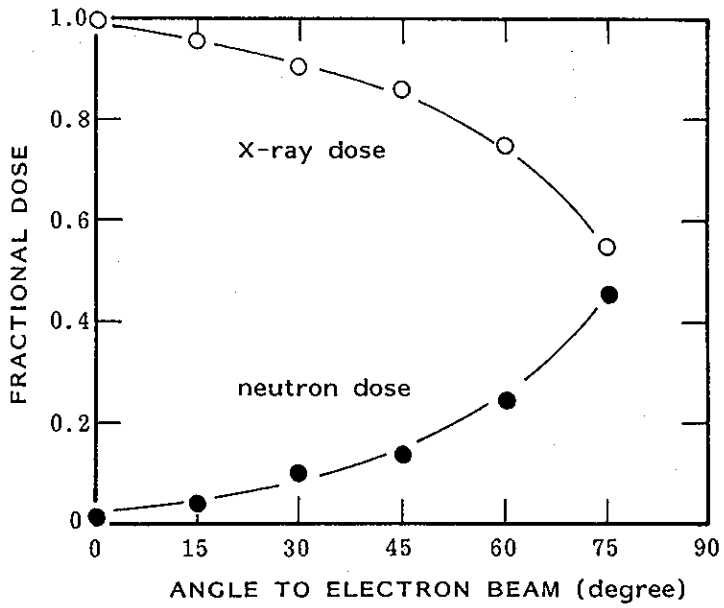

Fig. 5.21. Fractional doses due to X-rays and neutrons as a function of the angle to electron beam. Electron energy: 28 MeV.

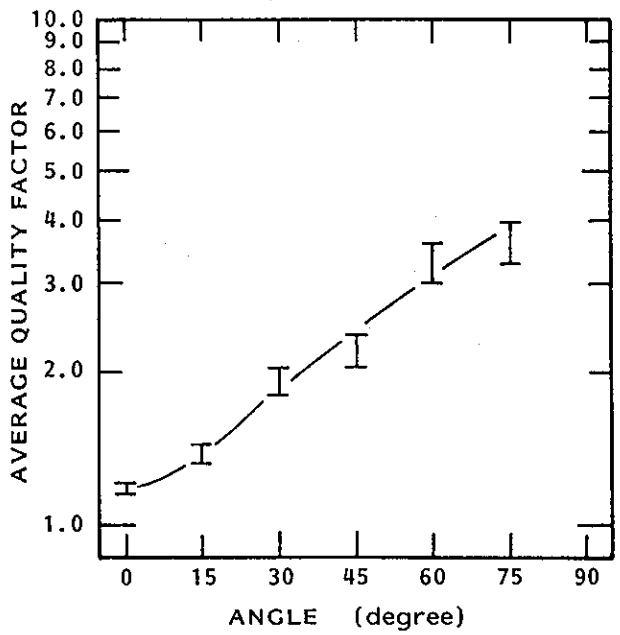

Fig. 5.22. Angular dependence of average QF evaluated from separate measurement of absorbed doses with two ionization chambers.

The average QF's evaluated by various methods are summerized in Table 5.2 and Fig. 5.23 as a function of the angle to the electron beam. It is found from the comparison with the results obtained by proposed methods that a method using the effective LET gives a lower value of the average QF, and that using the average recombination coefficient gives a higher value. Namely, the latter method is on the safety side from a standpoint of radiation protection. It is concluded that a proposed method for estimating DE from the average recombination coefficient has a satisfactory applicability to pulsed and mixed radiations. There is, however, a room for improvement of the method for a mixed or neutron field of extremely high fluence rate. In such a field, it is desirable to apply the method in combination with others auch as a method using the effective LET, separate neasurement, and so on.

5.5. Concluding remarks

Radiations emitted from high energy particle accelerators and apparatus for fusion research have marked characteristics such as extremely high energy, extremely high fluence rate, single burst, and mixture of various particles. Dosimetry of such radiations has been discussed in the present chapter, and the following results were obtained:

(1) Basic concept of dosimetry of mixed radiation fields has been refined for practical purpose.

(2) Methods for evaluating the dose equivalent were classified into three categories according to the radiation quantity to be measured. Merits and demerits of each method to various types of radiation fields were clarified.

(3) Two procedures based on the ionization chambers have been pro-

Angle	Effective LET	Average α	Energy Spectra	LET Spectrum	Separate Doses
0	1.0	1.08 1.11	1.00	–	1.16 1.21
15	1.0	1.23 1.33	1.03	–	1.33 1.44
30	–	1.68 2.08	1.10	–	1.81 2.04
45	–	2.25 2.71	1.21	2.2	2.06 2.37
60	–	3.11 3.69	1.48	2.8 3.6	3.01 3.59
75	–	4.16 4.79	3.23	4.0 5.3	3.24 3.94

Table 5.2. Comparison of various methods for estimating the average QF. The second and the third columns represent the results obtained by the proposed methods.

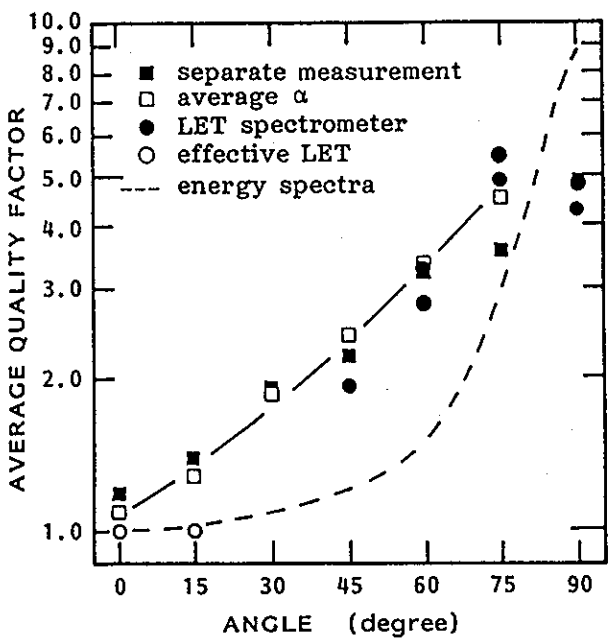

Fig. 5.23. Angular dependence of the average QF estimated by various methods.

posed for estimating the average quality factor in a mixed radiation field consisting of neutrons and X-rays. It was found that the quality factor could be estimated by measuring the effective stopping power or the average recombination coefficient which was regarded as a parameter characteristic of mixed fields.

(4) The proposed methods have been actually applied to a pulsed and mixed radiation field consisting of bremsstrahlung X-rays and photoneutrons generated by an electron linear accelerator.

(5) The proposed methods have been compared with other ones, i.e. theoretical calculation of energy spectrum of bremsstrahlung X-rays, measurement of neutron energy spectrum by TOF and activation methods, measurement of LET distribution of the absorbed dose with a Rossi counter, separate measurement of neutron and X-ray doses with two ionization chambers, Applicability of the proposed methods was experimentally confirmed.

Appendix 5.A. Effective stopping power in X- and γ-ray fields

It is the purpose of the section to confirm a possibility of direct measurement of the effective LET. Experiments are carried out in ^{60}Co γ-ray field.

The definition of the effective LET described in eq. (5.9) is rewritten with a saturation current of a parallel-plate ionization chamber, I_s, and a current without a voltage applied, I_0, in the following formula:

$$\bar{L} = \frac{\text{absorbed energy per unit volume}}{\text{electron fluence}}$$

$$= \frac{WI_s/eSd}{I_0/eS} = \frac{WI_s}{dI_0} , \qquad (5.A.1)$$

where S is the area of collecting electrode, d the gap distance. Experimentally, the effective LET becomes as follows provided that the CPE condition should be satisfied, the practical range of Compton electrons and the linear attenuation coefficient are denoted by R and μ, respectively, and the condition that $\mu R \ll 1$ should be satisfied:

$$\bar{L}_e = \mu_{en} E/\mu R . \qquad (5.A.2)$$

On the other hand, the effective LET is theoretically expressed by

$$\bar{L} = \int_0^{T_{max}} \phi(E,T)\, L(T)\, dT \Big/ \int_0^{T_{max}} \phi(E,T)\, dT, \qquad (5.A.3)$$

where $\phi(E,T)\,dT$ is the fluence of scattered electrons of which energy lies between T and $T + dT$ for a primary photon with an energy of E, and $\phi(E,T)$ is written with cross section for photon interactions, σ, as follows:

$$\phi(E,T) = \frac{1}{\sigma(E)} \frac{d\sigma}{dT} . \qquad (5.A.4)$$

Figure 5.A.1 shows the result of calculations of eqs. (5.A.2) and

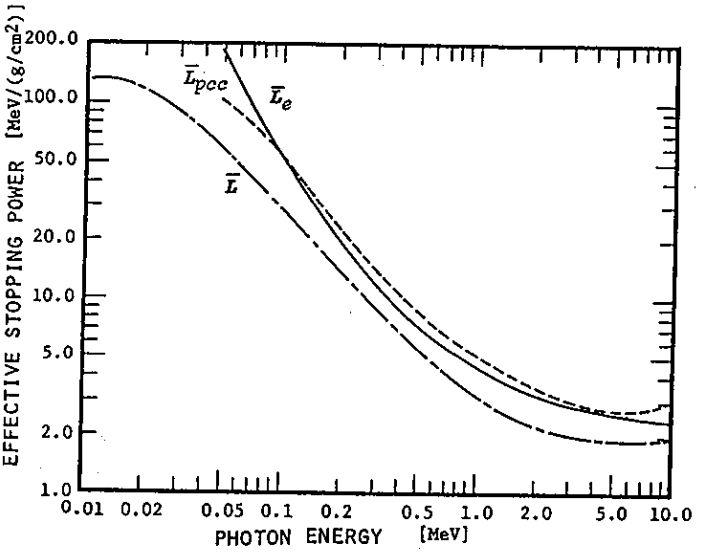

Fig. 5.A.1. Effective stopping power as a function of photon energy.

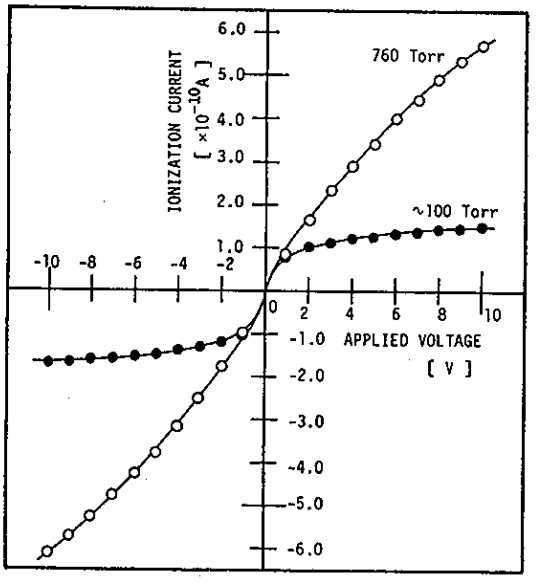

Fig. 5.A.2. Ionization current as a function of applied voltage for two gas pressures, which were observed with a parallel-plate ionization chamber exposed to ^{60}Co γ-rays.

(5.A.4). Both $\bar{L}$- and $\bar{L}_e$-values have the same dependence on the photon energy in the region where the Compton effect dominates other ones. A difference of 30 % between two values is probably attributed to underestimate of the electron fluence in case of eq. (5.A.2).

Experiments were carried out in ^{60}Co γ-ray field with an air-equivalent ionization chamber of parallel plate. An applied voltage-current curve is shown in Fig. 5.A.2 by circles. In general, negative current is a little higher than positive one, and a current can be observed with no voltage applied to the chamber.[41-44] The current was also observed at a low gas pressure of about 100 Torr as shown in the figure by dots. The result shows that the current without a voltage is independent of the existance of gas filling the chamber. Furthermore, a relation that

$$I_0 = \frac{1}{2} (I_{s+} + I_{s-}) \qquad (5.A.5)$$

is found among the current, I_0, positive saturation current, I_{s+}, and negative one, I_{s-}.

The current, I_0, is not equal to a true photo-Compton current,[45-52] but involves a so-called a stem current. It is very difficult to measure directly the stem current because it varies with the shape of the ionization chamber, a length of cables, etc. Thus, the stem current was estimated from measurement by cutting a lead wire near the electrodes and guard ring of the chamber.

The results of experiments at a distance of 100 cm from a 10000 Ci ^{60}Co source are compared with theoretical ones in Table 5.A.1. The experimental LET, $\bar{L}_{exp}$, is found to be larger than the theoretical value by about 40 % in most cases. About 70 % this error is attributed to a difference shown in Fig. 5.A.1. In Fig. 5.A.3 is shown

EXPERIMENTAL RESULTS

100 cm from Co-60 source

Data

$I_{s-} = -5.31 \times 10^{-8}$ A

$I_{s+} = 5.24 \times 10^{-8}$ A

$J_s = (I_{s+} - I_{s-})/2S = 1.86 \times 10^{-9}$ A/cm^2

$I_0 = -3.51 \times 10^{-10}$ A

$I_{stem} = -7.80 \times 10^{-12}$ A

$J_0 = (I_0 - I_{stem})/S = 1.24 \times 10^{-11}$ A/cm^2

Effective Stopping Power

experimental $\bar{L}_{exp} = 0.511$ keV/μm

theoretical $\bar{L} = 0.360$ keV/μm

$\bar{L}_e = 0.395$ keV/μm

$\bar{L}_{pcc} = 0.460$ keV/μm

Table. 5.A.1. Experimental results obtained with the ionization chamber placed at a distance of 100 cm from ^{60}Co source. Comparison with theoretical values is carried out.

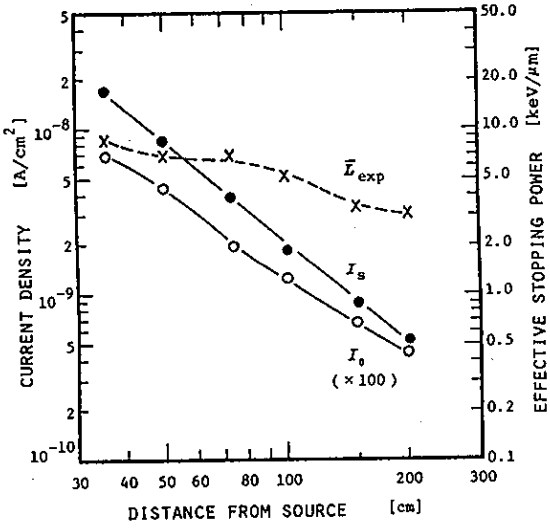

Fig. 5.A.3. Dependence of saturation current, zero-corrent and effective stopping power upon the distance from ^{60}Co source.

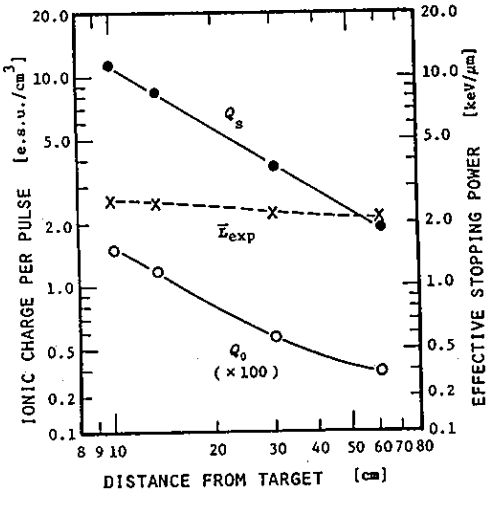

Fig. 5.A.4. Dependence of corrected charge, ionic charge without a voltage applied and effective stopping power upon the distance from W-target bombarded by 20 MeV-electrons.

the dependence of the effective LET on the distance from the source. It is considered that the spatial variation of the effective LET is caused by the influence of scattered photons and electrons, and underestimate of the stem current. The spatial variation becomes negligible in case of high-exposure-rate X-rays generated by the linear accelerator, as shown in Fig. 5.A.4.

It is concluded that the effective LET can experimentally be evaluated if about 40 % errors could be permitted.

Appendix 5.B. Distribution of absorbed doses in collision stopping power

The concept of measurement of LET distribution of the absorbed doses has been established by Rossi.[7-11] A so-called Rossi counter, a spherical TE proportional counter shown in Photo 5.B.1, is used in this measurement, which is connected with the gas flow system as shown in Fig. 5.B.1. The effective diameter in tissue becomes 1 μm when the counter is filled with 56 Torr TE gas. In this case, ionization processes in the counter simulate those in tissue.

The output signals of the counter do not represent the LET of incident charged particles, but the energy deposited by a particle in the sphere, E_y. Thus, Rossi defined the lineal energy, Y, by the deposit energy divided by a diameter of the sphere, d.[9] Namely,

$$Y = E_y/d \ . \qquad (5.B.1)$$

Accordingly, the pulse height spectrum observed with a PHA is equivalent to Y distribution of charged particle fluence. From a simple calculation, the LET distribution of absorbed dose, $D(L)$, is derived from Y distribution of the fluence, $N(Y)$, as follows:[11]

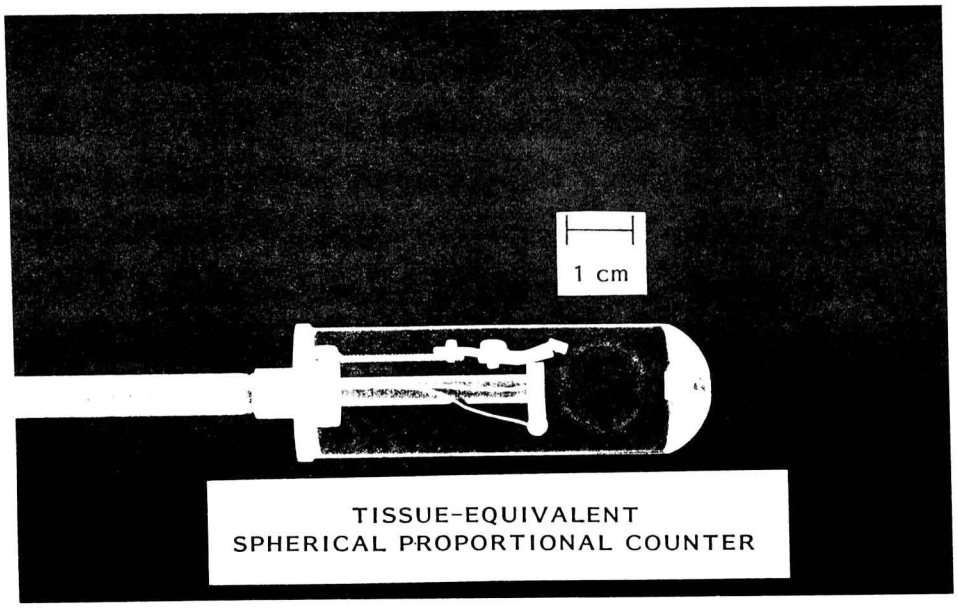

Photo 5.B.1. X-ray photograph of a tissue-equivalent spherical proportional counter. An effective diameter in tissue becomes 1 μm in case that a pressure of tissue-equivalent gas is adjusted to be about 56 Torr.

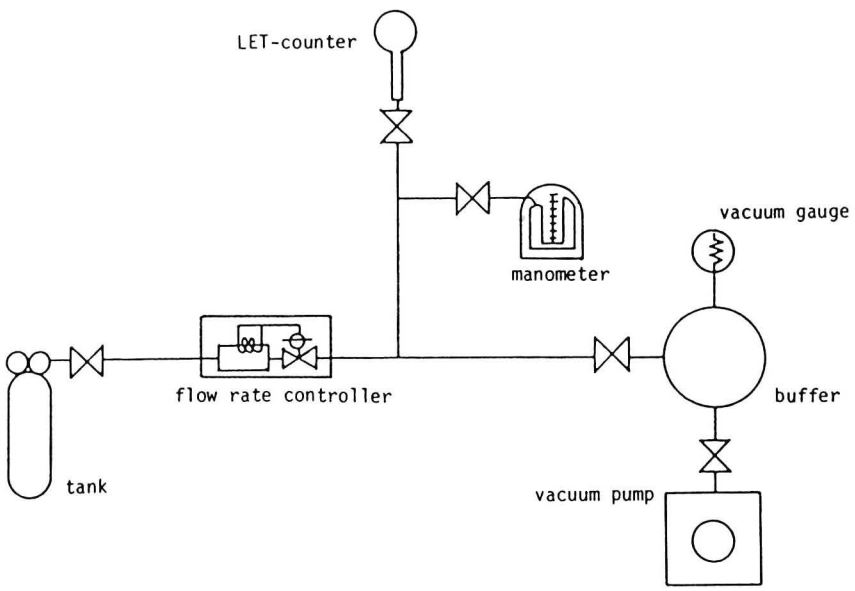

Fig. 5.B.1. Schematic diagram of a gas flow system for a TE proportional counter shown in Photo 5.B.1.

$$D(L) = \frac{2.547 \times 10^{-8}}{r^2} \left[Y N(Y) - Y^2 \frac{dN(Y)}{dY} \right]_{Y=L} . \quad (5.B.2)$$

The counter was placed around the target bombarded by 28 MeV electrons. In order to avoid the duplication of radiation pulses, the electronic current of the linear accelerator was adjusted to be as low as possible. A typical Y spectrum is shown in Fig. 5.B.2, where the lineal energy is calibrated beforehand with ^{244}Cm reference source. The signals due to electrons are neglected in the figure because of pile-up of pulses due to electronic noises. The data are converted into LET distribution of absorbed dose according to eq. (5.B.3) as shown in Fig. 5.B.3.

In order to obtain the normalized distribution and thereby obain the average QF (DE), one must know either X-ray dose or total absorbed dose. Thus, we use an ionization chamber in combination with a Rossi counter. In this case, the DE can be obtained by the following formula:

$$\begin{aligned} H &= \int_0^\infty QF(L)\, D(L)\, dL \\ &= \int_0^{3.5} D(L)\, dL + \int_{3.5}^\infty QF(L)\, D(L)\, dL \\ &= D_t - \int_{3.5}^\infty [\, QF(L) - 1 \,]\, D(L)\, dL , \end{aligned} \quad (5.B.3)$$

where D_t is the total absorbed dose to be measured with the ionization chamber and $D(L)$ is the absorbed dose per unit LET to be measured with a Rossi counter for an LET higher than about 3.5 keV/μm. The average QF, then, is obtained by dividing the DE by the total dose.

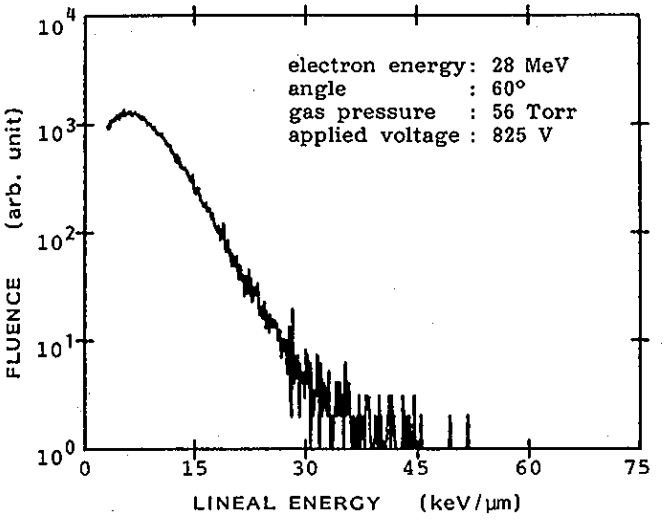

Fig. 5.B.2. A typical Y-spectrum observed with a Rossi counter, where the lineal energy is calibrated beforehand with ^{244}Cm reference source. Electron energy: 28 MeV, angle: 60°, effective diameter: 1 μm.

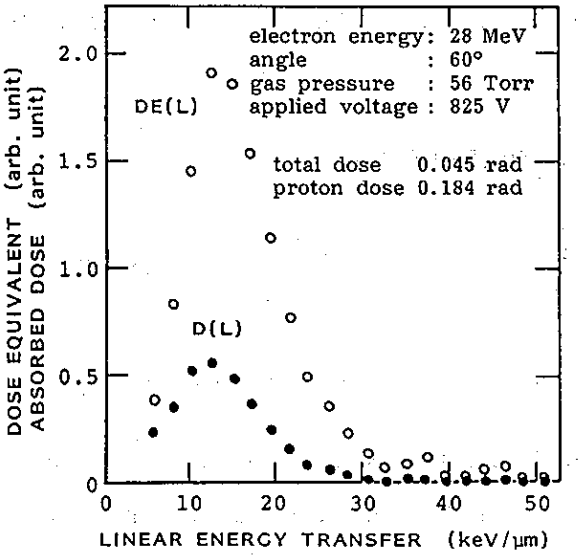

Fig. 5.B.3. A typical LET distribution of absorbed dose and DE obtained from data shown in Fig. 5.B.2. Fractional doses could be obtained by dividing the dose by the total absorbed dose measured with an ionization chamber.

Appendix 5.C. Separate measurement of absorbed doses with two ionization chambers

For this method are required two detectors having different sensitivities to radiations. Let k and h be the relative sensitivities to neutrons and X-rays, respectively, the response of the detector, R_i, is expressed as follows:

$$R_i = \int_0^\infty k_i(E_n)D_n(E_n)\,dE_n + \int_0^\infty h_i(E_x)D_x(E_x)\,dE_x \quad , (5.C.1)$$

where $D(E)\,dE$ is the absorbed dose due to particles of which energy lies between E and $E + dE$. In principle, each separate dose can be obtained by solving the simultaneous equation. But in mathematics, it is very disfficult to solve the equation because of complicated dependences of the relative sensitivities on the particle energy. In this sense, it is desirable to choose a TE ionization chamber and a C-CO_2 chamber as two detectors. The selection allows the approximation that $k_1 = h_1 = h_2 = 1.0$ for all particle energies. Then, the separate doses are easily obtained as follows:[6)]

$$D_n = (R_1 - R_2)/(1 - \bar{k}_2)$$

and

$$D_x = (R_2 - \bar{k}_2 R_1)/(1 - \bar{k}_2) \quad , \qquad (5.C.2)$$

where $\bar{k}_2$ denotes the dose-averaged sensitivity of C-CO_2 chamber. Namely,

$$\bar{k}_2 = \int_0^\infty k_2(E_n)D_n(E_n)\,dE_n \Big/ \int_0^\infty D_n(E_n)\,dE_n \quad . \qquad (5.C.3)$$

As a first step, experiments have been performed with a polyethylene-air ionization chamber (PE chamber) and a graphite-air one (C chamber). The PE and C chambers is regarded to simulate a TE and a C-CO_2 chambers, respectively. An assumption that $k_1 \simeq h_1 \simeq h_2 \simeq 1.0$ was

made for greater simplicity. Experimental and theoretical values of k_2 for C chamber have been published by several authors,[53-55] and they lies bewteen 0 and 0.32 in the neutron energy region lower than 14 MeV.

Separate measurement has been actually applied to a mixed radiation field consisting neutrons and photons generated by the electron linear accelerator. Angular dependences of the responses of both PE and C chambers is shown in Fig. 5.C.1, where the electron energy is 28 MeV and the wall thickness is adjusted to be between 0.5 and 0.55 $g\,cm^{-2}$. Substituting the data into eq. (5.C.2), and the separate doses can be obtained as shown in Fig. 5.C.2. The bars are not due to experimental errors in measuring the ionic charges but to energy dependence of k_2-value.

A procedure for calculating the average QF from the experimental values of separate doses is as follows. Firstly, the formula for definition of DE is rewritten with the separate doses as follows:

$$H = \int_0^\infty QF(L)\, D(L)\, dL = \int_0^\infty [D_x(L) + QF_n(L)\, D_n(L)]\, dL$$
$$= D_x + \overline{QF}_n D_n , \qquad (5.C.4)$$

where D_n and D_x are the separate doses ($D = \int D(L)\, dL$). The average QF for neutrons, $\overline{QF}_n$, is rewritten with the neutron fluence per unit energy, $\phi(E)$, as follows:

$$\overline{QF}_n = \int_0^\infty QF_n(L)\, D_n(L)\, dL \Big/ \int_0^\infty D_n(L)\, dL$$
$$= \int_0^\infty p(E)\, \phi(E)\, dE \Big/ \int_0^\infty p'(E)\, \phi(E)\, dE , \qquad (5.C.5)$$

where $p(E)$ is the fluence-to-DE conversion factor, and $p'(E)$ the flu-

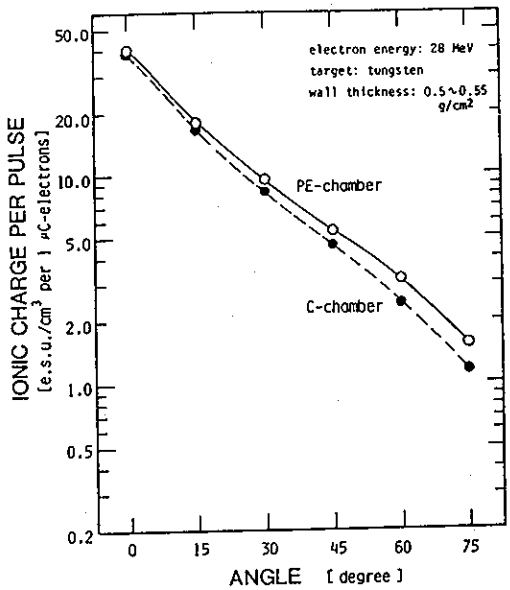

Fig. 5.C.1. Angular dependence of responses of both PE- and C-chambers. Electron energy: 28 MeV, distance from W-target: 30 cm, wall thickness: $0.5 \sim 0.55$ g cm^{-2}.

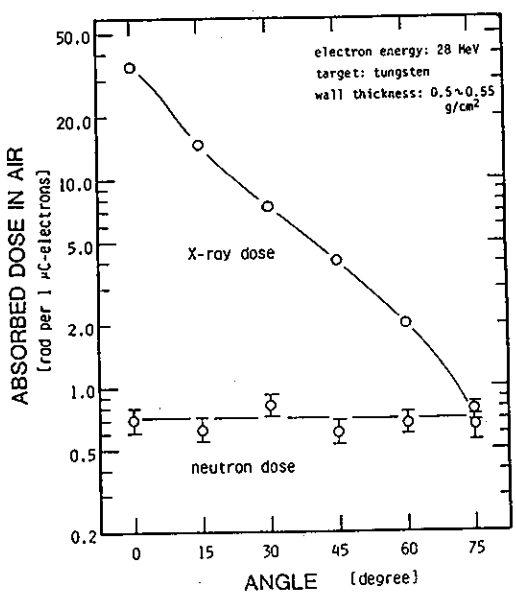

Fig. 5.C.2. Angular dependence of separate deses due to X-rays and neutrons. The bars are not attributed to experimental arrors in measuring the ionic charges, but to energy dependence of the sensitivity of C-chamber to neutrons varying widely with the neutron energy.

ence-to-dose one. The neutron energy spectrum was measured by TOF and activation methods as stated in Fig. 5.17 in the section 5.4, and then a $\overline{QF}_n$-value of 10.2 was obtained. Then, the average QF can be obtained by dividing DE by the total dose.

REFERENCES

1) ICRP Publication 15 (1970).

2) ICRU Report 19 b (1973).

3) ICRU Report 25 (1976).

4) ICRP Publication 4 (1964).

5) *Accelerator Health Physics*, eds. H.W.Patterson and R.H.Thomas (Academic, New York, 1973) Chap.2.

6) ICRP Publication 26 (1977).

7) H.H.Rossi and W.Rosenzweig: Radiology 64 (1955) 404.

8) H.H.Rossi and W.Rosenzweig: Rad. Res. 2 (1955) 431.

9) H.H.Rossi: Rad. Res. 10 (1959) 522.

10) W.Rosenzweig and H.H.Rossi: Rad. Res. 10 (1959) 532.

11) H.H.Rossi: *Radiation Dosimetry, vol. I*, eds. F.H.Attix and W.C. Roesch (Academic, New York, 1968) Chap.2.

12) S.Pszona: Health Phys. 16 (1969) 9.

13) S.Pszona and M.Höfert : Nucl. Instrum. & Methods 146 (1977) 509.

14) M.Zel'chinskii: *Neutron Dosimetry, vol.2* (IAEA, Vienna,1977), p.397.

15) M.Zel'chinskii and S.Pszona: CERN Internal Report CERN-71-16 (1971) 403.

16) A.H.Sullivan and J.Baarli: CERN Internal Report CERN-63-17 (1963) 1.

17) G.Jaffé: Ann. Physik 42 [4] (1913) 303.

18) G.Jaffé: Ann. Physik 1 [5] (1929) 977.

19) J.W.Boag: Brit. J. Radiol. 23 (1950) 601.

20) T.Yamamoto, K.Oda, H.Kobayashi and M.Kawanishi: Nucl. Instrum. & Methods 172 (1980) 447.

21) T.E.Burlin: *Radiation Dosimetry, vol. I,* eds. F.H.Attix and W.C. Roesch (Academic, New York, 1968) Chap.8.

22) K.Tsumori, N.Kimura, T.Yamamoto, T.Hori, S.Takeda, J.Okuma, T.Sawai, M.Kawanishi, H.Sakurai and K.Hayashi: *Proc. 3rd Symp. Accelerator Science & Technology, Osaka, 1980,* p.49.

23) H.Sakurai, M.Kawanishi, K.Hayashi, T.Okada, K.Tsumori, S. Takeda, N.Kimura, T.Yamamoto, T.Hori, J.Ohkuma and T.Sawai: Mem. Inst. Sci. Ind. Res., Osaka Univ. 39 (1982) 21.

24) K.Oda, H.Kobayashi, T.Yamamoto and M.Kawanishi: J. Nucl. Sci. Technol. 19 (1982) 89.

25) H.W.Koch and R.E.Carter: Phys. Rev. 77 (1950) 165.

26) J.W.Mots, W.Miller and H.O.Wyckoff: Phys. Rev. 89 (1953) 968.

27) H.W.Koch and J.W.Mots: Rev. Mod. Phys. 31 (1959) 920.

28) M.J.Berger and S.M.Seltzer: Phys. Rev. C2 (1970) 621.

29) T.Nakamura, M.Takemura, H.Hirayama and T.Hyodo: J. Appl. Phys. 43 (1972) 5189.

30) L.B.Levy, R.G.Waggner, W.D.McDavid and W.H.Payne: Med. Phys. 1 (1974) 62.

31) T.Nakamura and H.Hirayama: Nucl. Sci. Eng. 59 (1976) 237.

32) G.A.Price and D.W.Kerst: Phys. Rev. 77 (1950) 806.

33) R.Montalbetti, L.Kats and J.Goldemberg: Phys. Rev. 91 (1953) 659.

34) W.C.Barber and W.D.George: Phys. Rev. 116 (1959) 1551.

35) D.B.Gayther and P.D.Goode: J. Nucl. Energy 21 (1967) 733.

36) R.G.Alsmiller Jr. and H.S.Moran: Nucl. Instrum. & Methods 48 (1967) 109.

37) R.G.Alsmiller Jr. and H.S.Moran: Nucl. Instrum. & Methods 51 (1967) 339.

38) R.G.Alsmiller Jr., T.A.Gabriel and M.P.Guthrie: Nucl. Sci. Eng. 40 (1970) 365.

39) N.N.Kaushal, E.J.Winhold, R.H.Auguston, P.F.Yergin and H.A. Medicus: J. Nucl. Energy 25 (1971) 91.

40) J.Ohkuma: Private communication (1982).

41) H.E.Johns, N.Aspin and R.G.Baker: Rad. Res. 9 (1958) 573.

42) K.Moriuchi: Oyo Butsuri 34 (1965) 435.

43) K.Moriuchi: Oyo Butsuri 35 (1966) 84.

44) R.Tanaka: Thesis (Osaka Univ., 1980).

45) B.Gross: Z. Physik 155 (1959) 479.

46) T.A.Dellin and J.C.MacCallum: SCL-RR-720086 (1972) 1.

47) K.G.Kerris, C.C.Berggren, D.B.Carter and G.G.Spehar: IEEE Trans. Nucl. Sci. NS-16 (1969) 264.

48) R.L.Fitzwilson, M.J.Bernstein and T.E.Alson: IEEE Trans. Nucl. Sci. NS-21 (1974) 276.

49) W.L.Chadsey, B.L.Beers, V.W.Pine and C.W.Wilson: IEEE Trans. Nucl. Sci. NS-23 (1976) 1933.

50) D.M.Clement, C.E.Wuller and E.P.Chivingston: IEEE Trans. Nucl. Sci. NS-23 (1976) 1946.

51) E.P.Chivingston, L.E.Shaw and T.E.Alston: IEEE Trans. Nucl. Sci. NS-23 (1976) 1952.

52) C.E.Wuller, L.C.Nielsen and D.M.Clement: IEEE Trans. Nucl. Sci. NS-25 (1978) 1961.

53) R.D.Colvett, H.H.Rossi and V.Krishnaswamy: Phys. Med. Biol. 17 (1972) 356.

54) F.M.Waterman, F.T.Kuchnir and L.S.Skaggs: Phys. Med. Biol. 22 (1977) 880.

55) M.Makarewicz and S.Pszona: Nucl. Instrum. & Methods 152 (1978) 423.

CHAPTER 6. CONCLUSIONS

In this thesis, basic problems have been discussed about radiation dosimetry in a high-fluence-rate, singly pulsed and mixed field. The purposes of the dosimetry have been focused on an absolute evaluation of exposure (or kerma), absorbed dose and dose equivalent in such a radiation field. The first two quantities are in general proportional to the number of ion pairs liberated in air or irradiated materials. Hence, it is indispensable to measure accurately the ion density. An ionization chamber was selected as a dosimeter in this work, which is one of reference dosimeters for both exposure and ansorbed dose. Concerning the dose equivalent, it is necessary to estimate the average quality factor in a mixed radiation field. From theoretical and experimental approaches to such problems, the following results have been obtained:

(1) Among several correction factors for absolute measurement of exposure or absorbed dose with an ionization chamber, a collection efficiency for ion recombination is most important, especially in a pulsed X-ray field of high exposure rate. In order to obtain the relation of the collection efficiency with various parameters, temporal and spatial variations of the ion density in the chamber were calculated numerically. It was pointed out that the well-known Boag's formula should deviate from the true collection efficiency in a pulsed X-ray field where the exposure rate became extremely high or a field where the pulse duration became of the order of the ion transit time between electrodes of the ionization chamber. Furthermore the effects caused by existance of space charge or difference in mobility between positive and negative ions.

(2) It is very difficult to determine the collection efficiency in an unknown X-ray field, because the efficiency itself is a function of the exposure rate to be evaluated. Thus, a convenient method has been proposed, by which a true collection efficiency could be determined by finding a best fit of theoretical saturation curves to measured one. It is indispensable to measure ionic charges collected at two different applied voltages at least. An abreast-type ionization chamber was designed and constructed for single-burst X-rays.

(3) Experiments on determination of the collection efficiency have been carried out in a pulsed X-ray field generated by an electron linear accelerator. A good agreement in output currents of a parallel-plate ionization chamber between theoretical and experimental results was found. It was also confirmed that the proposed method could be applied to an X-ray field of which exposure rate up to 10^{10} R s^{-1}, i.e. collection efficiency higher than about 0.03.

(4) The dose evaluation has been discussed in an X-ray field in the other region where the Boag's formula became invalid, that is, the pulse duration became long to be comparable with the ion transit time. It was found from numerical calculations that the collection efficiency in such a field was affected by the pulse shape as well as the pulse duration. In order to ascertain the fact, experiments were carried out in a field generated by an X-ray tube for medical diagnosis. A good agreement in output current shapes and saturation curves was confirmed between experimental and theoretical results. It was pointed out that the proposed method was also applicable to an X-ray field of relatively long duration.

(5) Dosimetry of mixed radiations have also been discussed. At first,

a basic concept of mixed field dosimetry was refined for practical purpose, and the methods for evaluating dose equivalent were classified into three categories according to radiation quantity to be measured, that is, energy spectra, LET spectrum and ionic charge density. Two kinds of procedures based on the ionization chamber have been proposed for singly pulsed and mixed radiation fields. The methods were applied to a field consisting of bremsstrahlung X-rays and photo-neutrons generated by the electron linear accelerator, and the results were compared with those obtained by other methods in common use, i.e. calculations of X-ray energy spectrum, measurement of neutron energy spectrum by TOF and activation methods, measurement of LET distribution of absorbed dose with a Rossi counter, and separate measurement of X-ray and neutron doses with two ionization chambers. The applicability of the proposed method in the mixed field could be confirmed.

It seems that the study on radiation dosimetry in a high-fluence-rate, singly pulsed and mixed field has just begun and is still in development. There remain many problems in the dosimetry, e.g. definition of exposure for high energy X-rays, description of mixed field by mixed air-kerma, multiplication of radiation effects in mixed fields, representation of radiation effects by entropy change, and so on. In order to catch up with future rapid development in accelerator science and nuclear fusion technology, enthusiastic endeavors by many dosimetrists are required.

ACKNOWLEDGEMENTS

The author would like to express the heartful appreciation to Professor M. Kawanishi for his guidance and unfailing encouragement.

The author is also grateful to Professor K. Sumita and Professor T. Okada for their valuable discussions and warm encouragement.

Thanks are also due to Professor M. Shinagawa, Professor T. Sano, Professor S. Imoto and Professor T. Sekiya for their guidance in the course of nuclear engineering.

The author cannot find proper words to express the gratitude to Dr. T. Yamamoto for his rigorous guidance, without which this work could never have accomplished.

The author is also indebted to Dr. N. Abe of the Welding Research Institute of Osaka University for his helpful discussions and constant encouragement.

The author wishes to thank all the staffs of Radiation Laboratory of the Institute of Scientific and Industrial Research, Osaka University, especially Assistant Professor K. Tsumori for their stable operation of the electron linear accelerator and useful suggestions about experimental techniques.

The author is also grateful to Mr. H. Terada and Miss K. Yamazaki of the Research Institute for Microbial Diseases, Osaka University for their fruitful discussions about medical diagnosis and operation of the X-ray tube.

Thanks are also due to Mr. S. Takeda for valuable discussions about numerical calculations, Dr. J. Ohkuma for measurement of neutron energy spectrum, Dr. M. Miyake and Dr. R. Kikuchi for useful

discussions.

The author would like to express his sincere thanks to Dr. Y. Moriuchi of Electrotechnical Laboratory Headquarters, Professor S. Okabe of Fukui University, Dr. T. Nakamura of the Institute for Nuclear Study, University of Tokyo, Dr. K. Yatsui of the Technological University of Nagaoka, Dr. S. Miyake of the Welding Research Institute of Osaka University, Dr. C. Yamaguchi of National Laboratory for High Energy Physics, and Dr. R. Tanaka of Japan Atomic Energy Research Institute for their kind interest and helpful suggestions.

Mr. H. Kobayashi, Mr. Y. Moriguchi and Mr. H. Koyama enthusiastically cooperated with the author in the experiments and numerical calculations.

The author wishes to thank Mr. K. Fujii, Miss M. Nakagawa and post-graduate students in Kawanishi Laboratory for their warm encouragement.

This work was partially supported by the Grant-in-Aid for the Scientific Research from the Ministry of Education, Science and Culture.

LIST OF LECTURES BY THE AUTHOR

1. Highly Ionizing Mechanism in the ECR Type Heavy Ion Source.
   The 2nd Symp. Accelerator Science & Technology, 1978.
2. Trial Manufacture of an ECR-Type Generator of Characteristic X-Rays.
   The 25th Vernal Meeting of the Japan Society of Applied Physics, 1978.
3. Production of Multiply-Charged Ions in an ECR Plasma.
   The 39th Autumnal Meeting of the Japan Society of Applied Physics, 1978.
4. Production of Multi-Charged Ions in ECR Plasma.
   The 3rd Symp. Ion Sources & Application Technology, 1979.
5. Response of an Ionization Chamber to Pulsed Radiations of High Fluence Rate (Space Charge Effect).
   The 26th Vernal Meeting of the Japan Society of Applied Physics, 1979.
6. Production of Multiply-Charged Ions and Characteristic X-Rays in an ECR Plasma.
   The 40th Autumnal Meeting of the Japan Society of Applied Physics, 1979.
7. Dose Evaluation in a Pulsed and Mixed Radiation Field with an Ionization Chamber.
   The 40th Autumnal Meeting of the Japan Society of Applied Physics, 1979.
8. Pulse Dosimetry in Mixed Radiation Fields.
   The 1st Symp. Generation of Pulsed Radiations & Its Application, 1980.
9. Dosimetry in Pulsed and Mixed Radiation Field with an Ionization Chamber.
   The 27th Vernal Meeting of the Japan Society of Applied Physics, 1980.
10. Production of Multiply-Charged Ions in an ECR Plasma (II).

The 27th Vernal Meeting of the Japan Society of Applied Physics, 1980.

11. Characteristics of an ECR-Type Ion Source.
    The 4th Symp. Ion Sources & Application Technology, 1980.

12. Response of an Ionization Chamber to a Radiation Field of High Fluence Rate.
    The 17th Annual Meeting on Radioisotopes in the Physical Science and Industry, 1980.

13. Dosimetry of Pulsed, High-Exposure-Rate X-Rays of Pico-Second Duration.
    The 5th Symp. Linear Accelerators, 1980.

14. Characteristics of an ECR-EB Hybrid-Type Multiply-Charged Ion Source.
    The 3rd Symp. Accelerator Science & Technology, 1980.

15. Pulse Dosimetry of Mixed Radiation Field around an Electron Linear Accelerator.
    The 3rd Symp. Accelerator Science & Technology, 1980.

16. Dosimetry of Pulsed Radiations with a Parallel-Plate Ionization Chamber
    1980 Fall Meeting of the Atomic Energy Society of Japan, 1980.

17. Method for Determining f-Value of an Ionization Chamber Exposed to Pulsed X-rays.
    The 41st Autumnal Meeting of the Japan Society of Applied Physics, 1980.

18. Improvement of an ECR-Type Multiply-Charged Ion Source by Electron Beam Injection.
    The 41st Autumnal Meeting of the Japan Society of Applied Physics, 1980.

19. A Problem in Absolute Measurement of Absorbed Dose Due to Diagnostic X-Rays with an Ionization Chamber.
    The 40th Sectional Meeting of the Japan Radiological Society, 1980. Branch: Radiological Physics.

20. Pulse Dosimetry of Mixed Radiations of High Fluence Rate.
The 19th Annual Meeting of the Atomic Energy Society of Japan, 1981.

21. Recombination Coefficient-of Ionization Chamber in Mixed Radiation Field.
The 28th Vernal Meeting of the Japan Society of Applied Physics, 1981.

22. Characteristics of an ECR-EB Hybrid-Type Ion Source.
The 28th Vernal Meeting of the Japan Society of Applied Physics, 1981.

23. Characteristics of an ECR-EB Hybrid-Type Multiply-Charged Ion Source.
The 5th Symp. Ion Sources & Ion-Assisted Technology, 1981.

24. Characteristics of an ECR-EB Hybrid-Type Ion Source (II).
The 42nd Autumnal Meeting of the Japan Society of Applied Physics, 1981.

25. Evaluation of Dose Equivalent in Pulsed and Mixed Radiation Field.
1981 Fall Meeting of the Atomic Energy Society of Japan, 1981.

26. A Problem in Absolute Measurement of Absorbed Dose Due to Diagnostic X-Rays with an Ionization Chamber (II).
The 41st Sectional Meeting of the Japan Radiological Society, 1981. Branch: Radiological Physics.

27. Pulse Dosimetry in (γ + n) Mixed Radiation Fields.
Technical Meeting on Neutron Experiments with Accelerators, 1981.

28. Separate Measurement of Absorbed Dose in Mixed Radiation Fields Consisting of Neutrons and X-Rays.
The 20th Annual Meeting of the Atomic Energy Society of Japan, 1982.

29. Characteristics of an ECR-EB Hybrid-Type Ion Source (III).
The 29th Vernal Meeting of the Japan Society of Applied Physics, 1982.

30. Plasma Heating in an ECR-EB Hybrid-Type Ion Source.
The 6th Symp. Ion Sources & Ion-Assisted Technology, 1982.

31. Effective Stopping Power in X- and γ-ray fields.
The 19th Annual Meeting on Radioisotopes in the Physical Science and Industry, 1982.

32. Comparison among Methods for Evaluating Dose Equivalent in Pulsed and Mixed Radiation Fields.
The 42nd Autumnal Meeting of the Japan Society of Applied Physics, 1982.

33. Dose Equivalent Evaluation from LET Spectrum in a Mixed Radiation Field around an Electron Linear Accelerator.
1982 Fall Meeting of the Atomic Energy Society of Japan, 1982.

34. Evaluation of Dose Equivalent in Pulsed and Mixed Radiation Field (II).
1982 Fall Meeting of the Atomic Energy Society of Japan, 1982.

35. LET Distribution of Absorbed Dose in a Mixed Radiation Field around an Electron Linear Accelerator.
The 4th Symp. Accelerator Science & Technology, 1982.

LIST OF PAPERS BY THE AUTHOR

1. T.Yamamoto, N.Abe, K.Oda and M.Kawanishi: Highly Ionizing mechanism in the ECR Type Heavy Ion Source, *Proc. 2nd Symp. Accelerator Science & Technology, Tokyo, 1978,* pp. 29 - 30.

2. K.Oda, N.Abe, T.Yamamoto and M.Kawanishi: Production of Multi-Charged Ions in ECR Plasma, *Proc. 3rd Symp. Ion Sources & Application Technology, Tokyo, 1979,* pp. 47 - 50.

3. K.Oda, N.Abe, T.Yamamoto and M.Kawanishi: Charge State Distribution of Argon Ions Extracted from ECR Plasmas, *IONICS —— Ion Sources & Technology ——* 5 (1979) 5 - 10, [in Japanese].

4. T.Yamamoto, K.Oda, H.Kobayashi and M.Kawanishi: Response of a Parallel-Plate Ionization Chamber to Pulsed X-Rays of High Exposure Rate, *Proc. 2nd KEK Symp. Radiation Dosimetry, Tsukuba, 1978, KEK-79-17 R* (1979) 129 - 154.

5. N.Abe, T.Yamamoto, K.Oda and M.Kawanishi: Production of Multiply-Charged Ions in an ECR Plasma, *Jpn. J. Appl. Phys.* 19 (1980) 149 - 155.

6. T.Yamamoto, K.Oda, H.Kobayashi and M.Kawanishi: Collection Efficiency of a Parallel-Plate Ionization Chamber Exposed to Pulsed X-Rays, *Nucl. Instrum. & Methods* 172 (1980) 447 - 454.

7. T.Yamamoto, K.Oda, H.Kobayashi and M.Kawanishi: Radiation Dosimetry in Pulsed, Mixed Field of High-Fluence Rate with Ionization Chamber, *Proc. 3rd KEK Symp. Radiation Dosimetry, Tsukuba, 1979, KEK-80-1 R* (1980) 75 - 101.

8. T.Yamamoto, M.Kawanishi, K.Oda and H.Kobayashi: Dosimetry of Mixed field of Single Burst Consisting of X-Rays and Neutrons, *Kakuyugo Kenkyu* (*Nuclear Fusion Research*) 43 Suppl.7 (1980) 127 - 138, [in Japanese].

9. M.Kawanishi, T.Yamamoto, K.Oda and H.Kobayashi: Pulse Dosimetry in Mixed Radiation Fields, *Proc. 1st Symp. Generation of Pulsed Radiations & Its Application, Osaka, 1980,* pp. 29 - 36, [in Japanese].

10. K.Oda, N.Abe, T.Yamamoto and M.Kawanishi: Characteristics of an ECR-Type Ion Source, *Proc. 4th Symp. Ion Sources & Application Technology, Tokyo, 1980,* pp. 19 - 22.

11. T.Yamamoto, K.Oda and M.Kawanishi: Dosimetry of Pulsed, High-Exposure-Rate X-Rays of Pico-Second Duration, *Proc. 5th Symp. Linear Accelerators, Tsukuba, 1980,* pp. 155 - 158, [in Japanese].

12. K.Oda, Y.Moriguchi, T.Yamamoto and M.Kawanishi: Characteristics of sn ECR-EB Hybrid-Type Multiply-Charged Ion Source, *Proc. 3rd Symp. Accelerator Science & Technology, Osaka, 1980,* pp. 69 - 70.

13. T.Yamamoto, K.Oda and M.Kawanishi: Pulse Dosimetry of Mixed Radiation Field around an Electron Linear Accelerator, *Proc. 3rd Symp. Accelerator Science & Technology, Osaka, 1980,* pp. 101 - 104.

14. K.Oda, N.Abe, T.Yamamoto and M.Kawanishi: Production Mechanism of Multiply-Charged Ions in an ECR-Type Ion Source, *Jpn. J. Appl. Phys.* 20 (1981) 955 - 961.

15. K.Oda, Y.Moriguchi, T.Yamamoto and M.Kawanishi: Characteristics of an ECR-EB Hybrid-Type Multiply-Charged Ion Source, *Proc. 5th Symp. Ion Sources & Ion-Assisted Technology, Tokyo, 1981,* pp. 157 - 160.

16. T.Yamamoto, K.Oda and M.Kawanishi: Pulse Dosimetry in Mixed Radiation Field, *INS-NUMA-29* (1981) 116 - 123, [in Japanese].

17. K.Oda, T.Yamamoto and M.Kawanishi: Pulse Dosimetry in (γ + n) Mixed Radiation Field, *Research Reports on Neutron Experiments with Accelerators, Research Reactor Institute of Kyoto University, 1981,* pp. 13 - 15, [in Japanese].

18. K.Oda, H.Kobayashi, T.Yamamoto and M.Kawanishi: Experimental Determination of Collection Efficiency of Ionization Chamber in Field of Pulsed X-Rays, *J. Nucl. Sci. Technol.* 19 (1982) 89 - 95.

19. K.Oda, Y.Moriguchi, T.Yamamoto and M.Kawanishi: Plasma Heating in an ECR-EB Hybrid-Type Ion Source, *Proc. 6th Symp. Ion Sources & Ion-Assisted Technology, Tokyo, 1982,* pp. 17 - 20.

20. T.Yamamoto, K.Oda, H.Kobayashi and M.Kawanishi: Dosimetry of Pulsed X-Rays of High Exposure Rate Generated by an Electron Linear Accelerator with an Ionization Chamber, *Nucl. Instrum. & Methods* 196 (1982) 469 - 476.

21. K.Oda, T.Yamamoto and M.Kawanishi: Saturation Correction for an Ionization Chamber in a Pulsed X-Ray Field for Medical Diagnosis, *Hoken Butsuri* (*J. Jpn. Health Phys. Soc.*) 17 (1982) 143 - 150.

22. K.Oda, T.Yamamoto and M.Kawanishi: Evaluation of Average Quality Factor in a Mixed Radiation Field with an Ionization Chamber, *Nucl. Instrum. & Methods* 202 (1982) 481 - 486.

23. K.Oda, H.Koyama, T.Yamamoto and M.Kawanishi: LET Distribution of Absorbed Dose in a Mixed Radiation Field around an Electron Linear Accelerator, *Proc. 4th Symp. Accelerator Science & Technology, 1982, Saitama,* pp. 77 - 78.

24. K.Oda, H.Koyama, T.Yamamoto and M.Kawanishi: Comparison of Methods for Estimating Average Quality Factor in a Mixed Field around an Electron Linear Accelerator, [in preparation].